LIQUID PHASE METHANATION/SHIFT, MARSHALL E. FRANK, Chem Systems Inc., 747 Third Ave. New York, N.Y. 10017 - David B. Blum, Chem Systems Inc.-Research Center, 275 Hudson Street, Hackensack N.J.

Chem Systems' Liquid Phase Methanation/Shift (LPM/S) process economically converts high concentration CO synthesis gas to high Btu Gas. A development program with ERDA/AGA sponsorship has been under way since 1973. Recently the process concept has been extended to handle synthesis gas feeds wherein the hydrogen to carbon monoxide molar ratio is less than 3/1. In the liquid phase system, the methanation reaction and the water-gas shift reaction proceed simultaneously. The hydrogen produced by the shift reaction is utilized immediately for the methanation reaction. With synthesis gas feeds containing less than a 2/1 hydrogen to carbon monoxide ratio, a small amount of additional water (usually in the form of steam) must be added to the system to provide the necessary hydrogen for bulk CO conversion. The effluent gas from the liquid phase reactor is sent to a small, fixed bed, polishing reactor for complete conversion of the carbon monoxide. This paper describes recent experimental work in a bench scale unit and in a larger process development unit (PDU). Results have been correllated using an empirically derived kinetic model. The effect of water addition rate on carbon monoxide conversion and effluent gas composition has been determined for synthesis gas feeds with H_2/CO ratios ranging from 1/1 to 2/1. Life tests have been performed on catalysts under various polishing reactor conditions. Based on the bench scale and PDU results, the economics of the liquid phase methanation/shift process as it would be applied in a commercial size coal gasification plant have been determined.

Pilot Plant Operation of a Nonadiabatic Methanation Reactor

R. R. Schehl, H. W. Pennline, J. P. Strakey and W. P. Haynes

Energy Research and Development Administration
Pittsburgh Energy Research Center
4800 Forbes Avenue
Pittsburgh, PA 15213

INTRODUCTION

The development of efficient catalytic methanation reactors is essential to the commercialization of plants for converting coal to substitute natural gas. One of the most important problems facing researchers in this area is that of effective removal of the heat of reaction from the catalyst bed. The Energy Research and Development Administration, Pittsburgh Energy Research Center, is conducting bench-scale and pilot-plant scale studies of a variety of types of catalytic methanation reactors. Some of the earlier investigations (1, 2) included fixed-bed and fluidized-bed experiments using an assortment of supported catalysts and promoters. Later studies (3, 4, 5, 6) concentrated on Raney nickel catalyst thermally deposited onto stainless steel substrates and operated in reactors of varying geometrical configurations and differing modes of operation.

Two distinctly different types of methanation reactors utilizing thermally sprayed Raney nickel catalyst had heretofore been investigated; one, an isothermal reactor in which the Raney nickel was thermally sprayed onto either the internal or external surface of a tube with the heat of reaction being removed by circulating Dowtherm, the other, an adiabatic reactor with the catalyst bed consisting of parallel plate grid assemblies. The plates were constructed of stainless steel and coated on both sides with Raney nickel. The catalyst temperature in the adiabatic reactor is controlled by diluting the reactants in the feed stream to the reactor with recycled product gas. There are advantages and disadvantages to both reactor schemes and the present work is an effort to encorporate desirable features of each methanation scheme into a more efficient reactor system.

The hybrid reactor, as we have christened it, employs a Dowtherm jacket to remove an appreciable amount of the heat of reaction, while at the same time, some product gas is recycled through the reactor to control the reaction rate. The catalyst bed is in the form of an x-shaped stainless steel insert, thermally sprayed with Raney nickel. This insert may be easily replaced when the catalyst becomes deactivated.

REACTOR DESCRIPTION

The hybrid reactor experiments, HYB-17, 18, 19 and 20, were performed in a pilot plant scale reactor constructed of type 304 stainless steel 2 inch schedule 40 pipe. Surrounding the two inch reactor tube was a four inch diameter pipe jacket containing boiling Dowtherm in the annular space to remove a portion of the heat of reaction. The Dowtherm cooling system is depicted in figure 1. The temperature of the coolant is regulated by controlling the pressure in the cooling system. Nucleate boiling is assumed to take place on the outer surface of the reactor tube thereby providing a natural convective circulation of the Dowtherm. Dowtherm vapor is condensed via cooling water and returned to the reservoir.

The catalyst bed consisted of an x-shaped insert coated with Raney nickel catalyst. The cross member insert was two stainless steel 1 x 1 x 1/8 inch angles welded together, 14 ft long. The catalytic surface of the insert was prepared by sand-blasting the stainless steel surface with an iron-free grit and then depositing a

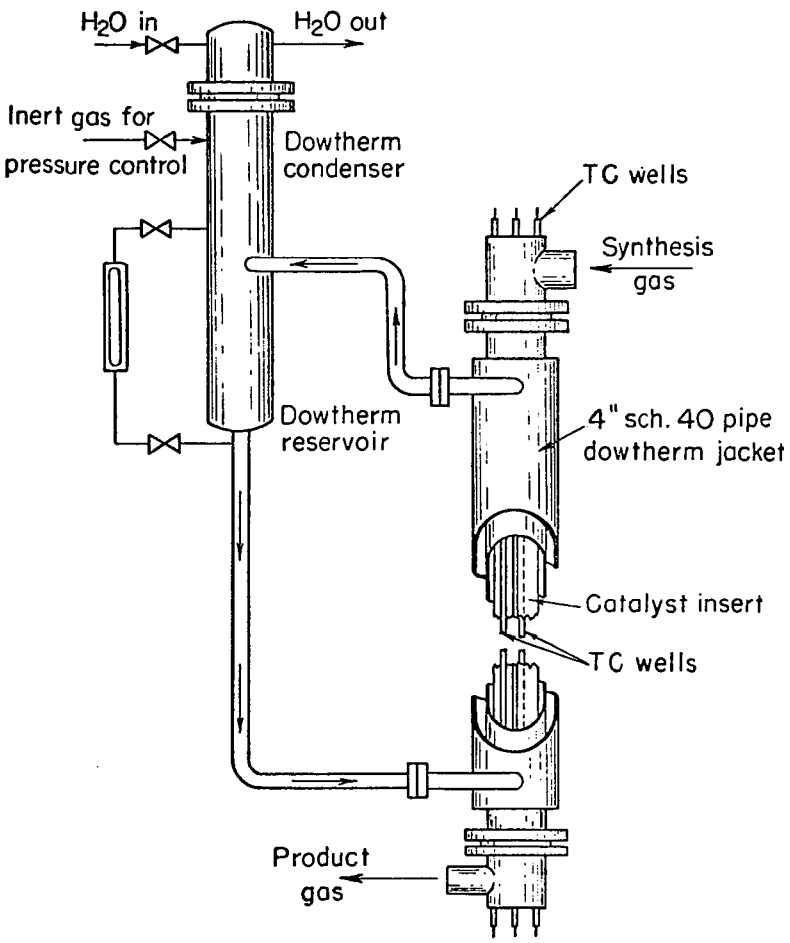

Figure 1. - Hybrid methanation reactor with Dowtherm cooling system.

light coat of bonding material consisting of 80% Ni and 20% Al to a thickness of about .007 inches. Subsequent to the bond coat, Raney nickel alloy powder (80-200 mesh) was thermally deposited onto the bond surface until the desired thickness was achieved (.023 inches). Two different methods were employed for the thermal deposition of Raney nickel onto the substrate. In runs 17 and 18 the catalyst was flame sprayed onto the surface with an oxy-hydrogen flame. A plasma arc with nitrogen as the carrier gas was used to deposit the catalyst for runs 19 and 20. Prior bench-scale studies indicated that plasma sprayed catalyst exhibited longer stability, hence, the method of catalyst deposition was one of the more important parameters studied in this sequence of runs.

The catalyst insert was placed in the reactor and then activated by passing a 2 wt. percent solution of NaOH through the reactor until approximately 70 percent of the aluminum in the Raney alloy was reacted. The extent of reaction was determined by measuring the quantity of hydrogen which evolves according to 3 moles of H_2 for every 2 moles of Al reacted. After activation, the catalyst was washed with distilled water until the pH of the effluent water was within one or two tenths that of the distilled water. The reactor was maintained under hydrogen until the temperature and pressure of the system was brought to synthesis conditions. Synthesis feed gas was then introduced gradually to the system to initiate the run.

Figure 2 illustrates a simplified flowsheet of the hybrid methanation pilot plant. Synthesis gas consisting of approximately 3 parts hydrogen and one part carbon monoxide is blended with recycled product gas. Product water vapor is condensed from the recycle stream before the recycle is mixed with the fresh feed gas. The ratio of recycled gas to fresh gas was from 5 to 8, depending upon the exposure velocity, for a fresh catalyst bed. The recycle ratio required to maintain some preselected maximum catalyst temperature then tended to increase as the catalyst activity declined with age. The mixed gas stream was preheated to the desired temperature before being introduced to the reactor. This temperature was generally the same temperature as that of the Dowtherm coolant.

A second stage clean-up methanator, not shown in figure 2, was used only during the latter periods of the runs when conversion in the primary reactor was declining. The clean-up reactor, an adiabatic reactor charged with a supported commercial nickel catalyst, was utilized to upgrade the quality of the product gas from the primary reactor.

OPERATING PROCEDURES AND RESULTS

The system pressure for all four hybrid reactor runs was 300 psig. The Dowtherm temperature in the cooling jacket as well as the inlet gas temperature was maintained at 300° C throughout all of the runs except for the last few hundred hours of Run 20, when these temperatures were raised to 325° C. Similarly, the maximum catalyst temperature was held at 400° C by adjusting the rate of recycled product gas. The maximum catalyst temperature was allowed to increase to 425° C during the latter portion of Run 20.

Catalyst temperature and gas temperature were measured at 3 inch intervals throughout the reactor on a daily basis. This was accomplished through the use of movable thermocouples in thermowells positioned as shown in figure 3. The thermocouple measuring the gas stream temperature was positioned in the geometrical center of one of the quandrants defined by the x-shaped insert and held in place by ceramic spacers. The thermowell designed to measure the catalyst temperature was first fastened into the "vee" formed by two fins. The bond and catalyst coatings were then sprayed over the thermowell at the same time that the fins were coated. A configuration of this type, with the catalyst essentially surrounding the thermowell,

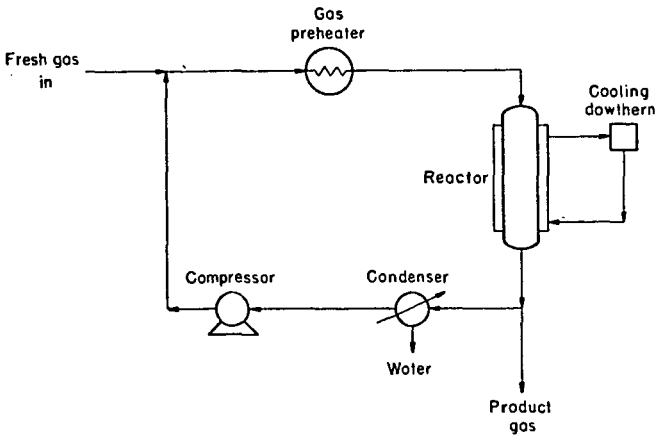

Figure 2. - Flow scheme of HYBRID reactor system.

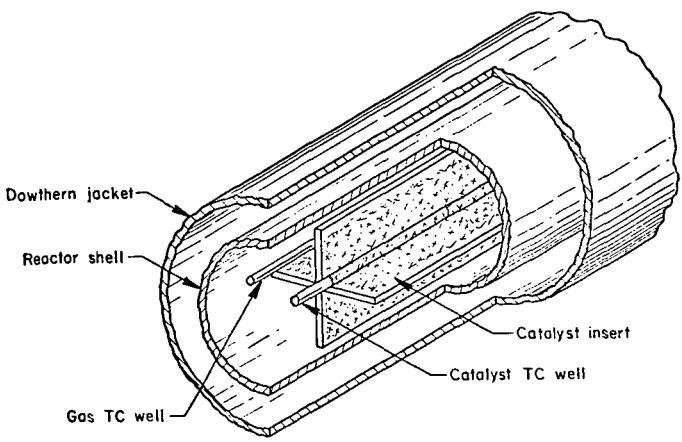

Figure 3. - View of catalyst insert and thermocouple wells.

should yield an excellent measurement of maximum temperature that the catalyst experiences. The gas stream composition was also measured as a function of distance through the catalyst bed. Gas samples were taken every one-eighth of the reactor length with a movable probe which was guided by a slit tube. The gas composition profile was measured only when operating conditions were changed rather than on a daily basis.

Run HYB-17: Seven two ft. inserts coated with flame sprayed Raney nickel were used in Run HYB-17. The reactor was operated at exposure velocities of 20, 30, and 40 scfh/ft^2. Exposure velocity is calculated as the ratio of scfh of synthesis gas (3 parts H_2 to 1 part CO) to the superficial catalyst surface area. An exposure velocity of 30 scfh/ft^2 corresponds to a space velocity of 806 hr^{-1}. Once again, the space velocity is based on a 25 percent CO fresh feed gas flow rate. This first hybrid reactor experiment lasted only 671 hours. The run was terminated when CO conversion decreased to 96.6 and the concentration of CO in the product gas reached 3 percent. Overall performance of this catalyst bed was not outstanding with a production of only 15.0 mscf of CH_4 per pound of catalyst (before leaching). Operating parameters and product gas characteristics are presented in figure 4. Catalyst bed data for Run HYB-17 as well as the three successive runs are listed in Table 1.

Table 1. - Catalyst Bed Data

	HYB-17	HYB-18	HYB-19	HYB-20	HYB-21
Catalyst Type	Flame-Sprayed Raney		Plasma Sprayed Raney		Cast Raney
Wt Pct Nickel	42[a]	42[a]	42[a]	42[a]	42[a]
Pct Activated	71.4[b]	70.6[b]	70.1[b]	70.0[b]	100.0[c]
Reactor Diameter X Length, in.	2 x 168	2 x 168	2 x 168	2 x 168	2 x 170
Reactor Volume, ft^3	0.326	0.326	0.326	0.326	0.330
Weight of Unactivated Catalyst, lb	2.78	2.24	2.43	1.70	10.64
Superficial Area of Catalyst, ft^2	8.75	8.75	7.58	8.46	11.20
Fin Thickness, in.	0.124	0.122	0.125	0.129	0.150
Avg. Bond Coat Thickness, in.	0.008	0.007	0.007	0.006	—
Avg. Catalyst Thickness, in.	0.03	0.023	0.023	0.013	0.050

[a] before leaching

[b] theoretical (based on H_2 evolution)

[c] 100% theoretical leaching of 0.05 inches

Run HYB-18: Flame sprayed Raney nickel was again used in Run HYB-18. Operating conditions were comparable to those of HYB-17 with the exception that the catalyst was exposed to a higher space velocity (1344 hr^{-1}, 50 scfh/ft^2) during a large portion of the run. This experiment lasted almost 3 times longer than the previous run. The run was voluntarily terminated after 2073 hours on stream when the CO conversion reached 95.6 percent and the CO concentration in the product gas was nearly 4 percent. It should be noted in figure 5 that decreasing the Dowtherm temperature from 300° C to 275° C at about 1950 hours on stream was responsible for a large decrease in conversion. CO conversion just prior to this time was

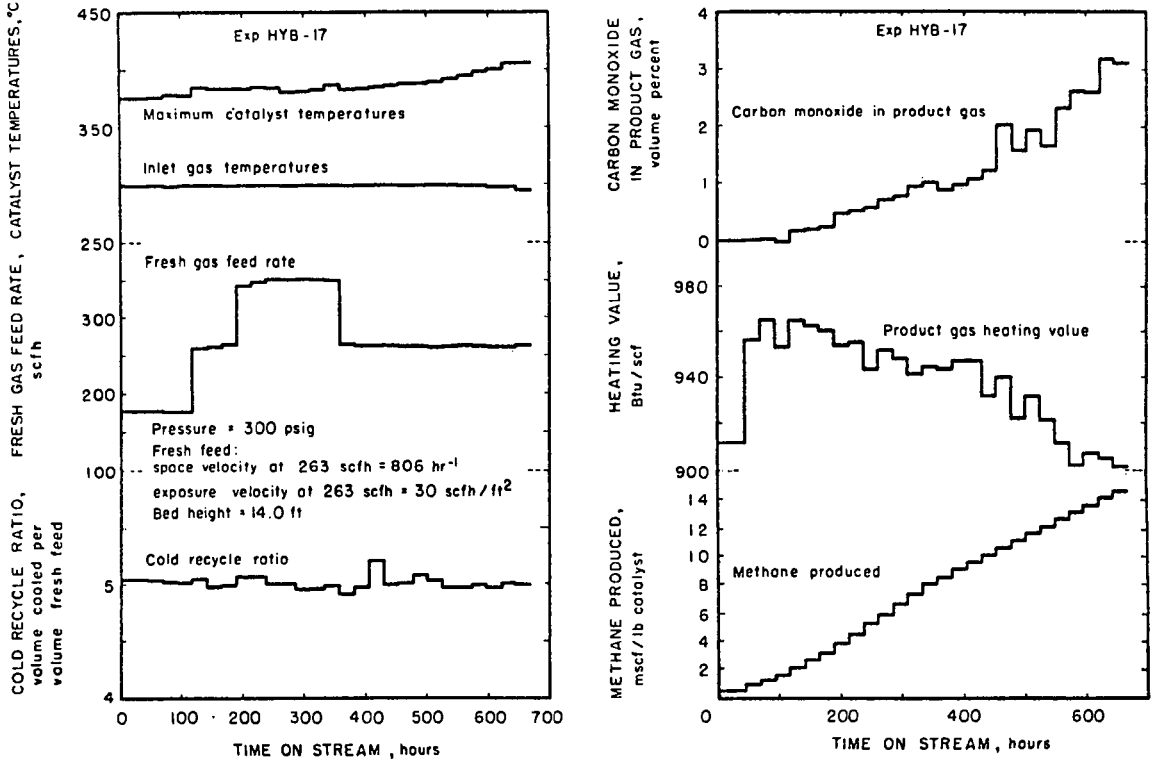

Figure 4. - Reactor conditions and product gas characteristics for Run HYB-17.

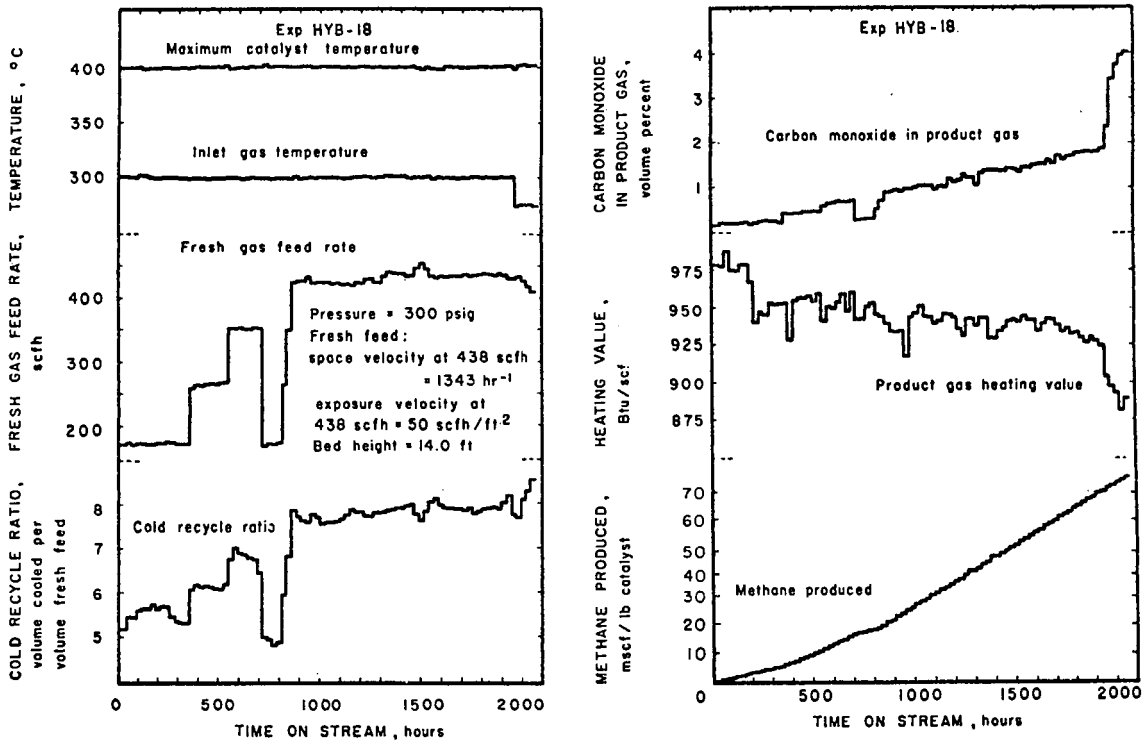

Figure 5. - Reactor conditions and product gas characteristics for Run HYB-18.

still rather acceptable at 98 percent. Due to greater catalyst stability, methane production was much higher for Run HYB-18 with a total of 75.2 mscf per pound of catalyst. Data pertinent to Run HYB-18 are illustrated in figure 5.

Typical stream flowrates and compositions are listed in table 2 for experiment HYB-18. These are data averaged over a 24 hour period and representative of the operating conditions during each of the exposure velocities investigated (20, 30, 40 and 50 scfh/ft^2). The last period represents the reactor operation with a Dowtherm temperature of 275° C. It should be noted that, at this temperature, CO conversion decreased significantly, and as a direct result, the heating value of the product gas decreased to 898.1 Btu/scf.

Run HYB-19: Recent experiments performed on bench-scale methanation reactors using plasma sprayed Raney nickel catalyst indicated that catalyst coatings prepared in this manner demonstrated a longer life. In an effort to test these findings in a larger scale reactor, an x-shaped substrate, identical to that used in runs HYB-17 and HYB-18 was plasma sprayed with catalyst and operated under conditions similar to those used in the previous two runs. Deactivation of the catalyst was rather rapid, with the experiment lasting only 1100 hours. Final CO conversion declined to 97.3 percent with 2.35 percent CO in the product gas. Methane production for this run was 36.6 mscf per pound of catalyst. Operating conditions for this run are shown in figure 6. One plausible explanation for the relatively poor performance of the catalyst in this experiment might lie in the leaching procedure. The activation time required for 70% aluminum leaching was much shorter, 4.6 hours compared to 18 hours in Run HYB-18. It was discovered that the NaOH solution was inadequately mixed resulting in an initial caustic concentration higher than the usual 2 percent.

Run HYB-20: This experiment was, essentially, a duplication of Run HYB-19. Operating parameters and product gas characteristics are given in figure 7. Methane production for this plasma sprayed catalyst was significantly better than HYB-19 with a total of 75 mscf per pound of catalyst. Final CO conversion stood at 97 percent with 2.55 percent CO in the product gas. The reactor was on stream for a total of 2081 hours. As indicated in figure 7, the Dowtherm temperature was increased to 325° C during the last portion of this run. Correspondingly, the maximum catalyst temperature was allowed to increase to 425° C. The increase in catalyst temperature was accompanied by a decrease in the quantity of recycled product gas required. Contrary to what might be expected, however, an increase in catalyst temperature did not significantly improve CO conversion. The conversion remained about the same, at 97.7 percent.

HYB-21: A fifth hybrid test has just been initiated. Preliminary results of this run are given in figure 8. The catalyst bed in this run differs from the previous four in that cast Raney nickel inserts were used rather than a thermally spray coated stainless steel insert. The castings were made of 42-58 percent Ni-Al alloy; each being six inches long and having 8 fins. The castings were formed with a hole along the axis to accomodate a thermocouple well to measure catalyst temperature. The catalyst surface was activated to a depth of .05 inches and operated under conditions similar to those for Run HYB-20. The data shown in figure 8 for the first 384 hours on stream indicate greater initial CO conversion and no detectable catalyst deactivation.

At the termination of each run, samples of spent Raney nickel catalyst were removed from the catalyst insert and subjected to wet chemical analysis, x-ray diffraction, BET surface and pore size distribution analysis. Two catalysts, one flame sprayed Raney nickel and one plasma sprayed Raney nickel, were measured for nickel surface area. Table 3 summarizes the results from chemical analysis and x-ray diffraction of the samples taken from the four runs. An appreciable carbon

Table 2. - Experiment HYB-18, Selected Test Data

Time on Stream.....hr	335	527	695	1640	2000
Temperatures					
Dowtherm.....°C	300	300.	300.	300.	275.
Gas Inlet.....°C	300.	300.	300.	300.	276.
Maximum Catalyst.....°C	400.	400.	400.	400.	401.
Pressure.....psig	300.	300.	300.	300.	300.
Feed Gas					
Rate.....scfh	175.	269.5	354.1	433.6	433.7
H_2.....vol pct	75.5	76.1	74.6	75.9	75.9
CO..... "	23.8	3.0	23.6	23.7	23.4
CO_2..... "	.3	.3	.1	.2	.2
N_2..... "	.2	.4	1.5	.1	.4
CH_4..... "	.2	.2	.2	.1	.1
H_2O..... "	.0	.0	.0	.0	.0
Exposure Velocity.....scfh/ft^2	20.	30.8	40.5	49.6	49.6
Space Velocity.....hr^{-1}	673.	1036.5	1361.9	1667.7	1668.1
Mixed Feed Gas					
Rate.....scfh	1112.2	1912.4	2748.4	3870.1	3779.1
H_2.....vol pct	17.9	16.0	16.1	14.5	19.4
CO..... "	3.9	3.7	3.7	4.0	5.1
CO_2..... "	0.2	.2	.2	.7	.5
N_2..... "	0.7	.8	.7	1.2	.3
CH_4..... "	77.2	79.2	79.2	79.5	74.0
H_2O..... "	.1	.1	.1	.1	.1
Inlet Velocity.....ft/sec	1.4	2.5	3.6	5.0	4.7
Inlet Reynold's No..... "	3357.	5885.	8465.	12042.	11548.
Exposure Velocity.....scfh/ft^2	127.1	218.6	314.1	442.3	431.9
Space Velocity.....hr^{-1}	4278.	7355.	10571.	14885.	14535.
Volume Recycle/Volume Fresh Gas	5.4	6.1	6.8	7.9	7.7
Product Gas					
Rate..... scfh	40.9	64.4	88.4	105.9	112.1
H_2.....vol pct	6.8	6.0	7.2	6.6	11.6
CO..... "	.2	.5	.7	1.5	3.3
CO_2..... "	.1	.2	.2	.7	.6
N_2..... "	.8	.9	.6	1.2	.3
CH_4..... "	87.9	89.2	87.9	87.1	81.3
H_2O..... "	4.2	3.2	3.4	2.9	2.9
Conversion					
CO..... pct	99.7	99.5	99.2	98.4	96.2
H_2..... pct	97.7	98.0	97.4	97.8	95.9
Heating Value.....Btu/scf	953.7	955.6	948.4	935.1	898.1
Carbon Recovery..... pct	91.6	98.3	98.8	93.5	95.6
Hydrogen Recovery..... pct	92.2	89.1	97.2	90.0	90.7
Oxygen Recovery..... pct	98.9	89.1	103.3	99.1	100.4

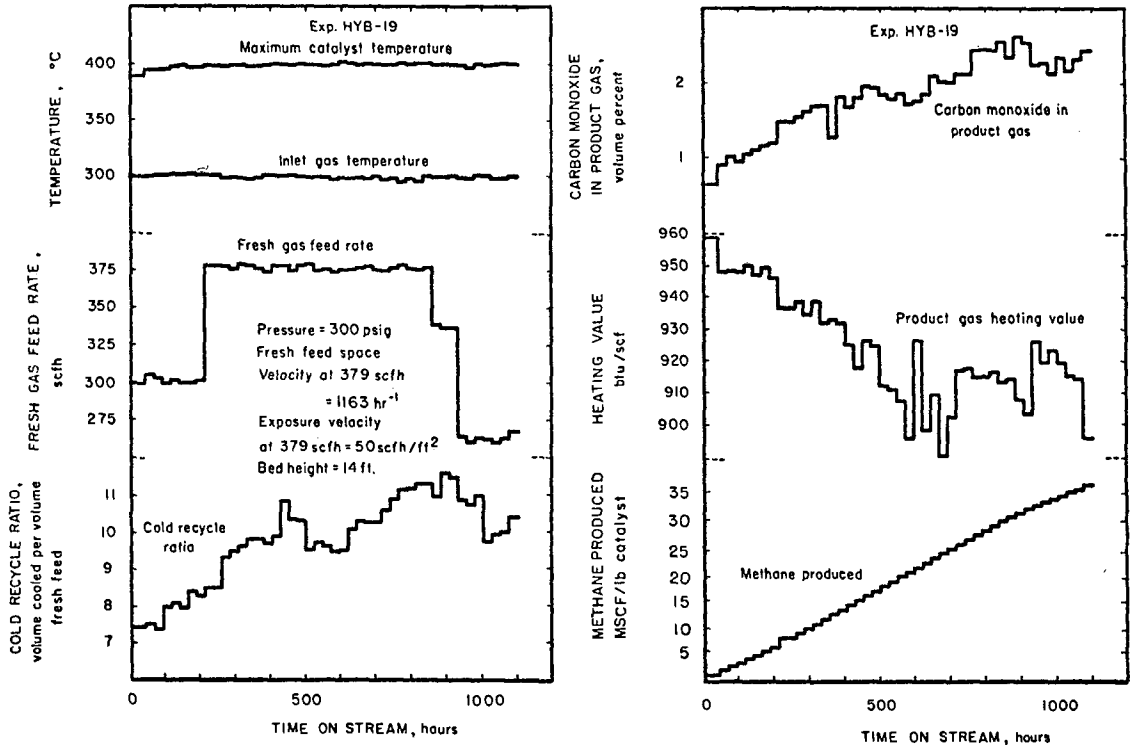

Figure 6. - Reactor conditions and product gas characteristics for Run HYB-19.

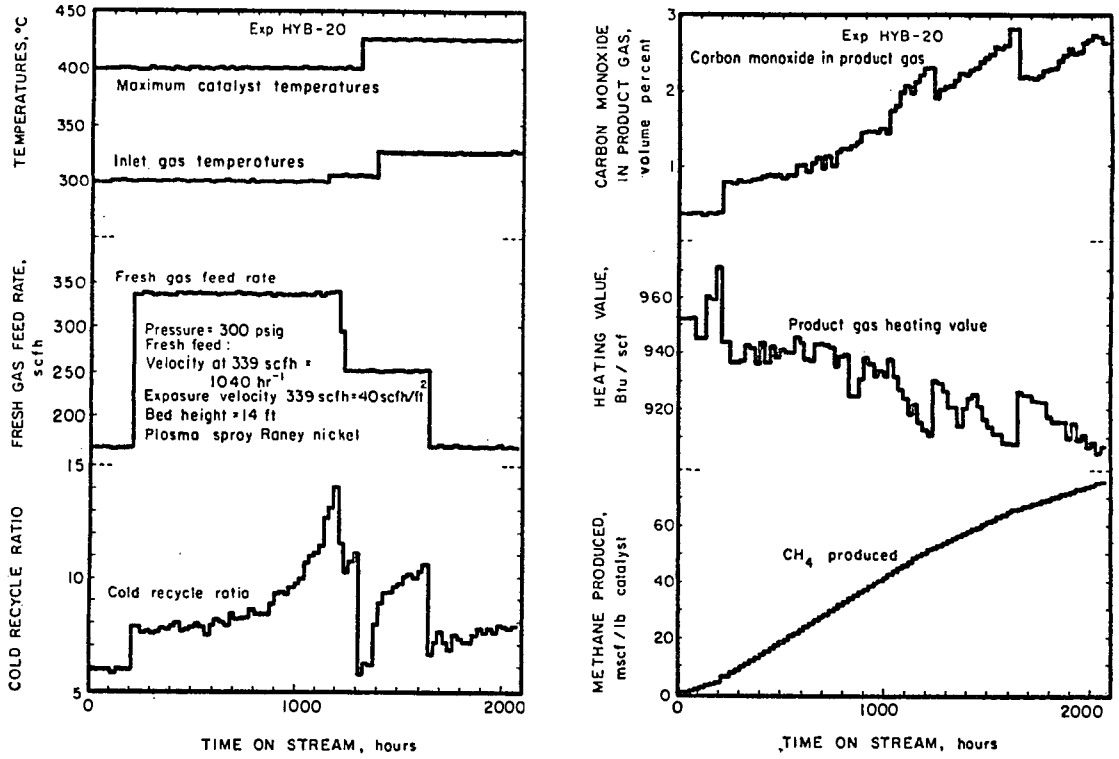

Figure 7. - Reactor conditions and product gas characteristics for Run HYB-20.

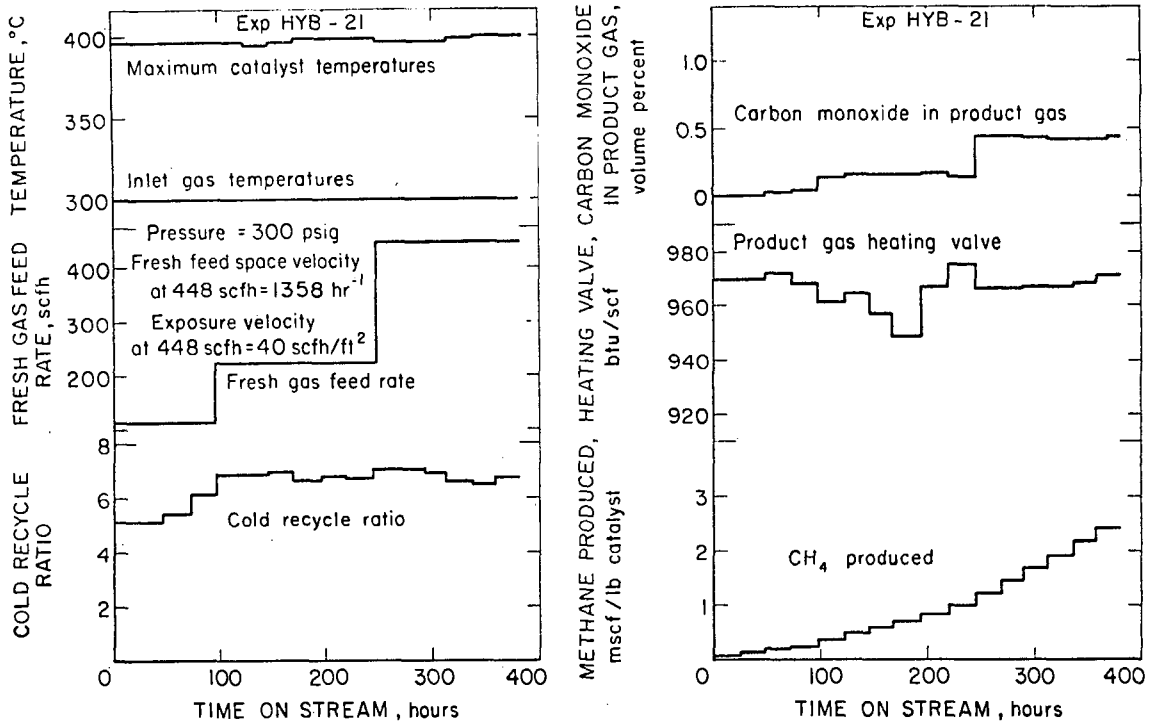

Figure 8. - Reactor condition and product gas characteristics for Run HYB-21.

Table 3. - Analysis of Spent Catalysts

	Ni	Al	C	S	Fe	Na	Species
HYB-17							
Inlet	68.1	8.6	4.68	-	0.27	0.08	Ni_3C
Center	74.6	8.8	1.71	-	0.24	0.08	Ni_3C, Ni
Outlet	72.3	9.0	0.20	-	0.25	0.08	Ni
HYB-18							
Inlet	64.1	10.4	2.0	0.3	0.5	4.5	Ni_3C
Center	68.0	11.7	0.7	0.2	0.4	4.9	Ni_3C
Outlet	69.0	11.6	0.5	0.3	0.7	6.5	Ni
HYB-19							
Inlet	75.7	8.6	3.0	0.2	0.5	0.08	Ni, Ni_3C
Center	77.1	7.3	1.6	0.3	0.5	0.03	Ni
Outlet	75.7	6.6	1.1	0.2	0.4	0.03	Ni
HYB-20							
Inlet	76.5	8.8	3.4	0.1	0.3	<0.01	Ni_3C
Center	80.3	8.3	1.0	0.4	0.4	<0.01	Ni
Outlet	79.4	8.4	0.3	2.2	0.4	<0.01	Ni

profile along with nickel carbide is found in every case. Other contaminants such as S, Fe, and Na are not present in amounts significantly greater than those found in unactivated catalyst except for high sodium concentrations on Run HYB-18 catalyst. This probably is indicative of insufficient rinsing of the catalyst subsequent to the activation step. The high sulfur concentration measured at the exit of HYB-20 is unexplained. Possibly sampling and/or analysis errors are involved. Analysis of this sample is being repeated. Iron contamination had been a problem in experiments prior to the hybrid reactor tests. Iron carbonyl can form by reaction of CO at high pressure and low temperature (100° - 200° C) with carbon steel piping. The carbonyl is carried into the hot reactor where it thermally decomposes according to the reaction:

$$2Fe\ (CO)_5 \rightarrow 5C + 2Fe + 5CO_2$$

and deposits on the nickel catalyst creating an iron catalyst. At methanation temperatures, carbon deposition occurs on the iron and further fouls the catalyst. Iron concentrations as high as 22 percent in the catalyst at the reactor inlet had been detected in previous runs. This was accompanied by high carbon content. Before initiating the hybrid reactor experiments, all carbon steel piping in the pilot plant was replaced with stainless steel. Examination of the iron concentrations found on the spent catalyst samples from the hybrid runs in table 3 indicates that this was successful in alleviating the iron contamination problem. The BET surface areas, pore volumes and pore radii are shown in table 4. Measured BET surface area for HYB-17 and HYB-20 appear to be somewhat smaller than those for the other runs. No other trends in the data were clearly evident. Also shown on table 4 are the nickel metal surface area measurements as determined by hydrogen chemisorption. Metal surface area measurements were performed on a flame-sprayed catalyst, Run HYB-18, and a plasma sprayed catalyst, Run HYB-20. In both instances, metal surface area is lower at the reactor exit than at the inlet while in general, being lower for HYB-20 than for HYB-18. There is no immediate explanation for these trends in the data. Nickel metal surface area for freshly activated catalyst is in the neighborhood of 12 m^2/gm. The tentative conclusion regarding the cause for catalyst deactivation for this series of experiments, in view of the limited amount of data available, is the formation of nickel carbide and possibly additional carbon formation on the catalyst surface. It was not possible to distinguish free carbon from carbidic carbon.

Table 4. - Surface Areas Of Spent Catalysts

	Surface Area m^2/gm	Pore Volume cm^3/gm	Avg. Pore Radius A	Nickel Surface Area m^2/gm
HYB-17				
Inlet	30.5	.076	50.07	
Outlet	23.7	.055	46.07	
HYB-18				
Inlet	53.4	.053	45.05	6.0
Outlet	50.2	.060	53.51	4.5
HYB-19				
Inlet	44.3	.095	42.8	
Outlet	32.8	.11	66.7	
HYB-20				
Inlet	32.77	.067	40.6	2.5
Outlet	23.73	.078	65.7	<1.0

MATHEMATICAL MODELING

Several recent publications (7, 8, 9, 10, 11) have discussed a one-dimensional mathematical model along with several applications of the model to tube-wall and parallel-plate, adiabatic (hot-gas-recycle) methanation reactors. Incorporated in the model was a postulated poisoning mechanism which obeyed an irreversible Langmuir-Hinschelwood type of rate equation. This one-dimensional model has been appropriately modified to describe the chemical and physical processes occurring in the hybrid methanation reactor.

The kinetic rate expression for the conversion of carbon monoxide to methane according to the reaction

$$CO + 3H_2 \rightarrow CH_4 + H_2O,$$

is taken to be that proposed by A. L. Lee (12, 13) which provides a reasonable fit to data reported by IGT. Lee's rate expression, developed from data for supported commercial nickel catalysts is of the form,

$$-r_{CO} = \frac{A\, e^{(-E/RT_C)}\, \tilde{C}_{CO}\, \tilde{C}_{H_2}^{1/2}}{1 + k_1 \tilde{C}_{H_2} + k_2 C_{CH_4}} \qquad 1)$$

Since the catalyst is deposited in a very thin layer, the catalyst thickness is neglected in the model and is considered to be only an active superficial surface. The kinetic rate is expressed as the number of moles of CO converted per unit time per unit superficial surface area of catalyst. The symbols, $\tilde{C}$, signify that these are concentrations at the surface of the catalyst as opposed to concentrations in the bulk stream. It should be noted that the concentration of methane at the catalyst surface is assumed to be the same as the bulk methane concentration. Due to the relatively large quantity of product gas that is recycled through the catalyst bed, methane is the major constituent in the gas at every point in the reactor. The assumption is made that negligible error is introduced by ignoring the methane concentration gradient between the bulk gas and the catalyst surface.

The construct envisioned for the description of the processes occurring in the hybrid reactor is the following. The reacting gas, flowing through a conduit in turbulent flow, is considered to be thoroughly mixed in the radial direction, i.e., there are no thermal or concentration gradients across the turbulent core (see figure 9). The reactants (CO and H_2) are transported across the laminar sublayer, adsorbed, react to form methane and water, and the products diffuse back into the turbulent core. There will be thermal and concentration gradients across the laminar film, the magnitudes of which depend upon the extent of diffusion control. Energy released in the methanation reaction is removed from the catalyst by convective heat transfer to the cooler bulk gas and thence to the cooling jacket and by radiation from the catalyst to the cooling jacket. A portion of the heat of reaction is also removed as sensible heat to the gas.

At steady state conditions there is no net change in reactant concentrations at the catalyst surface, thus, the rate of reaction must equal the rate at which CO and H_2 diffuse to the surface. The mass transfer rates are given by,

$$-r_{CO} = k_C (C_{CO} - \tilde{C}_{CO}) = j_{CO} \qquad 2\text{-a)}$$

$$-r_{H_2} = -3r_{CO} = k'_C (C_{H_2} - \tilde{C}_{H_2}) = j_{H_2} \qquad 2\text{-b)}$$

where k_C and k'_C are the film mass transfer coefficients for CO and H_2 respectively. The mass transfer coefficients are calculated, for a given Reynold's number, from the standard j-factor correlation (14, 15).

The following equations are taken to describe the heat transfer in the system.

$q = r_{CO} \mathcal{H}$ rate of heat generated by reaction 3-a)

$q_1 = h(T_C - T_G)$ heat flux between catalyst and turbulent core 3-b)

$q_2 = k\varepsilon (T_C^4 - T_W^4)$ radiation heat flux between catalyst and cooling jacket 3-c)

$q_3 = h' (T_C - T_W)$ heat flux by conduction through direct contact of insert with cooling wall 3-d)

$q_4 = h (T_G - T_W)$ heat flux between turbulent core and cooling wall 3-e)

$C_P M \frac{\partial T_G}{\partial a} \delta a = q_1 \delta a - q_4 \delta a'$ rate change of sensible heat of the gas 3-f)

In addition, we have the equation for the conservation of energy,

$$q = q_1 + q_2 + q_3. \qquad 3\text{-g)}$$

In order to calculate the global rate of reaction at any point in the reactor, equations 1), 2), and 3) must be solved simultaneously. The method of finite differences is utilized to calculate local bulk concentrations and temperatures throughout the length of the reactor. The model used to describe catalyst deactivation in previous experiments has been reported elsewhere (7, 8) and will not be reiterated. This deactivation mechanism was found to inadequately predict deactivation rates for the hybrid methanation reactor. It is possible that, due to system plumbing

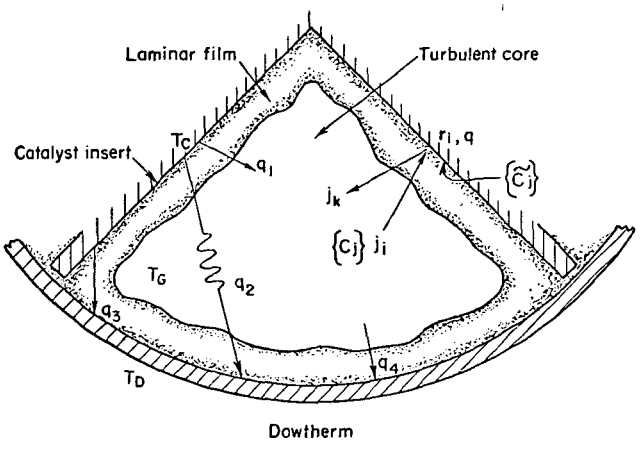

Figure 9. - Cross-section view of a quadrant of the reactor.

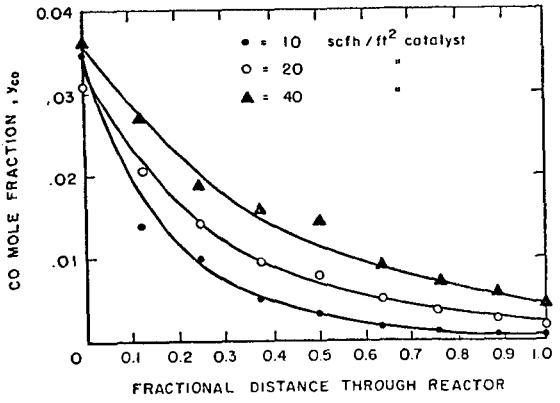

Figure 10. - Carbon monoxide mole fraction profiles for Run HYB-21. Solid lines indicate model predictions.

modifications, i.e. the substitution of carbon steel with stainless steel pipes, catalyst activation procedures, or the intrinsic difference in mode of reactor operation, the principal agent responsible for catalyst deactivation differs between the hybrid reactor and reactors previously operated. Nevertheless, the model is capable of satisfactorily predicting initial reactor performance. As an example, figures 10 and 11 illustrate the fit of the model to experimental composition and temperature profile data from Run HYB-21. Figure 10 is a plot of CO mole fraction as a function of distance through the reactor. Gas stream compositions were measured at 21 inch intervals through the reactor. The data represente operation at exposure velocities of 10, 20 and 40 scfh/ft^2 catalyst and wer taken early in the run before any deactivation of the catalyst was evident. The points indicate experimentally measured values whereas the solid lines represent the profiles calculated from the model. Agreement between model and experiment is seen to be quite good.

Temperature profiles for both catalyst and gas phase are illustrated in Figure 11. The three plots, once again, represent operation at 10, 20 and 40 scfh/ft^2 catalyst. The open circles are measured catalyst temperature while the ▲'s are gas phase temperatures. The temperatures predicted by the model (solid lines) are in good agreement with measured values. At the higher exposure velocities, the differences between model and measured values are, at most, 10-15° C. The percentages of the total heat liberated by the reaction which is transferred to the Dowtherm coolant are 86, 73 and 61% for the exposure velocities 10, 20, and 40 scfh/ft^2 catalyst, respectively.

SUMMARY

Four experiments were completed using the hybrid methanation reactor. A fifth experiment utilizing cast Raney nickel inserts has been initiated and preliminary results are encouraging. Each of the first four runs was terminated voluntarily with final CO conversions no less than 95-97 percent. The reactor was satisfactorily operated at an exposure velocity of 50 scfh/ft^2, comparable to those attainable in the tube-wall reactor, yet, as a result of the bed design, the catalyst can be easily replaced. The recycle ratio in a hot-gas-recycle methanator required to maintain a 100° C gas temperature difference across the catalyst bed is about 10/1. At comparable exposure velocities, the recycle ratio required to hold the catalyst temperature below 400° C in the hybrid reactor is as little as 5/1 - 6/1.

Although the hybrid reactor had a higher average productivity of methane per pound of catalyst than previous TWR and HGR experiments, it is possible that this is the result of decreasing the amount of iron carbonyl in the system rather than the nature of the reactor. Data, resulting from the four completed runs, do not indicate that plasma sprayed Raney nickel catalyst demonstrates a greater life at the pilot plant scale than flame sprayed Raney nickel. Data from the test using cast Raney nickel inserts are, of course, incomplete at the present time. Catalyst stability continues to be of prime concern in the research efforts at Pittsburgh Energy Research Center.

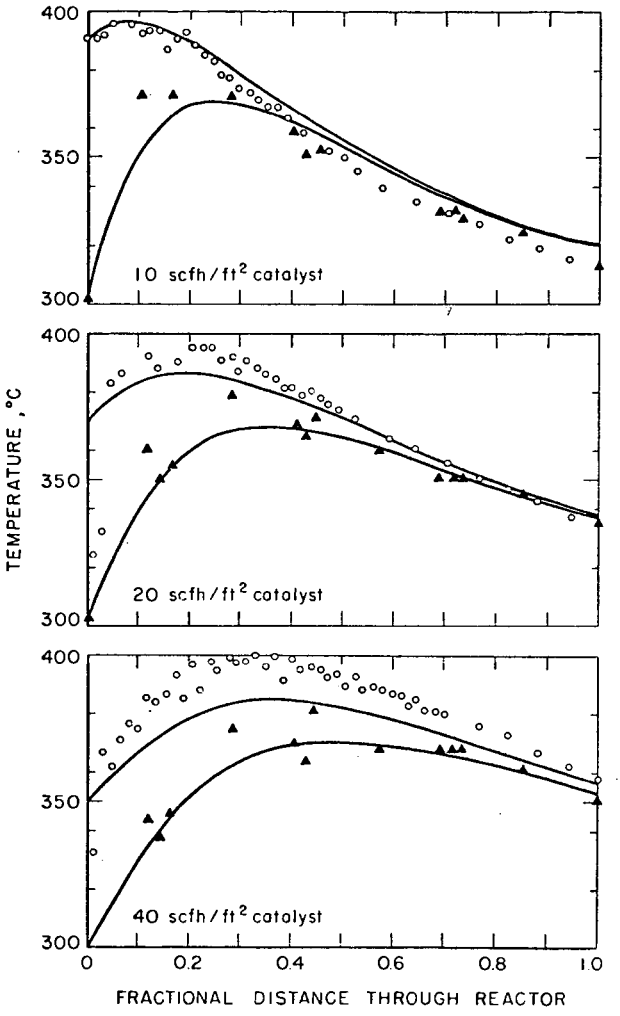

Figure 11. - Catalyst (O) and Gas (▲) temperature profiles for Run HYB-21. Solid lines indicate model predictions.

NOMENCLATURE

A= preexponential factor

C= concentration in bulk gas (lb mol/ft^3)

$\overset{s}{C}$= concentration at catalyst surface (lb mol./ft^3)

C_p= specific heat of gas (Btu/lb.mol. - °F)

E= activation energy (Btu/lb mol)

$\mathcal{H}$= heat of reaction (Btu/lb mol)

h= heat of transfer coefficient (Btu/hr-ft^2 - °F)

j= mass flux (lb. mol./hr-ft^2)

k= constant (Btu/hr-ft^2 - $°R^4$)

k_c= mass transfer coefficient (lb.mol./hr-ft^2-concentration difference)

k_1, k_2= equilibrium constant's

M= gas molar flowrate (lb.mol./hr)

q= rate of heat generated (Btu/hr-ft^2)

q_1= heat flux from catalyst to gas (Btu/hr-ft^2)

q_2= radiation heat flux between catalyst and cooling jacket (Btu/hr-ft^2)

q_3= heat flux by conduction through direct contact of insert with cooling wall (Btu/hr-ft^2)

q_4= heat flux from gas to cooling wall (Btu/hr-ft^2)

R= gas constant (Btu/lb.mol. - °R)

r= rate of reactant conversion (lb.mol./hr-ft^2 catalyst)

T= temperature (°R)

ε= emissivity (dimensionless)

δa= incremental catalyst surface area (ft^2)

δa'= incremental cooling wall surface area (ft^2)

REFERENCES

1. Grayson, M., Demeter, J.J., Schlesinger, M.D., Johnson, G.E., Jonakin, J., and Meyers, J.W., "Synthesis of Methane", BuMines RI-5137, July 1955, 32 pp.

2. Schlesinger, M.D., Demeter, J.J., Greyson, M., "Catalyst for Producing Methane From Hydrogen and Carbon Monoxide", Industrial and Engineering Chemistry, 48, pp. 68-70, 1956.

3. Forney, A. J., Demski, R. J., Bienstock, D., and J. H. Field, "Recent Catalyst Developments in the Hot-Gas-Recycle Process". BuMines RI-6609, 1965, 32 pp.

4. Demeter, J.J., Youngblood, A.J., Field, J.H., and Bienstock, D., "Synthesis of High-Btu Gas in a Raney Nickel Coated Tube-Wall Reactor", BuMines RI-7033, 1967, 17 pp.

5. Haynes, W.P., Elliott, J.J., and Forney, A.J. "Experience with Methanation in Catalysts", 163rd National Meeting of American Chemical Society, Boston, Mass. April 10-14, 1972, Vol. 16, No. 2 pp. 47-63.

6. Haynes, W.P., Forney, A.J., Elliott, J.J., Pennline, H.W., "Synthesis of Methane in Hot-Gas-Recycle Reactors Pilot Plant Tests", ACS Fuels Division Preprint, Sept., 8-13, 1974, Vol. 19, No. 3, pp 10-42.

7. Haynes, W.P., Schehl, R.R., Weber, J.K., and Forney A.J., "Pilot Plant Study of An Adiabatic Parallel Plate Methanation Reactor " Paper presented at the 68th annual meeting of the American Institute of Chemical Engineers, LosAngeles, Calif., Nov. 16-20, 1975.

8. Schehl, R.R., Haynes, W.P., and Forney, A.J., "Catalyst Deactivation in Hot-Gas-Recycle Methanation Reactors, A Mathematical Model," ERDA PERC/RI-75/3, 1975, 22 pp.

9. Schehl, R.R., Haynes, W.P., and Forney, A.J., "Calculating Catalyst Temperature in a Hot-Gas-Recycle Methanation Reactor", ERDA PERC/RI-75/1, 1975, 12 pp.

10. Ralston, T.D., Haynes, W.P., Forney, A.J. and Schehl, R.R., "Tube-Wall Methanation Reactors With Combined Diffusion and Kinetic Resistance", BuMines RI-7941, 1974, 15 pp.

11. Wei, V.T., and Chen, J., "Tube-Wall Methanation Scale-up for Bureau of Mines SYNTHANE Coal Gasification Process Prototype Plant", Presented at the Fourth Joint Chemical Engineering Conference, Vancouver, British Columbia, Canada, September 10, 1973.

12. Lee, A.L., "Methanation for Coal Gasification" Clean Fuel for Coal Symposium, Chicago, Illinois, September, 1973.

13. Lee, A.L., Feldkirchner, H.L. and Tajbl, D.J., "Methanation for Coal Hydrogasification" Symposium on Hydrogen Processing of Solid and Liquid Fuels, American Chemical Society, Chicago, Illinois, September 13-18, 1970, Vol. 14, No. 4, Part I, pp 126.

14. Treybal, R.E., Mass Transfer Operations McGraw-Hill Book., Co., Inc., New York, 1955, p. 55.

15. Welty, J.R., Wicks, C.E. and Wilson, R.E., Fundamentals of Momentum, Heat and Mass Transfer, John Wiley and Sons, Inc., New York, 1969, p. 580.

A HIGH-TEMPERATURE METHANATION CATALYST FOR SNG APPLICATIONS

COLIN WOODWARD

Imperial Chemical Industries Limited, Agricultural Division, Billingham, Cleveland, TS23 1LD, England.

INTRODUCTION

The political and economic background to the development of coal-based Substitute Natural Gas processes will be familiar to readers and, therefore, need not be detailed herein. The technical problem can be regarded very simply as having two parts, namely the gasification of coal followed by conversion of the product gas into SNG. Proven commercial processes, eg Koppers-Totzek, Lurgi, etc exist for coal gasification and several second generation processes are in various stages of development in the United States and elsewhere. The compositions of gases produced by these processes differ depending upon operating conditions ie pressure, temperature, steam addition, etc. In general, however, dry gas compositions are typically in the range:

CO_2	0 - 30%
CO	10 - 60%
H_2	25 - 75%
CH_4	0 - 20%

Alternative methods of upgrading such a gas to pipeline quality exist, the major problem being to combine the degree of, highly exothermic, methanation required with a low final exit temperature compatible with favourable thermodynamic equilibrium for methane formation. A process incorporating a high recycle ratio of product gas back through the methanator has been described (1) as a means of moderating the temperature rise in the methanator. A more elegant and economic solution, however, is a straight-through process using a series of methanators operating at successively lower exit temperatures (2,3). The viability of such a scheme depends upon the availability of a methanation catalyst, or catalysts, capable of operating under the design conditions for commercially acceptable periods. The purpose of the work described in this paper was to develop and demonstrate such a catalyst. This work comprised part of a collaborative agreement between ICI and Krupp-Koppers GmbH to develop processes for the production of SNG from coal based upon the Koppers-Totzek coal gasification process.

EXPERIMENTAL

Process Design

The basic philosophy during this programme was to take a "typical" gas composition, to subject it to the type of methanation process necessary to produce SNG and to evaluate the performance of various catalysts, commercially proven and experimental, in the duties involved. The gas composition selected appears in Table 1 (column 1) and will be seen to have $H_2 + CO = 74\%$ (dry basis). While not referring specifically to a particular gasification process, this is representative of the composition of gas to be methanated. In fact, the virtual absence of methane from the original gas increases the demand on the methanation section in comparison with processes in which the incoming gas already contains a significant proportion of methane.

Table 1 Gas Compositions and Temperatures in Methanation Process

Position	1	2	3	4	5	6
CO	31.14	14.47	14.47	4.29	4.29	0.34
CO_2	24.66	40.15	40.15	53.93	53.93	62.70
H_2	42.91	35.50	35.50	20.26	20.26	5.83
CH_4	0.08	8.52	8.52	19.84	19.84	29.13
N_2 + Ar	1.21	1.36	1.36	1.68	1.68	2.00
	100.00	100.00	100.00	100.00	100.00	100.00
H_2O	67.3	72.3	72.3	94.4	94.4	118.2
T°C	398	729	325	590	300	428

The process design studied is illustrated in Figure 1, the gas composition and temperature at each stage appearing in Table 1. Incoming gas is mixed with steam (67.3 vols : 100 vols dry gas) and preheated to approximately 400°C at the inlet to the first methanator. Operating pressure is 30 atas (425 psig). The gas leaves the methanator at an adiabatic equilibrium temperature of approximately 730°C, is cooled to 325°C by raising high pressure steam in a boiler and passes to the second methanator. Further methanation occurs and the gas leaves at the adiabatic equilibrium temperature of 590°C. It is again cooled, by raising steam, to 300°C and passes to the final "wet" methanator where it attains an adiabatic equilibrium temperature of about 430°C. At this stage, the gas has a methane content (dry basis) of approximately 29% (78% after CO_2 removal). Subsequent processing stages would include water removal, final "dry" methanation and CO_2 removal to produce the final SNG. Design constraints were incorporated on nickel carbonyl formation in the reactors, which defined the minimum inlet temperatures possible to the first two methanators, and on the amount of steam added which was used to control the maximum temperature in the first methanator below 750°C. Neither the latter, nor the inlet to the third methanator which was arbitrarily set at 300°C, has been rigorously optimised so some flexibility in these values exists.

Catalyst Evaluation

Our previous experience in development and use of catalysts for naphtha- and methane-steam reforming as well as for methanation processes meant that, at the outset of this work, we had "on the shelf" a number of catalysts expected to have activity for the reactions of interest. A laboratory screening test was therefore set up, operating at atmospheric pressure, by which the initial activity of these catalysts could be evaluated rapidly under appropriate conditions of temperature and gas composition. This permitted selection of catalysts for further testing in semi-technical reactors operating under simulated process conditions. Previous experience suggested that provision of a catalyst suitable for the third methanator would present no difficulty so attention was concentrated on the preceding two. In general, steam reforming catalysts were found to lose their low temperature activity relatively rapidly while commercial methanation catalysts were unstable at high temperatures (>600°C). However, with experimental preparations it was soon found that low temperature activity was no problem. This allowed evaluations to be performed under first methanator conditions, with the expectation that comparative results would also be valid under second methanator conditions. Numerous catalyst lifetests, of durations varying between one and seventy days, were carried out under these conditions.

In summary, the outcome of the first phase of the catalyst evaluation and development programme was the production of a new high-nickel, co-precipitated formulation (NiO approx 60% loss free) which appeared to have the necessary activity, stability and physical strength for the applications envisaged. When a preferred catalyst formulation had been selected, its preparation was scaled up from the laboratory to a pilot plant located at our catalyst manufacturing site in Clitheroe, Lancashire. This unit is a reduced-scale simulation of a commercial production unit and its use is an essential stage in the development of a procedure for manufacture of a commercial catalyst. Its normal batch size is 15-20 kg and the catalyst manufactured therein was used for all subsequent testing. To demonstrate its properties, three semi-technical reactors were linked in series to permit a long lifetest with the catalyst operating under the conditions of the three methanators.

In common with other nickel-based catalysts, this formulation is susceptible to poisoning by sulphur compounds in the process gas stream. The extent of this was therefore minimised by incorporation of a vessel of desulphurisation catalyst (zinc oxide, ICI catalyst 32-4), upstream of the point of steam addition, running with maximum temperature 250-300°C. By this means, the sulphur level in the process gas was reduced below 0.1 mg S/Nm^3 (dry basis), see below.

The semi-technical reactors used were fabricated from 18/8 Ti stainless steel tube, nominal 1 inch id, overall length 30 ins. The catalyst bed, 12 ins deep, was arranged centrally in the reactor which was also fitted with an internal thermocouple sheath containing six equally-spaced thermocouples positioned throughout the catalyst bed. The reactors were fitted with two external electrical heaters, the first to permit attainment of the selected bed inlet temperature and the second adiabatically controlled to compensate for heat losses. The whole assembly was then surrounded by several inches of inert insulation material. Figure 2 is a simplified illustration of one reactor assembly.

For the performance tests, each reactor was loaded with an undiluted bed, volume 135 ml, of catalyst in the form of pellets diameter 5,4 mm, height 3.6 mm. This was reduced to the active form by passage of pure, dry hydrogen for several hours at 450-500°C and space velocity about 25,000 hr^{-1}. Because these reduction conditions were easily obtained in our equipment, no specific study was made of the reducibility of this catalyst although it has been shown that effectively complete reduction is obtained by passage of hydrogen for two hours at 300°C. After the reduction period, the inlet temperature of each reactor was adjusted to the design setting and the appropriate rate of water fed to the vaporiser upstream of the first methanator. After a few minutes, the hydrogen was replaced by pre-mixed process gas at a flow-rate corresponding to a dry gas space velocity of 10,000 hr^{-1} relative to the catalyst volume in the first methanator. Reduction in dry gas volume through the methanators made the effective (dry) space velocity through the second and third reactors 8865 hr^{-1} and 7160 hr^{-1} respectively. Methanatinn began immediately and steady state conditions in all three reactors were reached within a few hours. The tests were then allowed to run under constant conditions for a prolonged period, catalyst performance being monitored by regular measurement of the temperature profile in each catalyst bed. Outlet gas compositions, which corresponded to the equilibrium composition at each outlet temperature, were monitored by an on-line gas chromatograph.

Figures 3, 4 and 5 show the temperature profiles in each bed at the start of these tests and after continuous operation for the periods indicated. The test ran without significant disturbance for 1500 hrs at which time a plant failure caused an interruption to the water supply and consequently massive carbon deposition in all three reactors. After this upset, it proved impossible to restart the second and third methanators so these were discharged and the catalyst submitted to post-mortem examination. The first methanator was restarted although the temperature profile was found to be displaced substantially down the catalyst bed. Within a few days, however, it recovered to almost its original position (see Figure 3) and then remained stationary until 2200 hrs at

which time the test was terminated.

Post-mortem examination of the catalyst discharged from several levels in each bed revealed that it had mean nickel crystallite sizes in the ranges 750-1000Å, 270-400Å and 160-190Å for the first, second and third methanators respectively. Considering the duration and operating conditions of these tests, this crystallite growth, from an original size of about 100Å, demonstrated the inherent stability towards sintering of this catalyst formulation. Further, the excellent performance during the lifetests showed that this degree of sintering had had no detrimental effect on catalyst activity under the relevant operating conditions. The inference to be drawn is that, with a catalyst of high active metal content operating in a relatively high temperature range, some crystallite growth can be tolerated. The small amount of growth of the catalyst in the second methanator which had run up to 590°C was particularly noteworthy. The results reported were obtained before a full catalyst composition optimisation was carried out. Therefore, although it is not required for these duties, we would expect to be able to design a catalyst with greater resistance to sintering if necessary.

Discharged catalyst from the first two methanators was found to contain sulphur corresponding to an absorption of about 0.015 mg S/Nm^3 of gas passed in the first reactor followed by about 0.065 mg S/Nm^3 in the second, ie a total concentration of 0.08 mg/Nm^3 in the process gas inlet to the first reactor. This concentration caused no significant deactivation of the catalyst in the first bed and a deactivation rate of 1.0-1.5 inches per 1000 hrs in the second which, it is reasonable to postulate, would have been lower at a lower inlet sulphur level. This could have been obtained by optimising the desulphurisation catalyst operating conditions but, in view of the length of test which would have been required to demonstrate an improvement over the performance already observed, this was not felt to be a worthwhile exercise. It will be seen that the distribution of sulphur between the two beds was as would be expected for their inlet and outlet temperatures and the known fact that formation of nickel sulphide is thermodynamically favoured at low temperatures.

DISCUSSION

The catalyst lifetests described above have demonstrated that a formulation has been developed with the activity and stability needed to methanate a variety of process gases at temperatures up to 750°C. By proving the catalyst under simulated process conditions in tests of 2-3 months duration we have been able to show that its rate of deactivation is low enough to be commercially acceptable. Further, by testing under "typical" coal gas methanation conditions, we have acquired the confidence to predict that this catalyst will also perform satisfactorily under the variety of conditions encountered in different proposed coal gas methanation processes. The high temperature capability of this catalyst has the particular advantage of permitting the use of a straight-through methanation system without the need for recycle of product gas for temperature control.

The applicability of this catalyst to processes other than coal gas methanation should also be noted. For example, high temperature methanation steps may be used as sources of heat for steam generation. In such a system, methanatable gas is produced in an endothermic methane-steam reforming stage, piped to the site where the steam is to be generated, methanated, cooled in boilers and feed water heaters, then piped back to the steam reforming stage (4). To use such a process optimally, it is clearly necessary for the methanation catalyst to function over as large a temperature range as possible.

REFERENCES

1 K.H. Eisenlohr, F.W. Moeller and M. Dry in "Methanation of Synthesis Gas," Advances in Chemistry Series 146, 1975, p 113.

2 J.E. Franzen and E.K. Goeke, paper presented at Sixth Synthetic Pipeline Gas Symposium, Chicago, Illinois, October 1974.

3 G.A. White, T.R. Roszkowski and D.W. Stanbridge in "Methanation of Synthesis Gas," Advances in Chemistry Series 146, 1975, p 138.

4 General Electric Co., U.S. patent application no 484802, German OLS 2528660.

FIGURE 1. METHANATION PROCESS

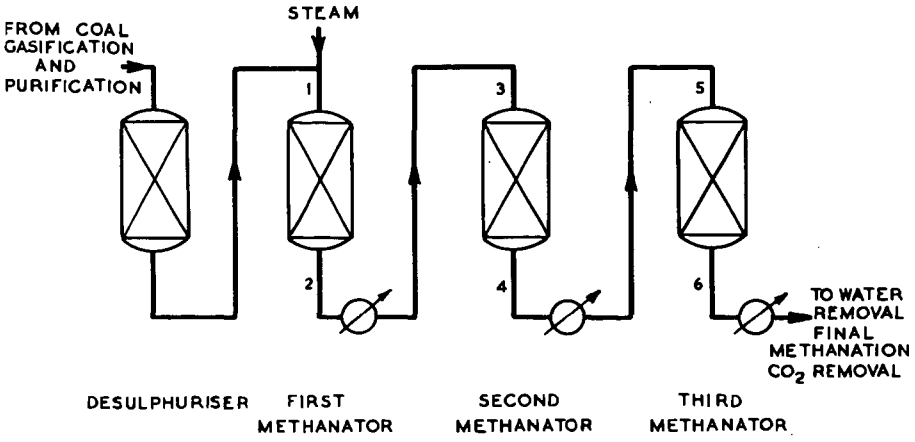

FIGURE 2. METHANATION SEMI-TECHNICAL PLANT REACTOR ARRANGEMENT (SIMPLIFIED)

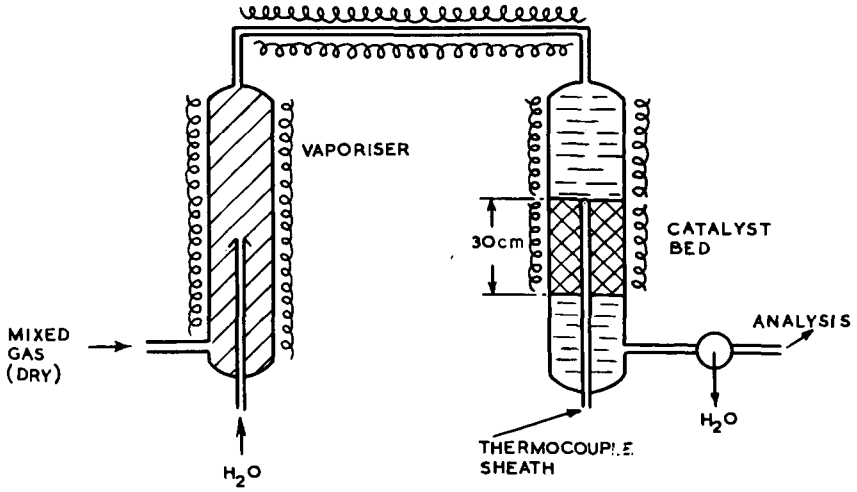

FIGURE 3. FIRST METHANATOR TEMPERATURE PROFILE

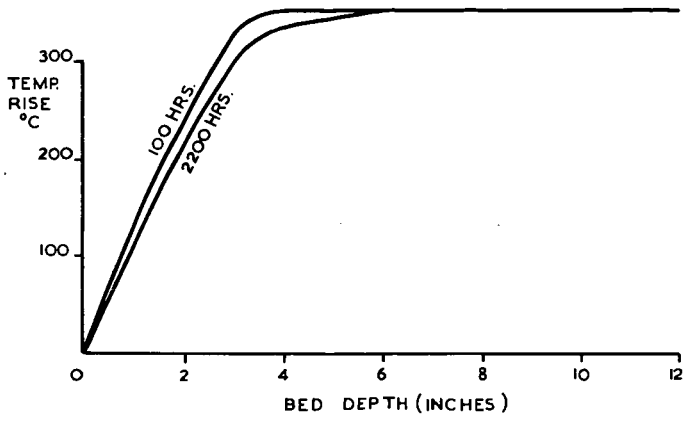

FIGURE 4. SECOND METHANATOR TEMPERATURE PROFILE

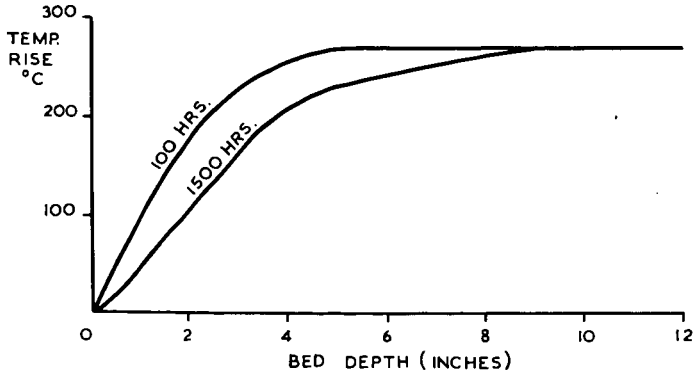

FIGURE 5. THIRD METHANATOR TEMPERATURE PROFILE

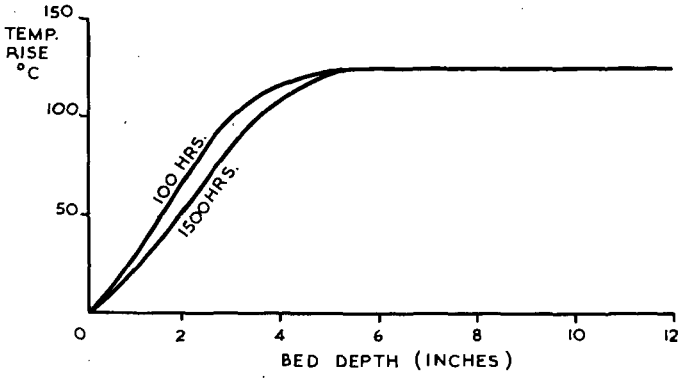

METHANATION ACTIVITY OF SUPPORTED NICKEL ALLOYS

Calvin H. Bartholomew and W. Blaine Barton

Brigham Young University
Department of Chemical Engineering
Provo, Utah 84602

INTRODUCTION

Natural gas is a highly desirable fuel because of its high heating value and nonpolluting combustion products. In view of the expanding demand for and depletion of domestic supplies of clean fuels, economical production of synthetic natural gas (SNG) from coal ranks high on the list of national priorities.

Presently there are several gasification processes under development directed toward the production of methane or SNG. Although catalytic methanation of coal synthesis gas is an important cost item in the process, basic technological and design principles for this step are not well advanced. Extensive research and development are needed before the process can realize economical, reliable operation. Specifically, there appears to be important economic advantages in the development of more efficient, stable catalysts.

Extensive general reviews of pertinent literature dealing with methanation catalysts and kinetics have been provided by Greyson (1) and Mills and Steffgen (2). However, only recently, were kinetic studies of selected Group VIII metals (Fe, Ni, Co, Ru, Rh, Pt, Pd, Ir) reported by Vannice (3,4) and of nickel and ruthenium catalysts by Dalla Betta et al. (5,6) for which the kinetic data were clearly determined under conditions free of heat and mass transfer (diffusional) influences and for which specific rates were based upon active catalytic surface areas.

There is very little mention in previous literature in regard to alloy catalysts for methanation, and no previous kinetic data have been reported for alloy systems. This paper discusses recently determined methanation activity data determined for alumina-supported alloys of nickel with ruthenium, rhodium, molybdenum oxide, iron, cobalt, platinum, palladium and copper. These data were determined under conditions such that effects of heat and mass transfer were minimized and specific rates are reported at 1 atm and 225 and 250°C, based upon active catalytic surface areas.

EXPERIMENTAL

Materials

Analytically pure metal salts (e.g. Baker Analyzed $Ni(NO_3)_2 \cdot 6H_2O$) and Kaiser SAS 5x8 mesh alumina (301 m^2/g) were used in preparation of the supported nickel alloy catalysts. Samples were prepared by simple co-impregnation to incipient wetness of the support with aqueous metal salt solutions followed by oven drying at 80-100°C for 24 hours. The impregnated, dried samples were reduced in flowing hydrogen at 1000-2000 GHSV while heating at less than 5°C/min to 450-500°C with a one hour temperature hold at 230°C and 10-16 hours at 450-500°C. Samples reduced in a separate reduction system were carefully passivated with 1% air in nitrogen before transferring to the reactor.

Hydrogen and nitrogen gases (99.99%) were purified by simultaneously passing both through a palladium Deoxo purifier (Engelhard) and dehydrated molecular sieve or liquid nitrogen trap. Carbon monoxide (Matheson Purity, 99.99%) was used without further purification.

Apparatus and Procedure

Metal surface areas were determined by means of hydrogen chemisorption at 25°C (Ni-Pd at 130°C) using a conventional volumetric apparatus capable of 10^{-6} Torr. Hydrogen adsorption uptakes were determined as a function of pressure and the isotherm was extrapolated to obtain the adsorption at zero pressure. It was assumed that exactly one hydrogen atom adsorbed on each surface metal atom, and site densities were calculated based on the three lowest index planes of each metal (except in the case of Ni-MoO_3 where hydrogen was found to adsorb only on the nickel sites). The surface composition of each alloy was assumed to be the same as the nominal metal composition. Compositions and metal surface areas for catalysts prepared and tested in this study are listed in Table 1.

Methanation activities were measured using a laboratory, single-pass differential flow reactor equipped with Matheson flow meters and pressure regulators, a Hewlett-Packard 7132 temperature recorder, and a Hewlett-Packard 5830 gas chromatograph. A schematic of the reactor system is shown in Figure 1. The stainless steel reactor contained a catalyst chamber of $35cm^3$ with adjustable thermocouples installed at each end of the chamber.

Differential activity measurements were carried out at low conversions with 2-4 grams of previously reduced (and passivated) catalyst in the reactor (the remainder of the bed was filled with pure Al_2O_3 pellets) in order to minimize the influence of heat and mass transfer. The sample was heated in flowing H_2 (approximately 500 cm^3/min) to 450°C and held for two hours at that temperature, then allowed to cool in flowing H_2 to about 225°C. Reactant gases (1% CO, 4% H_2 and 95% N_2) were next allowed to flow through the reactor at a space velocity of 30,000 or 60,000 hr^{-1} for 30 minutes during which time the reactor temperature was stabilized at 225, 250, or 275°C. Reactor pressure was usually about 5-8 psig. Three chromatographic samples of the product gas were obtained after which three additional chromatographic samples were taken to determine unconverted reactant gas concentrations. All important experimental conditions such as temperature and pressure were recorded at the time each chromatographic sample was taken.

RESULTS AND DISCUSSION

Methanation activity data in the form of percent CO conversion, CH_4 production, and specific rates are listed for nickel and nickel alloy catalysts in Tables 2-4 (225°C, GHSV = 30,000 and 60,000 hr^{-1} and 250°C, GHSV = 60,000 hr^{-1}) and the specific rates are shown schematically in Figures 2 and 3 for 250°C and GHSV = 30,000 hr^{-1}. For catalysts with low metal loadings, low conversions were obtained. For example, at 250°C (Table 4) conversions for the 3 wt.% catalysts (Ni-A-112, Ni-Ru, Ni-Rh, and Ni-MoO_3) range from 4 to 14% depending upon the space velocity, whereas conversions for the 15 to 20 wt.% catalysts (all other catalysts) range from 11 to 43%. At 225°C the conversion ranges are 4 to 7% and 6 to 35% for low and high metal loadings respectively. Thus, truly differential (low conversion) conditions can be approached at 225°C for the 3% catalysts but not for the 15-20 wt.% catalysts. Apparently then, for our reactor system and for typical methanation catalysts, truly chemically-limited rate data can only be obtained for catalysts with a low metal loading (3-5 wt.%). Accordingly it would be desirable in obtaining very accurate kinetic rate data to prepare all of the catalysts with metal loadings in the 3-5% range. Nevertheless, for purposes of screening, the data obtained at moderate conversions are adequate for comparative purposes.and satisify the objectives of this study.

The turnover numbers (N_{CO} and N_{CH_4}) shown in Tables 2-4 and Figure 3 indicate approximately the same order of magnitude activity for Ni, Ni-Ru, and Ni-Rh catalysts. Our turnover numbers agree well with the initial rates reported by Dalla Betta et al. (5) and Vannice (3) for 0.5% Ru/Al_2O_3 and 5% Ni/Al_2O_3. It

appears that a small uncertainty (1-5%) in our results may be attributed to small variations in gas concentrations, pressure and flow rates over the test period of a given catalyst. The measurement of both activity and selectivity also includes uncertainties of 1-5% in calibration and measurement of gas concentrations. Thus, it may be possible that selectivities for CH_4 are slightly higher than indicated, although there is undoubtedly significant hydrocarbon and CO_2 production (3, 5).

Dalla Betta et al. (6) have indicated that their steady-state rates for methanation (after a 24-hour exposure to a reaction mixture) are 25 times lower than their initial rates (5). Thus, exposure to a reaction mixture over a period of hours or even minutes may significantly reduce the activity of the catalyst. This may explain why the turnover numbers reported in this study which were measured after exposure for 1/2 to 4 hours under reaction conditions are significantly lower than initial rates reported in the literature for 5% Ni/ZrO_2 (5) and 5% Ru/Al_2O_3 (3). The discrepancy between initial rates measured by Dalla Betta (5) and Vannice (3) for nickel and ruthenium catalysts might be similarly explained by differences in their pretreatment of the catalyst. Also, Vannice based his turnover numbers on CO adsorption data, which in fact may explain differences of 100-400% between his data and ours or those of Dalla Betta.

Vannice (3) has reported selectivities for the methanation reaction over the group VIII metals to be in the following decreasing order: Pd>Pt>Ir>Ni>Rh>Co>Fe>Ru. This order correlates well with measured selectivities for alloys of these same metals with nickel as shown in Tables 2-4. Of special interest is Ni-Pt-A-100 which shows the highest selectivity, 99% at 250°C and higher temperatures. Changes in space velocity and temperature have appreciable effects on the selectivity as can be seen for example in the data for Ni-A-112, Ni-Pd-A-100 and Ni-Ru-A-105. Generally the selectivity increases with increasing temperature for a given space velocity and with increasing space velocity for a given temperature.

Figures 2 and 3 illustrate the magnitude of the rates per gram of catalyst, the turnover numbers, and selectivities at 250°C and a space velocity of 30,000 hr^{-1}. Nominal compositions and hydrogen uptakes used to calculate turnover numbers are listed in Table 1. It should be observed that the active metal loadings which vary significantly between catalysts have an obviously marked effect on the activity of the catalyst per unit catalyst weight as can be seen in Figure 2 where the listed order corresponds to the order of wt.% active metal. A comparison of these rates with the hydrogen uptake data shows that the rate is strongly influenced by the available surface area. For example, Ni-A-116 (14 wt.% Nickel) is more active (per unit mass) than G-87 (32 wt.% nickel) mainly because the surface area of the former catalyst is larger.

Turnover numbers for 250°C and a space velocity of 30,000 hr^{-1} are shown in decreasing order of activity in Figure 3. Ni-MoO_3-A-101, Ni-A-112 (3% nickel) and Ni-Co-A-100 are the most active and G-87 the least active. The details of these results are discussed below for each catalyst.

Ni-MoO_3-A-101 has a relatively low active surface area. Thus, its rate per unit weight is among the lowest tested. However, its turnover number is the highest of any catalyst tested. Assuming a method to increase the active surface area can be found, this catalyst is a most promising candidate for further study.

Ni-Ru-A-105 and Ni-Rh-A-100 behave typically as nickel catalysts showing comparatively little effects of alloying although both are slightly less active than Ni-A-112, a nickel catalyst of comparable weight loading. The Rh does cause some increased selectivity to methane but not as pronounced as for platinum. The data determined at 225°C (Table 2) show an unexpectedly low selectivity to methane for Ni-Rh. Thus, some of this work will be repeated.

Ni-Co-A-100 contains a high loading of metal with equal weight percents of nickel and cobalt. It is of special interest in that both the rate per unit weight and the turnover number are high. The selectivity of this catalyst for the methanation reaction (78% at 250°C and GHSV = 30,000) is the lowest of any nickel catalyst tested. Vannice (3) has reported cobalt to have a selectivity of 78% under similar reaction conditions and the selectivity for nickel to be 90% also in good agreement with our data. Thus, cobalt has a strong effect on the selectivity of the Ni-Co catalyst. Nevertheless, a recent test showed the same catalyst to have a 93.5% selectivity at 225°C and GHSV = 30,000 hr^{-1}. Since the selectivity should be lower at 225 than at 250°C, these data must be repeated.

Ni-Fe-A-100 was found to completely deactivate within two hours under normal reactor operating conditions. When the catalyst was removed from the reactor some of the beads showed a brown (rust) color as compared to the normal black. The observations suggest that the iron may scavange the oxygen from the CO to form various iron oxides and thus effectively poison the catalyst. It is also possible that the Ni-Fe catalysts was not completely reduced at the beginning of the test. Additional reactor tests are planned to investigate these possibilities.

Ni-Pd-A-100 was found to be less active than most of alloys tested thus far with a turnover number about the same as G-87. Ni-Pt-A-100 has rate characteristics which are not outstandingly different from the other catalysts. The selectivity, however, is significantly improved over nickel. Vannice (3) has shown platinum to be one of the most selective catalysts for methane--namely about 98% to CH_4. As an alloy with nickel in the amount of only one atomic percent platinum effects a 99% selectivity to methane.

Ni-A-116 is a high loading (15 wt.%) nickel catalyst used to compare against other catalysts containing 15-20 wt.% alloy. It has the highest rate per unit weight but has a turnover number the same as Ni-Pt-A-100 and somewhat lower than the cobalt alloy.

G-87 is a commercial nickel catalyst manufactured by Girdler Catalyst Corp. and is included as a comparison against other nickel catalysts. It is unique, however, from the other catalysts tested because it contains a different support of unknown composition which may influence the diffusional and mass transfer characteristics of the catalyst. Because of its high nickel loading (32 wt.%) it is expected that its rate per unit weight should be high. However, its turnover number is one of the lowest measured. This may be due in part to the effects of pore diffusion resistance at a relatively high conversion of CO.

Data on Ni-Cu-A-100 obtained at 250°C and a space velocity of 30,000 hr^{-1} show this to be the least active catalyst tested thus far with relatively low selectivity. No further work is expected to be done with this catalyst because of its low activity.

Apparent activation energies for some of the nickel-alloy catalysts are listed in Table 5. With the exceptions of Ni-MoO_3-A-101, Ni-Co-A-100, and Ni-Rh-A-100, the catalysts appear to have activation energies of 12-18 kcal/mole for both CO conversion and methane formation. Ni-Co-A-100 and Ni-Rh-A-100 have slightly higher values of 22.2 and 19.2 respectively. Ni-MoO_3-A-101 has a significantly higher value of 26 kcal/mole which is close to the value of 25 kcal/mole for nickel reported by Vannice (3). The far right column lists the activation energies for various metals as reported by Vannice and measured under kinetic limited (low conversion) conditions. Considerably lower activation energies for alloys compared to those of either alloy component very likely result at least in part from mass transfer (or diffusional) limitations. In addition, the variations are partly the result of alloy formation, the alloy having catalytic properties different from either of the pure metals.

CONCLUSIONS

1. Steady-state conversions of carbon monoxide at 225 and 250°C, 1 atm. (inlet composition of 1% CO, 4% H_2, 95% N_2) range from 3-43% for alumina-supported nickel alloy catalysts. Percent selectivities to methane range from 67-99%. Turnover numbers are not significantly different within experimental error for Ni-Rh, Ni-Ru, and Ni catalysts and compare favorably with initial rates reported for 5% Ni/Al_2O_3 and 0.5% Ru/Al_2O_3.

2. Steady-state conversion measured at 225 and 250°C, 1 atm and for space velocities of 30,000 and 60,000 hr^{-1} indicate that very nearly differential (low conversion) conditions obtain only for low (3-6 wt.%) metal loading catalysts. Screening data for 15-20 wt.% $metal/Al_2O_3$ catalysts are influenced by mass transfer or diffusional limitations.

3. $Ni-MoO_3/Al_2O_3$ is the most active catalyst on a per surface area basis. $Ni-Pt/Al_2O_3$ has the highest selectivity for methane production--namely 99% (250°C, 30,000 hr^{-1}). A 14 wt.% Ni/Al_2O_3 is the most active catalyst on a per mass basis--even more active than a commercial 32 wt.% Ni/Al_2O_3 simply because the 14% catalyst has a high nickel surface area.

REFERENCES

1. M. Greyson, "Methanation" in "Catalysis" Vol. IV, ed. P.H. Emmett, Rheinhold Pub. Corp., New York, 1956.

2. G.A. Mills and F.W. Steffgen, "Catalytic Methanation," Catalysis Reviews 8, 159 (1973).

3. M.A. Vannice, "The Catalytic Synthesis for Hydrocarbons from H_2/CO Mixtures over the Group VIII Metals," J. Catal, 37, 449 (1975).

4. M.A. Vannice, "The Catalytic Synthesis of Hydrocarbons from H_2/CO Mixtures over the Group VII Metals, III. Metal-Support Effects with Pt and Pd Catalysts," J. Catal. 40, 129 (1975).

5. R.A. Dalla Betta, A.G. Piken, and M. Shelef, "Heterogeneous Methanation: Initial Rate of CO Hydrogenation on Supported Ruthenium and Nickel," J. Catal, 35, 54 (1974).

6. R.A. Dalla Betta, A.G. Piken, and M. Shelef, "Heterogeneous Methanation: Steady State Rate of CO Hydrogenation on Supported Ruthenium, Nickel, and Ruthenium," J. Catal. 40, 173 (1975).

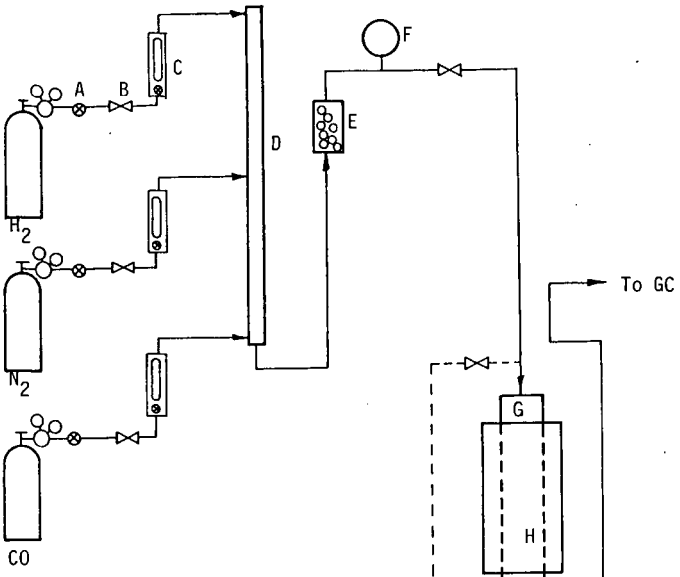

A. Pancake Regulator
B. Control Valve
C. Flowmeter
D. Manifold
E. Mixing Chamber
F. Pressure Gauge
G. Reactor
H. Furnace

Figure 1 Low Pressure Continuous Flow Reactor System for Methanation Studies

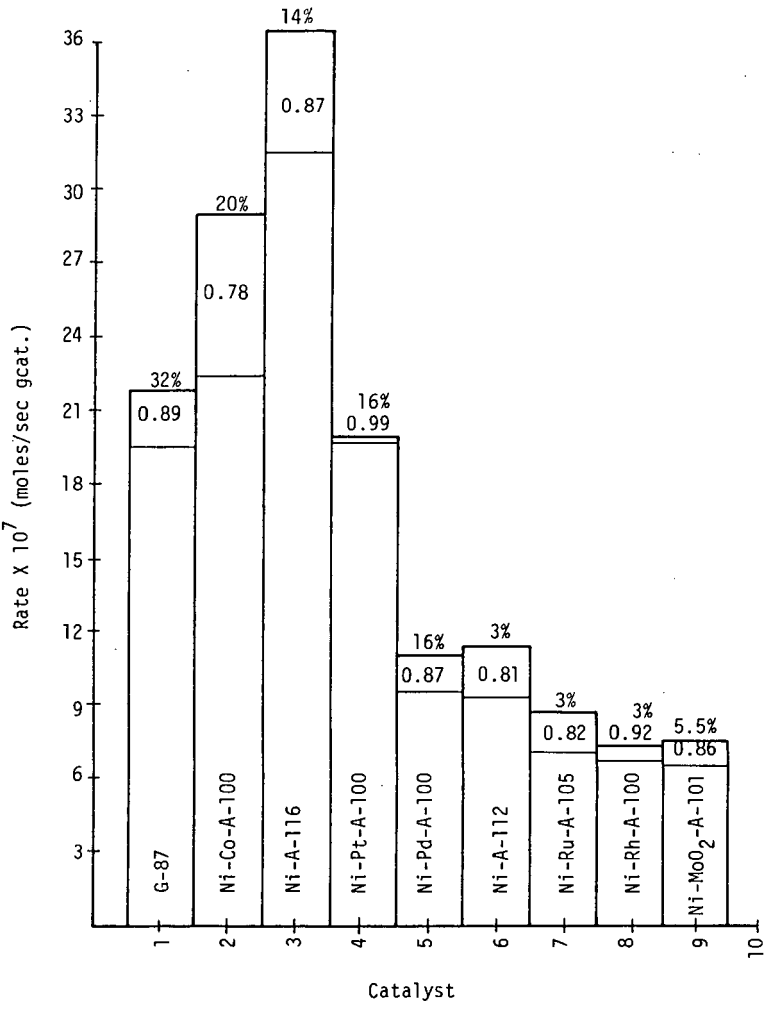

Figure 2 Specific Methanation Rates (mass basis) for Nickel and Nickel Alloy Catalysts. (Percentages are active metal loadings. Fractions represent selectivity to methane.) (T=250°C; GHSV=30,000 hr^{-1})

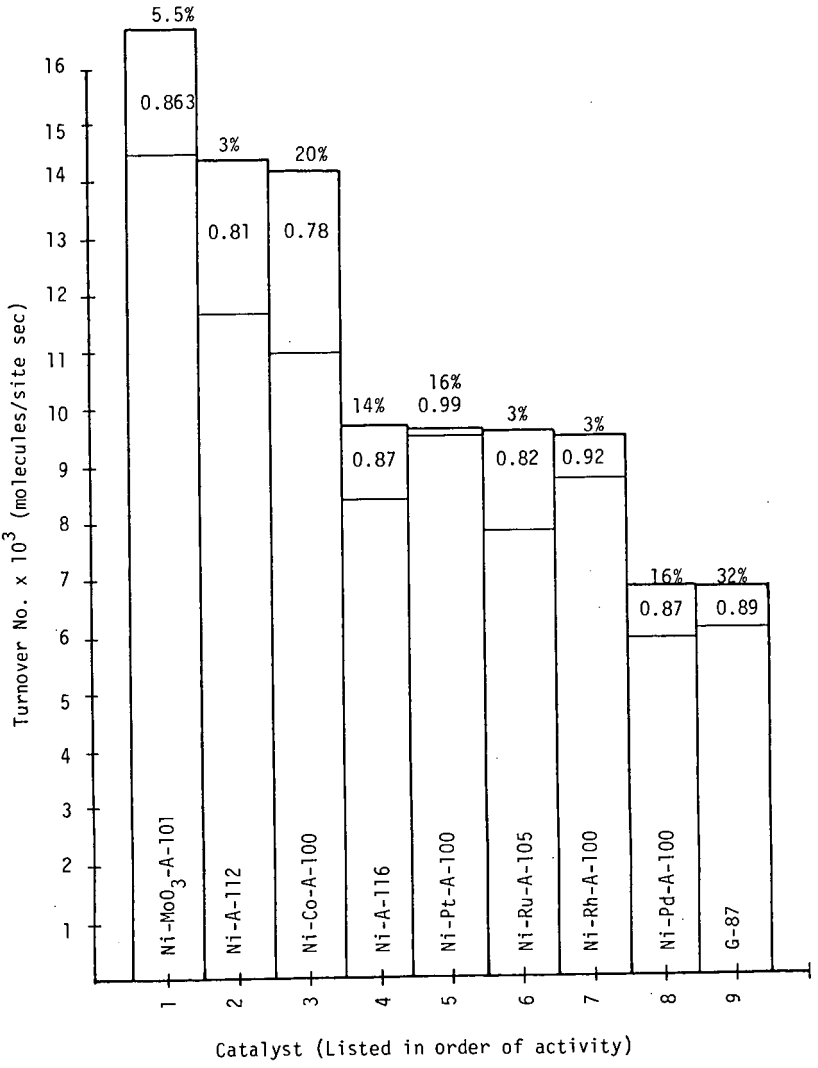

Figure 3 Turnover Numbers (molecules product/site sec) for Methanation on Nickel and Nickel Alloy Catalysts. (Percentages are active metal loadings. Fractions represent selectivity to methane.) (T=250°C; GHSV=30,000 hr^{-1})

TABLE 1

Hydrogen Chemisorptive Uptake Data for Alumina-Supported Nickel Nickel Alloy and Ruthenium Alloy Catalysts

Catalyst	Nominal Composition (wt%)	H_2 Uptake (μmoles/gram)	Metal Particle Size (A)	Percent Dispersion	Surface Area (m^2/g)
Ni-A-111	3% Ni	21.4	116	8.35	1.75
Ni-A-112	3% Ni	39.4	63	15.4	3.23
Ni-A-116	14% Ni	187.8	62	15.7	15.39
G-87 (Girdler)	32% Ni	161.6	163	5.93	13.24
Ni-MoO_3-A-101	2.5% Ni - 3% MoO_3	22.5	92*	10.6*	1.84*
MoO_3-A-101	3% MoO_3	1.0	--	--	--
Ni-Ru-A-105	2.5% Ni - 0.5 wt% Ru	44.6	52	18.76	3.71
Ni-Rh-A-100	2.5% Ni - 0.5% Rh	38.3	62	16.1	3.16
Ni-Co-A-100	10% Ni - 10% Co	114.9	142	6.76	9.54
Ni-Fe-A-100	10% Ni - 10% Fe	80.6	278	4.60	5.14
Ni-Pt-A-100	15.7% Ni - 0.5% Pt	106	119	8.22	8.66
Ni-Pd-A-100	15% Ni - 1.0% Pd	107.4	115	8.13	8.82

* Based upon nickel only

TABLE 2 Reactor Screening Data for Nickel and Nickel Alloy Catalysts
225°C, GHSV = 30,000 hr^{-1}, 16 psia

Catalyst	Conversion CO	Conversion CH_4	Production Other	Rate x 10^7 ($\frac{mole}{g\ sec}$) CH_4	Rate x 10^7 ($\frac{mole}{g\ sec}$) CO	Turnover # x 10^3 (sec^{-1}) CH_4	Turnover # x 10^3 (sec^{-1}) CO	Selectivity to CH_4
Ni-Co-A-100	16.2	15.15	1.05	9.31	9.96	4.56	4.88	0.935
Ni-Pt-A-100	16.77	15.20	1.60	9.91	10.95	4.77	5.27	0.906
Ni-Ru-A-105	5.18	3.48	1.73	2.79	4.17	3.12	4.68	0.672
Ni-Rh-A-100	3.3	2.2	1.1	1.48	2.21	1.93	2.88	0.671
Ni-Pd-A-100	6.9	6.67	0.2	4.62	4.79	2.87	2.97	0.97
Ni-MoO_3-A-101	2.9	2.5	0.4	1.83	2.11	4.07	4.69	0.87
Ni-Fe-A-100	De-activates under reaction conditions							
G-87	22.45	19.55	2.88	9.81	11.25	3.04	3.49	0.871
Ni-A-112	6.63	4.47	2.13	3.62	5.35	4.60	6.80	0.674
Ni-A-116	34.63	28.08	6.55	19.23	23.74	5.13	6.32	0.815

TABLE 3 Reactor Screening Data for Nickel and Nickel Alloy Catalysts
225°C, GHSV = 60,000 hr^{-1}, 20 psia

Catalyst	% Conversion CO	% Conversion CH_4	% Production Other	Rate x 70^7 (mole/g sec) CH_4	Rate x 70^7 (mole/g sec) CO	Turnover # x 10^3 (sec^{-1}) CH_4	Turnover # x 10^3 (sec^{-1}) CO	Selectivity to CH_4
Ni-Co-A-100								
Ni-Pt-A-100	15.53	14.03	1.43	18.47	20.33	8.88	9.80	0.903
Ni-Ru-A-105	4.15	3.25	0.88	5.23	6.63	5.87	7.44	0.788
Ni-Rh-A-100								
Ni-Pd-A-100	6.63	5.43	1.23	7.76	9.49	4.81	5.89	0.817
Ni-MoO_3-A-101	3.70	3.03	0.67	4.84	5.86	10.74	13.03	0.827
Ni-Fe-A-100	De-activates under reaction conditions							
G-87	20.37	17.43	2.93	18.53	21.63	5.75	6.72	0.856
Ni-A-112	5.70	4.63	1.03	7.12	8.71	9.04	11.05	0.812
Ni-A-116	24.05	21.98	2.05	30.88	33.76	8.47	8.99	0.914

TABLE 4 Reactor Screening Data for Nickel and Nickel Alloy Catalysts
250°C, GHSV = 60,000 hr^{-1}, 20 psia

Catalyst	% Conversion CO	% Conversion CH_4	% Production Other	Rate x 10^7 (mole/g sec) CH_4	Rate x 10^7 (mole/g sec) CO	Turnover # x 10^3 (sec^{-1}) CH_4	Turnover # x 10^3 (sec^{-1}) CO	Selectivity to CH_4
Ni-Co-A-100	38.7	30.43	8.27	38.03	48.3	18.6	23.7	0.787
Ni-Pt-A-100								
Ni-Ru-A-105	9.47	8.03	1.47	12.70	14.97	14.20	16.80	0.848
Ni-Rh-A-100								
Ni-Pd-A-100	11.2	10.3	0.9	14.67	15.93	9.09	9.85	0.92
Ni-MoO_3-A-101	9.3	8.7	0.65	13.56	14.58	30.14	32.41	0.92
Ni-Fe-A-100	De-activates under reaction conditions							
G-87								
Ni-A-112	14.43	13.58	0.88	20.64	21.99	26.19	27.91	0.941
Ni-A-116	43.53	38.17	5.43	53.38	60.94	14.21	16.22	0.877

TABLE 5 Apparent Activation Energies for Methanation Catalysts
Based on measurements at 225-250°C and a space velocity of 30,000 hr^{-1}

Catalyst	CO Conversion (Kcal/mole)	CH_4 Production (Kcal/mole)	Metal*	CH_4* Production Kcal/mole
Ni-Co-A-100	22.2	18.3	Co	27.0±4.4
Ni-Pt-A-100	12.4	14.3	Pt	16.3±0.8
Ni-Ru-A-105	14.8	19.0	Ru	24.2±1.2
Ni-Rh-A-100	19.2	21.1	Rh	24.0±0.4
Ni-Pd-A-100	17.1	14.8	Pd	19.7±1.6
Ni-MoO_3-A-100	26.2	26.2		
Ni-Fe-A-100			Fe	21.3±0.9
G-87	13.7	14.2	Ni	25.0±1.2
Ni-A-112	15.5	19.2		
Ni-A-116	8.8	10.2		

*Data of Al Vannice (Exxon) Ref.

HETEROGENEOUS METHANATION:

EFFECTS OF CARBON, SULFUR AND WATER

ON ACTIVITY MEASUREMENTS AT VARIOUS TEMPERATURES

R. A. Dalla Betta(*) and M. Shelef
RESEARCH STAFF
FORD MOTOR COMPANY
P. O. BOX 2053, DEARBORN, MI 48121

INTRODUCTION

A wide variety of experimental procedures has been used to measure catalytic activity and to compare catalysts for carbon monoxide hydrogenation. The comparison is generally carried out in flow reactors operating at high conversions. While such conditions are more realistic and may better duplicate catalyst performance in actual use, specific catalyst activities or specific reaction rates are difficult to estimate from such data. This is especially true for highly exothermic reactions such as CO hydrogenation where the temperature as well as concentrations change along the catalyst bed. Sulfur tolerance tests generally took the form of sulfidation capacity measurements with the sulfur being quantitatively taken up by the catalyst bed.

The first publications of this series presented data on initial reaction rates (1) on clean metal surfaces and on steady-state rates (2) on several catalysts both in sulfur-free and sulfur containing streams. In this paper a series of Ni catalysts is compared in several different tests. It will be demonstrated that conclusions derived from steady-state rates at 673 K are markedly different from those drawn at 523 K. Similar contradictions apply to tests designed to assess the activity in the presence of sulfur. Water vapor in the reactant stream is found to have a significant effect on both the high temperature steady-state activity and the final activity in the presence of sulfur.

EXPERIMENTAL

1. Apparatus

Initial rates were measured in a Pyrex glass batch recycle system as described previously (1). The reactor loop was filled with the reactants to the required pressure and mixed by circulating through a bypass. The catalyst sample was reduced in a stream of flowing hydrogen, cooled to the reaction temperature, evacuated and the reactants diverted over the catalyst. Samples of the reactant gas were analyzed by injection into a gas chromatograph equipped with a flame ionization detector. Both methane and total hydrocarbons were determined, steady-state rates were

(*) Current Address: Catalytica Associates, 2 Palo Alto Square, Palo Alto, California 94304

measured in an atmospheric pressure single pass flow reactor, also described previously (2). The flow of each reactant was set by controlling the upstream pressure on a stainless steel capillary. The catalyst was contained in a Pyrex reactor supported on a porous glass disc. The reactor effluent was analyzed as described above.

Water was introduced into the reactant stream through a Pyrex tube extending into the glass reactor and connected to a motor driven positive displacement syringe pump. The pump was constructed of stainless steel and had a volume of 500 cc. The inlet portion of the reactor, including a plug of glass wool, was heated resistively to vaporize the water. The pressure of water in the reactant stream was controlled by the pump speed which was set at 0.049 cc/min.

2. Materials

The catalysts have been described in detail in previous publications (1,2). The supported catalysts were prepared by impregnation of the oxide support with aqueous $Ni(NO_3)_2$ solution. The 5% Ni/ZrO_2 (I) (1) and 5% Ni/ZrO_2 (II) (2) were prepared from different batches of ZrO_2 obtained from the TAM Division of National Lead Co. This material was found to be quite impure, containing appreciable amounts of Cl, Ca, Mg, Fe and Hf (3). These batch to batch variations may, possibly explain some of the activity differences observed in the catalysts made with the ZrO_2 support. Raney Ni was prepared by extraction of a 50:50 Ni/Al alloy with NaOH to dissolve 60% of the Al. Hydrogen adsorption isotherms were determined on these catalysts (2) and the results are collected in Table 1.

RESULTS

After reduction of the catalyst at 723 K, initial reaction rates were measured on the clean metal surface using the batch recycle reactor. Reactant composition was $P(H_2)$ 0.5625 atm and P(CO) 0.1875 atm. The rate was calculated from conversion versus time data at short times (1). The system is well-behaved as shown by a typical set of data for 2% Ni/Al_2O_3 presented in Fig. 1. Results for a number of Ni catalysts are collected in Table 2.

Steady-state rates were measured in the single pass flow reactor at atmospheric pressure with a reactant stream composition of $P(H_2)$ 0.5938, P(CO) 0.1562, and P(He) 0.250 atm, corresponding to an H_2/CO ratio of 3.8. After the catalyst was reduced at 723 K, the temperature was lowered to 523 K and the reactants diverted over the sample. Steady-state was usually attained after 6 to 8 hrs. but 24 hrs. were allowed to elapse before at least four gas samples are analyzed and averaged to determine the catalyst activity. Then, 10 ppm H_2S was introduced into the reactant stream, and after 24 hrs., the activity again determined. In a similar manner, the H_2S flow was stopped and the activity recovery, if any, noted. These results are presented in Fig.2. In Fig.3 the catalyst activities are compared at 673 K. The procedure used in this case was to start the reactants over the samples at 520 to 550 K then slowly heat the samples to 673 K without exceeding a turnover number of 0.2/s. As before, 24 hrs. elapsed at each condition before activity data were taken.

Up to this point the activity measurements have been run without the addition of water. Although water is a reaction product, the differential conditions of the flow reactor experiment keep the partial pressure of water over the catalyst low.

In Figs.4 and 5 there are, respectively, collected steady-state results from runs in which water was added to the reactant stream for the 5% Ni/ZrO_2 (II) and 2% Ni/Al_2O_3 catalysts. The conditions at which each of the rate measurements, shown in Figs.4 and 5, were made are given in Table 3. Following a procedure similar to the previous measurements, the catalysts were reduced at 723 K, cooled to 523 K and the flow of CO and H_2 started. Data at condition A were obtained after 24 hrs. Water was then injected and 24 hrs. later the reaction rate was measured. Similarly, each subsequent data point was taken after waiting 24 hrs. for steady-state conditions to be established.

DISCUSSION

1. Steady-State Activity

Comparison of the initial rate data (Table 2) and the steady-state data at 523 K (Fig.2) shows that at this temperature the steady-state surface is similar, or at least has comparable catalytic activity to the clean metal surfaces studied by initial rate measurements. The relative ordering of the activity of the three catalysts is the same from either set of data. When the catalysts are heated to 673 K and again compared (Fig.3), the activity is significantly reduced in comparison to the rate expected from extrapolation according to the measured activation energy (Table 2). The activity is lower by a factor of approximately 30, indicating a surface deactivated by carbonaceous deposits either as a carbon overlayer or by the formation of a carbide-like species (2). Although the results presented here are at 673 K, it should be noted that the deactivation was observable at even lower temperatures and varied in its rate of approach to steady-state from one catalyst to another. A quantitative indication of this phenomenon is presented in Fig.6. After reduction, the catalyst was cooled to the temperature at which the initial rate was expected to be either 0.1 or 0.01 per second, and the reactants were passed over. The temperature was then adjusted to maintain a nearly constant turnover number. The Raney Ni at a specific rate of 0.01/s, corresponding to a temperature of 483 K, shows no apparent deterioration in activity after 5 days. At a temperature of 548 K and an activity of 0.1/s, the activity constantly decreased. To maintain a constant activity it was necessary to continuously raise the temperature. The rate of deactivation was observed to accelerate as the temperature was raised, as seen by the accelerating slope of the curve in Fig.6. The rate of activity deterioration appeared also to be dependent on the support, 5% Ni/ZrO_2 deteriorating much more rapidly than 2% Ni/Al_2O_3 or Raney Ni. The deterioration is not associated with thermal sintering of the Ni, since it was shown earlier that cleaning the catalyst of carbon could restore the higher activity (2).

As a result of this different susceptibility to deactivation by carbon overlayer formation at different temperatures the relative specific activity of a series of catalysts at steady state can be completely reversed at different test temperatures. At 523 K the relative activity is 5% Ni/ZrO_2 (II) $\triangleright$ 2% Ni/Al_2O_3 $\triangleright$ Raney Ni, while at 673 K the order is Raney Ni $\triangleright$ 2% Ni/Al_2O_3 $\triangleright$ 5% Ni/ZrO_2 (II).

2. Sulfur Poisoning

The temperature chosen for sulfur poisoning studies is also extremely important. At 523 K the deactivation is a factor of 170 in the best case, Raney Ni, while it is only 2.5 for 5% Ni/ZrO_2 (II) at 673 K. This decreased poisoning at

higher temperatures is consistent with the decreased stability of the sulfide. The ordering of the catalysts is substantially different, 2% Ni/Al_2O_3 showing the greatest susceptibility to poisoning at 523 K, while Raney Ni is most susceptible at 673 K. Such large changes in the ordering of catalyst sensitivity to sulfur, at least in this type of test, implies complex behavior. For example, at low temperatures, the presence of sulfur leads to the formation of a bulk metal sulfide (4) and the effect of the support may be to inhibit the formation of such sulfides. At higher temperatures other compounds may form such as sulfospinels in the case of the Raney Ni which contains elemental Al (2).

The H_2S pressure is too low to form a bulk sulfide at 673 K (4) and a surface sulfur layer may have to compete with the carbon containing layer that apparently forms at this temperature. This is in apparent agreement with the observation that the least active catalysts in sulfur-free environment at 673 K are the most active in the presence of H_2S.

3. Effect of H_2O

Yet another measurement procedure to compare catalysts for CO hydrogenation includes H_2O in the reactant stream at the catalyst inlet. Inclusion of a large partial pressure of water would more closely simulate the industrial process since water is purposely added to reduce carbon formation in the reactor and to generate hydrogen by the water gas shift reaction. The data of Figs.4 and 5 show that at 523 K water has an inhibiting effect. At 673 K, however, 5% Ni/ZrO_2 (II) and 2% Ni/Al_2O_3 behave quite differently in the presence of H_2O. The ZrO_2 supported catalyst shows inhibition by water (compare arrow - water free data from Fig.3), while 2% Ni/Al_2O_3 is substantially more active. The latter behavior is expected if it is assumed that the high temperature deactivation is due to carbon and that the presence of water inhibits carbon formation. The thermodynamic inhibition of carbon formation by water is well known (5). The behavior of 5% Ni/ZrO_2 (II) is difficult to explain.

When H_2S is added to the reactant stream, the 2% Ni/Al_2O_3 catalyst becomes totally inactive (Fig.5), the conversion being below the detection limit of the analytical system. The 5% Ni/ZrO_2 (II) is only slightly more active. The comparison of the effect of 10 ppm H_2S in a dry stream and in a reactant stream containing 13 mol% water reveals the significant impact water can have on the measured "sulfur resistance" of a catalyst. Whereas 5% Ni/ZrO_2 (II) appeared to deteriorate by only a factor of two with 10 ppm H_2S, the combination of water and 10 ppm H_2S results in a deterioration greater than 100-fold. When both the water and the H_2S were removed from the reactant stream, the activity recovered but for 5% Ni/ZrO_2 the highest recovery was obtained in a stream containing sulfur. In fact, with the system at reaction conditon D, i.e. both H_2O and H_2S in the reactant stream, removing the H_2O but keeping the H_2S in the reactant stream results in an increase in catalyst activity by two orders of magnitude. This behavior was completely reversible; the catalyst could be cycled between conditions D, E and G of Table 3 repeatedly without adverse effects.

The behavior described above emphasizes the importance of water when searching for sulfur resistant catalysts. But even more significantly it may give clues to the properties desired in a sulfur resistant methanation catalyst. The formation of a material stable toward reaction with H_2S is one route to sulfur resistance if this phase possesses some catalytic activity (6). The carbon containing phase may be such a material. A significant partial pressure of water may reduce its stability, permitting the inactive sulfide phase to form.

The measured specific activity and the relative ordering of CO hydrogenation catalysts can vary markedly depending on the temperature and reactant stream composition chosen for the catalytic test. Low temperature tests employing either initial or steady-state rate measurements, give activity data for a clean metal surface. Results obtained at 673 K apparently are representative of a carbon contaminated surface.

The choice of the test temperature and reactant stream composition is extremely important in designing an experimental test for catalyst resistance to sulfur poisoning. Water should be added to the reactant stream since it has a great effect on the sulfur tolerance of Ni catalysts.

REFERENCES

1. R. A. Dalla Betta, A. G. Piken, and M. Shelef
   J. Catal. 35, 54 (1974).
2. R. A. Dalla Betta, A. G. Piken, and M. Shelef
   J. Catal. 40, 173 (1975).
3. M. Bettman, Research Staff, Ford Motor Co, unpublished results.
4. T. Rosenquist, J. Iron and Steel Inst.176,37 (]954).
5. G. A. White, T. R. Roszkowski, and D. W. Stanbridge,
   Am. Chem. Soc., Div. Fuel Chem. Preprint 19 (3) 57 (1974).
6. M. Boudart, J. A. Cusumano, and R. B. Levy
   New Catalytic Material for the Liquefaction of Coal,
   Report RP-415-1, Electric Power Research Institute, October 30,(1975).

TABLE 1

Hydrogen Adsorption Results

Catalyst	H_2 Adsorption µmol/g	Dispersion H (ads)/M(tot)
5% Ni/ZrO_2 (I) (*)	33.7	0.079
5% Ni/ZrO_2 (II) (**)	19.2	0.045
2% Ni/Al_2O_3	5.6	0.033
Raney Ni	137	0.031

(*) Sample used in ref (1)
(**) Sample used in ref (2)

TABLE 2

Initial Rates of CO Hydrogenation (*)

Sample	N at 523 K s^{-1} x 100		E_a kcal/mol	
	HC(total)	CH_4	HC(total)	CH_4
5% Ni/ZrO_2 (I)	6.3	2.3	20	28
5% Ni/ZrO_2* (II)	27	9.6	30	33
2% Ni/Al_2O_3	5.1	2.0	30	31
Raney Ni	3.2	1.0	26	31

(*) $P(H_2)$ 0.5625 atm., P(CO) 0.1875 atm.

TABLE 3

Reaction Conditions at Steady-State for Runs in Figures 4 & 5

Reactions Conditions (*)	Temp (K)	Reactant Composition (Atm)				
		H_2O	H_2S	H_2	CO	He
A	523	0	0	0.5938	0.1562	0.250
B	523	0.133	0	0.515	0.135	0.217
C	673	0.133	0	0.515	0.135	0.217
D	673	0.133	10-5	0.515	0.135	0.217
E	673	0.133	0	0.515	0.135	0.217
F	673	0	0	0.5938	0.1562	0.250
G	673	0	10-5	0.5938	0.5938	0.250

(*) The conditions were maintained for 24 hrs before the steady-state reaction rate was determined.

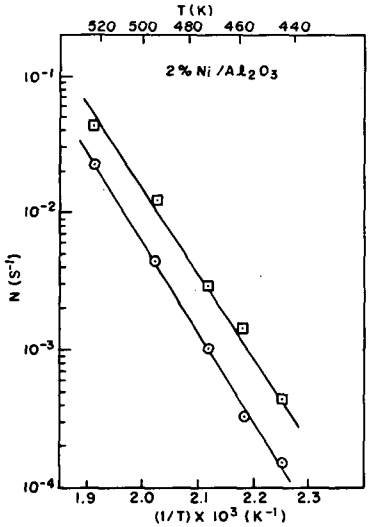

FIG. 1

Initial rate of CO hydrogenation on 2% $Ni/A\ell_2O_3$. □ - Total hydrocarbon synthesis rate; ○ - CH_4 synthesis rate.

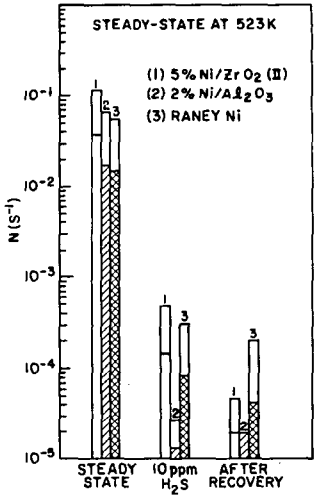

FIG. 2

CO hydrogenation at 523K on (1) 5% Ni/ZrO_2(II); (2) 2% $Ni/A\ell_2O_3$; (3) Raney Ni.

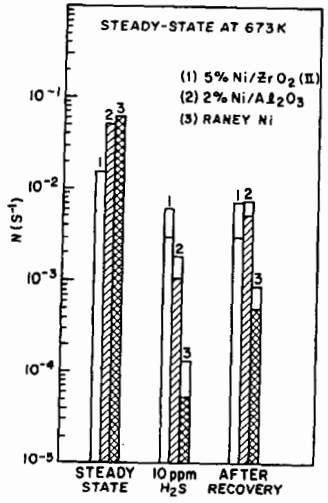

FIG. 3

CO hydrogenation at 673K on (1) 5% Ni/ZrO_2(II); (2) 2% Ni/Al_2O_3; (3) Raney Ni.

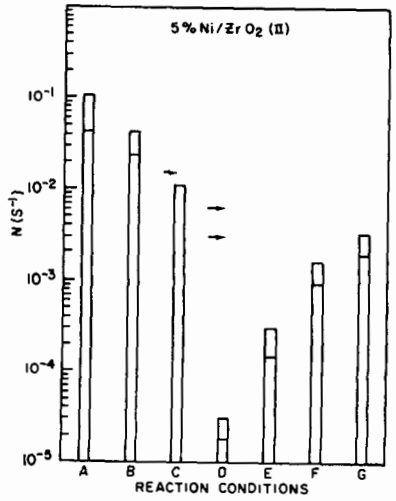

FIG. 4

CO hydrogenation at 673K on 5% Ni/ZrO_2(II), with H_2O in the reactant stream. See Table 3 for description of conditions. Arrows give rate in water-free system.

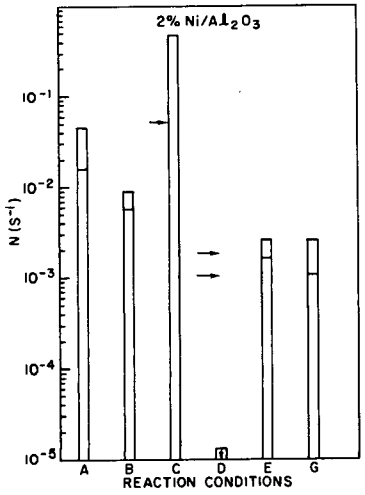

FIG. 5

CO hydrogenation at 673K on 2% Ni/Al_2O_3 with H_2O in the reactant stream. See Table 3 for description of conditions. Arrows give rate in water-free system.

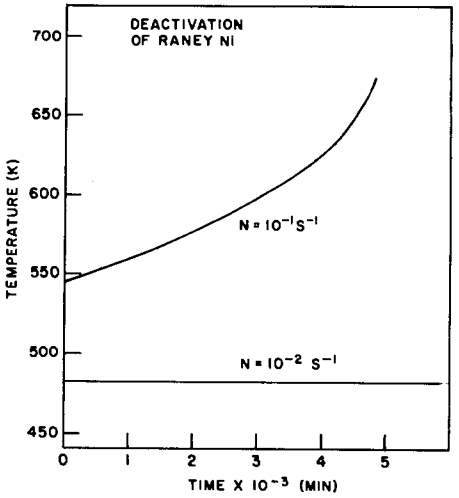

FIG. 6

Deactivation of Raney Ni for CO hydrogenation with reaction time.

FORMATION OF SURFACE CARBON AND METHANATION CATALYSIS ON ALUMINA SUPPORTED NICKEL

by

P. R. Wentrcek, J. G. McCarty, B. J. Wood and H. Wise
Solid State Catalysis Laboratory, Stanford Research Institute
333 Ravenswood Avenue, Menlo Park, California 94025

ABSTRACT

The mechanism of catalytic methanation on an alumina-supported nickel catalyst (25 wt% Ni) has been examined by means of (1) kinetic studies with a pulse microreactor, (2) surface studies with Auger electron spectroscopy (AES), and (3) temperature programmed surface reaction kinetics (TPSR) at the gas/solid interface. During exposure of the catalyst to pulses of CO (diluted with He) at elevated temperatures (> 450 K), we observed first-order formation of surface carbon. The surface carbon so formed exhibited high reactivity towards hydrogen with quantitative conversion to methane. The Auger electron spectra indicated that the surface carbon was bonded to the Ni as a carbidic-type surface species which converted to graphitic carbon of very low reactivity towards hydrogen at temperatures above 675 K. The kinetics of methane formation from surface carbon and gaseous H_2 were determined by means of TPSR. The formation of CH_4 is observed at temperatures as low as 375 K. The rates of methane formation follow first-order kinetics with respect to surface carbon. The activation energy for this process is 17.6 kcal/mol. The experimental data are analyzed in terms of a catalytic methanation mechanism in which dissociative adsorption of carbon monoxide and hydrogen is followed by reaction of surface carbon and surface oxygen with hydrogen adatoms to yield methane and water.

INTRODUCTION

In spite of considerable effort the methanation mechanism on nickel catalysts is not established unequivocally. At room temperature non-dissociative CO adsorption has been reported with the formation of several molecular bonding states on the surface of nickel.[1-5] However at elevated

---

*This research was supported by the American Gas Association.

temperatures (> 350 K) on an alumina-supported Ni catalyst[6] and on Ni films[7] the formation of CO_2 was observed and the reaction interpreted in terms of disproportionation. More recently dissociative chemisorption[8,9] has been suggested in accordance with:

$$CO(g) \rightleftarrows CO(s) \quad (1)$$

$$CO(s) \rightarrow C(s) + O(s) \quad (2)$$

$$CO(g) + O(s) \rightarrow CO_2(g) \quad (3)$$

However the surface carbon so formed was considered to have negligible reactivity in methanation and to deactivate the catalyst with the formation of bulk Ni_3C or graphitic carbon structures.[10]

The objectives of our research were (1) the kinetics of interaction of CO with a Ni/Al_2O_3 catalyst, (2) the reactivity of the surface carbon species toward hydrogen, and (3) the physical nature of the surface carbon and its bonding to Ni by Auger electron spectroscopy.

EXPERIMENTAL DETAILS

For measurement of the reaction of CO with the Ni/Al_2O_3 catalyst a pulse-microreactor system was used operating at 50 psig. Constant-volume pulses (1.3 cm^3) of CO, H_2, or CO/H_2 mixtures (CO + H_2) in a helium carrier stream passed through the catalyst bed and entered a gas chromatograph (GC) for quantitative analysis (CO, CO_2, and CH_4). The catalyst bed consisted of 13.7×10^{-3} g of hydrogen-reduced Girdler G-65 methanation catalyst (25 wt% Ni supported on Al_2O_3) crushed to finer than 200-mesh particle size. The catalyst was reduced for 15 hours at 725 K in a steady stream of pure H_2 at 1 atm, then purged for an hour in flowing He before the temperature was lowered to the desired operating level.

The rates of removal of the surface carbon species by hydrogen were determined by the technique of temperature programmed surface reaction (TPSR). This method represents a modification of the temperature programmed desorption technique (TPD) and is particularly well suited to the study of irreversible surface gas reactions, such as the interaction of hydrogen with surface carbon on nickel.[11] Interpretation of the experimental data in terms of kinetic parameters is based on the same theoretical analysis as employed in TPD.[12]

---

*(s) refers to a surface species and (g) to a gaseous species.

After depositing surface carbon on the catalyst (in the range from 3×10^{14} to 9×10^{14} atoms/cm^2 by exposure to a series of CO/He pulses at 450 - 550 K the sample was cooled to room temperature and the carrier gas changed to hydrogen. Subsequently the catalyst temperature was raised at a linear heating rate and the formation of methane resulting from the reaction of surface carbon with hydrogen was monitored as a function of time and temperature.

EXPERIMENTAL RESULTS

1. Pulse Microreactor Experiments

To establish the reaction order with respect to CO for surface-carbon formation the CO concentration in the pulse contacting the catalyst sample in the microreactor was varied from 1.0 to 10.0 vol% CO (in He) at 553 K. From the amount of CO_2 formed the mass of carbon deposited on the catalyst surface could be calculated (Equations 2 and 3). From the difference between the CO consumed (equivalent to twice the amount of CO_2 formed) and the total CO lost from the pulse the amount of non-dissociated CO left on the catalyst could be determined. The results of a series of such experiments are shown in Figure 1. The data depicted by curve (a) demonstrate that the fractional conversion of CO to surface carbon is proportional to the amount of CO in the pulse, indicative of a first order surface reaction. Thus, rather than disproportionation the mechanism involves rapid CO adsorption and rate-limited dissociation of the CO admolecule (reaction 2), followed by rapid removal of the oxygen adatoms by further reaction with CO [reaction (3)].

Of interest is the quantitative conversion of the surface carbon to methane on exposure to a hydrogen pulse at 553 K (curve b, Figure 1), except at very high surface densities of carbon (an estimated surface coverage of more than 50 percent relative to Ni surface atoms) at which the amount of the carbon converted to methane is somewhat less than that deposited. Under these conditions the temperature-labile characteristics of the surface carbon become apparent, as discussed in further detail in the following section.

For a first-order reaction, such as the dissociative chemisorption of CO on Ni/Al_2O_3, a pulse-reactor experiment can be employed for kinetic studies. Thus, from measurement of the amount of surface carbon formed over a range of temperatures, the activation energy for this heterogeneous reaction can be evaluated.[13] Over a temperature range from 553 K to 613 K we calculate, an activation energy of 39 kcal/mole for reaction (3) on the basis of a heat of adsorption of CO on nickel[7] of -35.0 kcal/mole.

2. TPSR Studies

The rate of formation of CH_4 by interaction of surface carbon with hydrogen, as studied by the TPSR technique, exhibits two distinct maxima (Figure 2). One methane peak is centered at 430 $\pm$ 20 K (α state), and the other at 630 $\pm$ 20 K (β state). The ratio of carbon coverages between the two states was found to be $N_\alpha/N_\beta = 2.5$ for exposure to CO at 523 K, and $N_\alpha/N_\beta = 1.0$ for exposure at 575 K. The shape of the TPSR curve and the maximum reaction temperatures were not influenced significantly by the temperature of surface-carbon deposition (from 510 to 570 K). In addition, the lack of dependence of these parameters on initial carbon coverage provides strong evidence that the reaction under study is of first order in surface-carbon coverage.

The apparent activation energies for the reaction of hydrogen with both the α and β states of adsorbed carbon were determined by varying the heating rate in a series of TPSR experiments.[12] Based on the theoretical analysis of a first-order surface reaction the apparent activation energies for the reaction of hydrogen with the α- and β- states of surface carbon were calculated:

$$k_\alpha = 1.3 \times 10^7 \exp(-17700/RT) \text{ sec}^{-1} \quad (4)$$

$$k_\beta = 3.0 \times 10^9 \exp(-33000/RT) \text{ sec}^{-1} \quad (5)$$

DISCUSSION

The experimental results strongly suggest the surface carbon formed by dissociative chemisorption of CO as an intermediate in the methanation reaction catalyzed by nickel. This mechanism is reinforced by experimental studies in which the surface carbon deposited to various degrees of surface coverage was exposed to pulses containing either hydrogen or mixtures of H_2 and CO ($H_2/CO = 9/1$). As summarized in Table 1 the surface carbon resulting from the exposure of the Ni/Al_2O_3 catalyst to six consecutive CO pulses can be converted rapidly and quantitatively to methane on exposure to a pulse of hydrogen. The resulting carbon mass balance between methane and surface carbon is excellent. On contacting a catalyst containing surface carbon with a pulse of $H_2/CO(9/1)$ the total amount of methane produced is greatly augmented over that measured on a clean nickel surface with the same gas mixture. As a matter of fact the total number of CH_4 molecules formed approaches the sum of the number of carbon atoms deposited on the catalyst surface and the number of CO molecules converted in passing a CO/H_2 pulse gas mixture over the clean catalyst (Table 1).

Furthermore it should be noted that in pulsing with CO some non-dissociated carbon monoxide is retained by the catalyst (Table 1). However these CO admolecules do not seem to contribute to methane formation on subsequent exposure to a pulse of H_2 at 553 K. This lack of participation of adsorbed CO molecules in methanation is substantiated by a calculation of the site occupancy of carbon and carbon monoxide adspecies on the catalyst surface resulting from exposure to pulses of different CO concentrations. In this analysis the assumption has been made that a bridge-bonded configuration [CO(B)] is particularly favorable for dissociative adsorption of CO, i.e., two neighboring nickel sites onto which CO is bound. The remaining sites are taken to be occupied by linearly bound CO admolecules [CO(L)], i.e., those bonded by sp-hybridized carbon to a single Ni atom. It will be noted from the data in Figure 1 (curve c) that during pulsing with progressively larger doses of CO, the finite number of Ni sites available is quickly preempted by CO(B)so that the adsorption of CO(L) goes through a maximum value. From a comparison of curves b and c in Figure 2 it is apparent that methane formation runs parallel to the surface density of C-atoms and not CO admolecules.

The chemical state of the carbon adatoms on the surface of the Ni/Al_2O_3 catalyst has been determined by means of Auger electron spectroscopic studies. A catalyst sample exposed to several CO pulses (10 vol% in He) at 553 K and cooled to room temperature exhibited the spectrum shown in Figure 3. The Auger electrons with energies near 250 eV and 260 eV exhibited by the Ni/Al_2O_3 sample and the carburized Ni foil are characteristic of a carbidic-type carbon structure.[14,15] The KLL Auger transition near 270 eV is common carbon in both the graphitic and the carbidic chemical states.

Since in the energy range of interest the Auger electrons emanate from a shallow depth near the surface of the solid (< 3 atomic layer) we may conclude that the dissociative chemisorption of CO on Ni results in the formation of a carbidic Ni-C surface bond. From the dissociation energy of CO (256 kcal/mole) and the Ni-O bond strength (89 kcal/mole) we estimate a value of 167 kcal/mole as the lower limit of the Ni-C binding energy required to make dissociative chemisorption of CO on Ni thermodynamically feasible. A bond strength of this magnitude for the Ni-C bond has been reported.[16]

Further evidence for dissociative adsorption of CO on Ni is provided by electron spectroscopy. In a study[17] of the photoelectron spectra of CO adsorbed on a polycrystalline nickel film at 300 K, a density-of-states distribution for the oxygen valence electrons was observed which could be attributed to CO admolecules. However at T > 400 K, the density-of-states distribution changed to that characteristic of O-adatoms resulting

from CO dissociation. Also, for CO adsorption on a disordered Ni(111) surface, Eastman and coworkers[18] reported rupture of the C–O bond.

The labile characteristics of the carbidic surface carbon species on nickel becomes apparent during prolonged exposure of the catalyst surface to the electron beam of the Auger electron spectrometer or to elevated temperatures. Under these conditions the Auger spectrum indicates a gradual transformation of the carbidic carbon to the graphitic form, i.e. disappearance of the spectral fine structure associated with the 250 and 260 eV Auger "peaks" and growth of the signal intensity of the 270 eV "peak." This form of surface carbon is relatively unreactive toward hydrogen. Possibly it has the properties of the C(β)-state (Figure 2) observed in the TPSR experiments. From the rate constants measured we would expect the reactivity of the graphitic carbon towards hydrogen to be 1/10,000 that of the carbidic species at 553 K.

Our experimental work strongly suggests the carbidic carbon surface species as an intermediate in the Ni-catalyzed methanation reaction. This surface carbon species, highly reactive towards hydrogenation and methane formation, should be distinguished from bulk nickel carbide, (Ni_3C), whose activity in methanation catalysis has been examined and found to be relatively low.[19-21] The rate determining step is to be found in the dissociative chemisorption of CO. The activation energy for this process is estimated to be 39 ± 2 kcal/mole, a value of the same magnitude found in our apparatus for steady state catalytic methanation at CO/H_2 = 1/9, as shown by the data in Figure 4.

REFERENCES

1. R. R. Ford, in Advances in Catalysis, eds. D. D. Eley, H. Pines, and P. B. Weisz, Academic Press, N.Y. 1970, Vol. 21; M. A. Vannice, J. Catalysis, 37, 449 (1975).

2. H. H. Madden, J. Kuppers, and G. Ertl, J. Chem. Phys., 58, 3401 (1973).

3. J. E. Demith and T. N. Rhodin, Surface Sci., 45, 249 (1974).

4. D. A. Degras, Nuovo Cimento Suppl., 5, 408 (1967).

5. G. Wedler, H. Papp, and G. Schroll, Surface Sci., 44, 463 (1974).

6. J. L. Bousquet, P. C. Gravelle, and S. Teichner, Bull. Soc. Chim. Franc., 1972, 3693.

7. M. McD. Baker and E. K. Rideal, Trans. Faraday Soc., 51, 1597 (1955).

8. H. H. Madden and G. Ertl, Surface Sci., 35, 211 (1973).

9. P. B. Tottrup, J. Catalysis 42, 29 (1976).

10. J. R. Rostrup-Nielsen, J. Catalysis 27, 343 (1972).

11. J. G. McCarty and H. Wise (to be published).

12. J. L. Falconer and R. J. Maddix, Surf. Sci. 48, 393 (1975).

13. D. W. Bassett and H. W. Habgood, J. Phys. Chem. 64, 769 (1960).

14. J. P. Coad and J. C. Riviere, Surf. Sci. 25, 609 (1971).

15. T. W. Haas and J. T. Grant. Appl. Phys. Letters 16, 172 (1970); T. W. Haas, J. T. Grant, and G. J. Dooley, J. Appl. Physics 43, 1853 (1972).

16. L. C. Isett and J. M. Blakely, Surf. Sci. 47, 645 (1975).

17. R. W. Joyner and M. W. Roberts, J. Chem. Soc. Faraday Trans. 1, 70, 1819 (1974).

18. D. E. Eastman, J. E. Demith, and J. M. Baker, J. Vac. Sci. Tech., 11, 273 (1974).

19. S. Weller, L.J.E. Hofer, and R. B. Anderson, J. Amer. Chem. Soc., 70, 799 (1948).

20. J. T. Kummer, T. W. DeWitt, and P. H. Emmett, J. Amer. Chem. Soc., 20, 3632 (1948).

21. A. K. Galwey, J. Catalysis 1, 227 (1962).

Table 1

INTERACTION OF H_2 AND H_2/CO WITH SURFACE CARBON ON Ni/Al_2O_3 CATALYST[a] AT 553 K

Experiment	Pulse[b]			Surface Species Deposited (moles x 10^6)		CH_4 Formed (mole x 10^6)
	Composition (vol%)		Total Number			
	H_2	CO		CO	C	
1	0	10	2	1.56	2.01	-
	100	0	1	0	0	1.96
2	0	10	2	0.83	2.12	-
	100	0	1	0	0	2.10
3	0	10	6	1.65	3.40	-
	100	0	1	0	0	3.39
4	90	10	1	-	-	5.25
	0	10	5	-	3.08	-
	90	10	1	-	-	8.01

[a] Ni/Al_2O_3 catalyst (Girdler G-65, 25 wt% Ni).

[b] CO pulse = 5.73×10^{-6} mole; H_2 pulse = 5.73×10^{-5} mole.

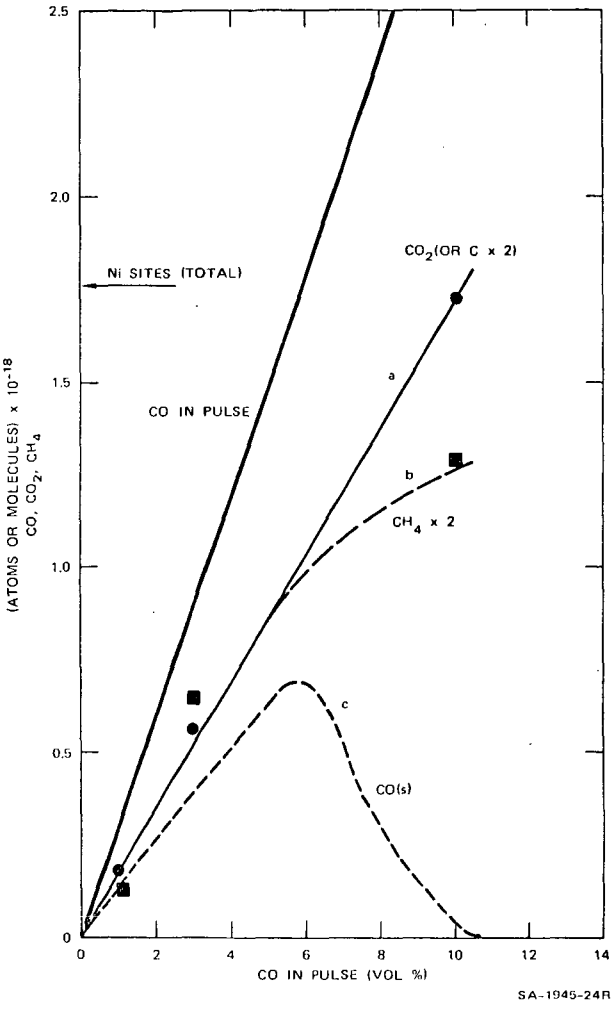

FIGURE 1 SURFACE CARBON INTERMEDIATE IN CATALYTIC METHANATION (Ni/Al_2O_3, 25 wt %)

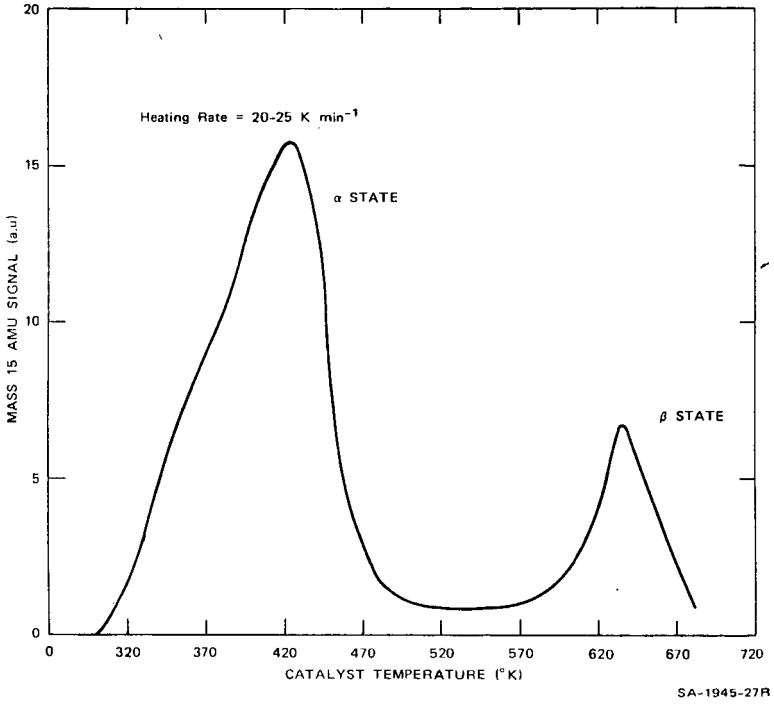

FIGURE 2 TEMPERATURE PROGRAMMED SURFACE REACTION BETWEEN SURFACE CARBON AND GASEOUS HYDROGEN CATALYZED BY Ni/Al_2O_3 (25 wt %)

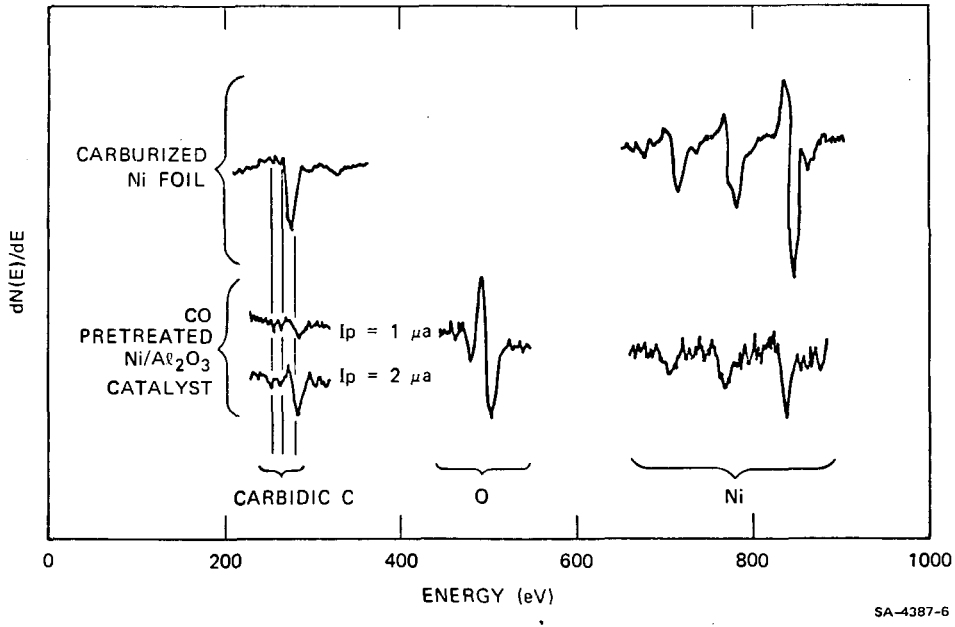

FIGURE 3 AES OF SURFACE CARBON MNi/Al_2O_3 CATALYST AFTER EXPOSURE TO CO AT 553 K

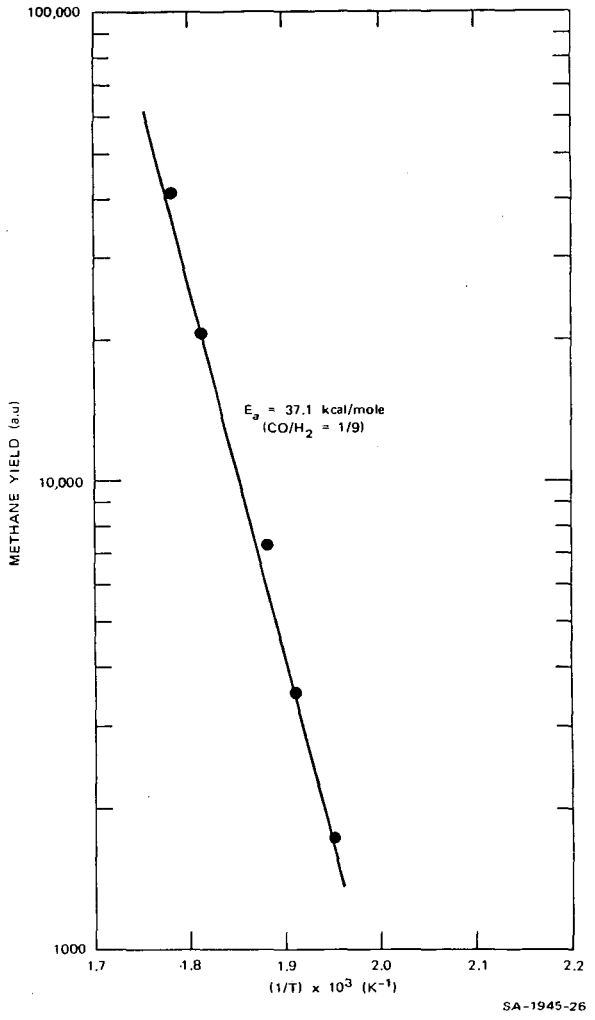

FIGURE 4 STEADY STATE METHANATION ACTIVITY OF Ni/Al_2O_3 (25 wt %)

PERMSELECTIVE MEMBRANES FOR THE REMOVAL OF H_2S FROM COAL GAS

S. L. Matson
S. G. Kimura

General Electric Corporate Research
and Development Center
Schenectady, New York 12301

INTRODUCTION

The integrated combined cycle power plant firing low BTU coal gas is one of the most attractive and efficient systems for production of electricity from coal. H_2S must be removed from the fuel gas stream when high sulfur coal is used in order to meet emissions requirements.

A permselective membrane which can be used to selectively separate H_2S from low BTU coal gas is being developed. The membrane is based on the principle of facilitated transport in which permeation is augmented by reversible chemical reaction with a carrier species incorporated in the membrane. In the case of facilitated H_2S transport, the liquid membrane is a film of immobilized carbonate solution with which H_2S reacts, yielding permeation rates and selectivities orders of magnitude greater than those of conventional polymeric membranes.

MEMBRANES FOR GAS SEPARATIONS

Membrane gas separations are attractive because they are fundamentally simple and can require less energy than conventional techniques. However, due to their generally low permeation rates and selectivities, the application of membranes to industrial gas separations has been limited. Low permeabilities result in excessively large membrane area requirements reflected in high capital costs. In order to achieve an adequate degree of separation with a membrane of low permselectivity, resort to multiple stage membrane cascades may be required, and both high capital and operating costs accompany this type of operation. To overcome these objections, General Electric is developing a new class of membranes called facilitated transport membranes, which promise both high permeation rates and high selectivity.

Permeation of gases through non-porous polymeric films occurs by a solution/diffusion mechanism. The permeant molecule first dissolves in the membrane phase and then diffuses across the film driven by its concentration gradient. The permeability of such a membrane is given by the product of permeant solubility and diffusivity

$$Pr = D_i \cdot S_i \qquad 1)$$

where permeability is generally defined by the equation

$$Pr_i = \frac{N_i \cdot \delta}{A \cdot \Delta P_i} \quad [=] \quad \frac{(cc/sec) - cm\ thickness}{cm^2 - cm\ Hg\ \Delta P} \qquad 2)$$

and

D_i = diffusivity of permeant i in the membrane, cm^2/sec

S_i = permeant solubility, cc(STP)/cc membrane-cmHg

N_i = permeant flux, cc(STP)/sec

A = membrane area, cm^2

δ = membrane thickness, cm

ΔP_i = transmembrane partial pressure difference, cm Hg

Membrane selectivity is expressed in terms of a separation factor which is simply the ratio of the permeation coefficients of two gases

$$\alpha_{ij} = Pr_i/Pr_j \qquad 3)$$

Unfortunately, both solubilities and diffusivities of gases in polymeric films are generally low and thus gas permeabilities are likewise low. Furthermore, since gas diffusivities and solubilities do not vary greatly for a given polymer, conventional polymeric solution/diffusion membranes also exhibit limited permselectivity as a rule.

Reasonable fluxes and area requirements can be obtained with relatively low performance membrane materials by employing ultrathin membrane technology, and silicone rubber and its copolymers have a number of useful applications when used in this form (1,2,3). Nonetheless, the problem of low selectivity is not resolved by decreasing membrane thickness.

A considerable improvement in performance results from using an immobilized liquid as the membrane phase rather than a polymer. Transport through the "immobilized liquid membrane" (ILM) again occurs by the solution/diffusion mechanism, but permeation rates are now improved because solubilities and diffusivities of permeating gases are generally higher in the liquid phase than in polymers. By immobilizing the membrane liquid by impregnation of a suitable porous support material, it is possible to combine the desirable permeation properties of the liquid with the physical properties and ease of handling of the polymeric support membrane. Such a membrane consisting of a supported polyethylene glycol film has been shown to have high permeability and selectivity for sulfur dioxide (4).

FACILITATED TRANSPORT

A more significant feature of immobilized liquid membranes may be that permeabilities and selectivities for gases in liquid membranes can further be augmented, often by orders of magnitude, through facilitated transport. This involves a non-volatile carrier species in the liquid membrane which reacts reversibly with the permeating gas. The reactive carrier shuttles back and forth between opposite sides of the membrane carrying the permeant with it in one direction. This process is very common in biological systems (5).

Consider the simplest case of facilitated transport in which a single permeating species, A, reacts reversibly with a carrier, C, to form a complex, AC; neither the carrier nor the carrier-permeant complex can cross the membrane boundaries. The sequence of events describing facilitated transport is the following:

(1) Species A dissolves in the membrane liquid;

(2) A reacts with the carrier near the feed side membrane boundary;

(3) The AC complex (as well as "free" A) diffuses across the immobilized liquid film;

(4) Near the other membrane boundary where the partial pressure of A is low, the reaction equilibrium shifts and the AC complex dissociates;

(5) Free A comes out of solution;

(6) The carrier diffuses back across the membrane and is again available to participate in the facilitated transport cycle.

The total flux of A is the sum of that by simple diffusion (as free A) and by facilitated diffusion (as AC). Because the concentration levels and gradients in carrier and complex can be made orders of magnitude greater than those of the "free" permeating component, transport of A can be dramatically enhanced by the carrier process. Moreover, membrane selectivity can be extraordinary, as advantage can be taken of the specificity of chemical reaction.

Some of the earliest work by engineers to exploit the separative efficiency of facilitated transport membranes is that of Ward and Robb (6), who identified the use of an aqueous carbonate solution immobilized in a cellulose matrix as a CO_2 transport membrane. They found that not only was CO_2 transport enhanced by orders of magnitude as compared to diffusion through water films, but also that the transport rate could further be enhanced by the addition of a hydrolysis catalyst. A number of mathematical analyses of facilitated transport have been published, including those by Ward (7) and Shultz *et al* (8).

FACILITATED TRANSPORT OF H_2S

Facilitated transport of H_2S occurs in liquid membranes consisting of aqueous carbonate solutions according to the following process (refer to Figure 1):

(1) H_2S dissolves in the membrane liquid at the high-pressure (h.p.) side of the film;

(2) H_2S decomposes near the h.p. side of the film by the reaction $H_2S \rightarrow H^+ + HS^-$;

(3) H^+ produced in step (2) is consumed by $CO_3^=$ that is diffusing toward the h.p. side by the reaction $H^+ + CO_3^= \rightarrow HCO_3^-$;

(4) HS^- and HCO_3^- diffuse from the h.p. to the low pressure (l.p.) side of the film;

(5) HS^- combines with H^+ near the l.p. side of the film by the reaction $HS^- + H^+ \rightarrow H_2S$;

(6) H^+ for step (5), is supplied by HCO_3^- by the reaction $HCO_3^- \rightarrow H^+ + CO_3^=$;

(7) $CO_3^=$ produced in step (6) diffuses back to the h.p. side;

(8) H_2S produced in step (5) leaves the membrane.

Carbon dioxide also reacts with the membrane liquid as described by the overall reaction

$$CO_2 + CO_3^= + H_2O \rightleftarrows 2HCO_3^- \qquad 4)$$

and, accordingly, it also experiences facilitated transport. However, because the reaction rate of CO_2 with the membrane liquid is slow relative to that of H_2S, alkaline absorbents demonstrate an inherent selectivity for absorption of H_2S in preference to CO_2. A means of improving this H_2S/CO_2 selectivity still further will be described later.

In its present configuration, the immobilized liquid membrane for facilitated H_2S transport consists of a concentrated (25-30 wt. %) aqueous solution of K_2CO_3, although other membrane liquids including K_3PO_4 solutions have been screened. The membrane liquid is immobilized as a film a few thousandths of an inch thick by virtue of surface tension forces in the pores of a hydrophilic polymeric support membrane.

Two approaches have been pursued for maintaining the transmembrane H_2S partial pressure gradient which drives membrane transport. The first and simplest involves "sweeping" one face of the membrane with low pressure steam to dilute the acid gases which permeate across the membrane and keep their partial pressures low. The sweep steam carries the acid gases from the membrane permeator to a condenser, providing a dry mixture of H_2S and CO_2 at a pressure sufficient for conversion of H_2S to elemental sulfur in a Claus plant or similar process. It is convenient to visualize the liquid membrane functioning as both the H_2S absorption column and steam stripping column which are conventionally used for H_2S removal. H_2S absorption and solution regeneration occur within the membrane liquid film thickness rather than in two separate vessels operated at different pressures with absorbent pumped between them. A drawback to steam sweeping is that a high pressure difference corresponding to the difference between the gasification pressure and the sweep steam pressure must be supported across the liquid film. While the membrane support problem is significant, it is indeed feasible to operate liquid membranes under such conditions, and the steam sweeping approach is being pursued in a parallel program. However, an alternative affords greater H_2S membrane reliability.

The alternative involves sweeping permeated acid gases from the membrane permeator by means of a pressurized liquid which is an H_2S absorbent. This liquid sweep may simply be a concentrated solution of K_2CO_3, identical in composition to the immobilized membrane liquid, which is isolated from the liquid membrane sandwich by a layer of non-wetted microporous polymer membrane which affords no significant resistance to H_2S transport. Relatively little power is required to pressurize the sweep

liquid to coal gas pressure, and by this means no significant pressure difference is applied across the membrane. The price of avoiding the membrane support problem is, of course, introduction of the requirement for absorbent regeneration. Dissolved acid gases are removed from solution by pressure reduction and steam stripping as is conventional practice. In this configuration, the membrane H_2S scrubbing process resembles a hot potassium carbonate plant in which the conventional packed tower absorber has been replaced by a membrane permeator. The advantages in this are enumerated below.

APPARATUS

Figure 2 shows the apparatus used to measure membrane permeability. A membrane is placed in the test cell, and the test cell is inserted into an oven set at the desired operating temperature, usually from 90° to 130°C. Feed and sweep streams pass countercurrently over opposite sides of the membrane. The feed gas--a mixture of H_2S, CO_2, N_2, and sometimes small amounts of other gases--is humidified by sparging through a boiler set at the temperature corresponding to the water pressure of the membrane liquid. Helium is likewise humidified and serves to meter the sweep steam. Flow rates of all streams are measured and gas compositions determined by chromatography. In liquid sweeping runs, a sweep liquid stream of appropriate composition pressurized by a metering pump replaces the low pressure sweep gas mixture of helium and steam.

While most tests have employed synthetic coal gas mixtures made from bottled gases, experiments have also been performed with actual coal gas. Coal gas supply pressure has been limited to one atmosphere to date.

H_2S MEMBRANE CHARACTERIZATION

The optimum operating temperature of the membrane is in the range of 90°C to 110°C, which coincides with that of the hot potassium carbonate systems. Total feed gas pressure is usually maintained at 300 psig--a typical operating pressure for fixed bed gasifiers. Inlet H_2S partial pressures are representative of gasification of high sulfur coals--2.5 to 3.5 psi.

Figure 3 shows the dependence of membrane H_2S permeability on the partial pressure of CO_2 in the feed gas. The inlet H_2S partial pressure was 2.8 psi, but since substantial amounts of H_2S were removed from the feed gas stream, the H_2S feed partial pressure varied several fold from package inlet to outlet and in certain instances significant H_2S partial pressures were present in the sweep stream. These data demonstrate the strong depressing effect of CO_2 partial pressure on H_2S permeability which results from competition of the two acid gases for the membrane carrier, the carbonate anion. Such an effect can be predicted qualitatively by the theory of facilitated transport, although a rigorous mathematical description would be extremely complex.

The CO_2 partial pressures of interest in low Btu coal gas range from about 15 to 30 psi, corresponding to an average permeability for H_2S of 3000-4000 x 10^{-9}cc(RTP)-cm/sec-cm^2-cmHgΔP. As a basis for comparison, the room temperature H_2S permeability of dimethyl silicone

rubber, the most permeable polymeric membrane available, is 850 x 10^{-9}. Unlike silicone rubber, the immobilized liquid membrane is virtually perfectly selective for acid gases; other coal gas components cross the membrane by the solution;diffusion mechanism, and solubilities in the hot, very concentrated salt solution are quite low.

H_2S permeability is essentially unchanged upon raising the operating temperature from 90 to 110°C, although an increase in CO_2 permeability results in a decreased selectivity for H_2S over CO_2 at the higher temperature. H_2S permeability is also relatively insensitive to carbonate solution concentration, apparently due to competing effects between higher carrier loading and decreased diffusivities and activity coefficients at the high concentrations employed.

The permeation coefficient for H_2S also depends on its own partial pressure in addition to that of CO_2; in Figure 4, the feed gas CO_2 partial pressure has been fixed while H_2S inlet concentration is varied. Since the extent of H_2S removal from the feed gas was limited to 15-30%, accurate point values of H_2S permeability were obtained. At high feed partial pressures of hydrogen sulfide, the membrane carrier mechanism is saturated--that is, the extent of the facilitation is limited by the availability of the carbonate carrier for reaction at the feed side of the membrane, and H_2S permeability falls off sharply at high partial pressures. For H_2S partial pressures below about 3 psi, the permeation coefficient increases modestly with decreasing reactant partial pressure. This saturation phenomenon is a general feature of facilitated transport systems. The performance of facilitated transport membranes is made more difficult to describe due to the dependence of permeation coefficient on permeant partial pressure. This contrasts with the relatively simple situation for polymeric membranes in which permeability is often a constant characteristic of the identity of the permeating gas but not its pressure.

Membrane permeability to H_2S depends on sweep side acid gas partial pressures as well as on those in the feed gas. In the liquid sweep runs summarized in Figure 4, the extent of conversion of incoming carbonate sweep solution to the bicarbonate form was varied to simulate different degrees of absorbent regeneration in the steam stripping process. The calculated equilibrium CO_2 partial pressures exerted by the incompletely regenerated sweep liquid are shown in Figure 4. The two dashed lines indicate that H_2S transport is further hindered by the presence of the competing permeant CO_2 on the sweep side of the membrane.

The presence of H_2S in the sweep stream influences transmembrane flux in two ways--(1) by decreasing the H_2S partial pressure difference across the membrane (i.e., the driving force for transport) and (2) by decreasing the facilitation factor due to the decreased concentration gradient in bisulfide and bicarbonate ions resulting from partial membrane liquid conversion by H_2S in the sweep stream.

As observed earlier, the transport of carbon dioxide is also facilitated by the carbonate membrane system. An important difference between H_2S and CO_2 facilitated transport is that, while the chemical reactions which augment H_2S flux are sufficiently rapid that H_2S transport is essentially diffusion rate limited, the reaction of

CO_2 with the membrane liquid is relatively slow due to the sluggish kinetics of CO_2 hydrolysis. Hence, reaction rates as well as equilibria are important in determining the permeation rate of CO_2. The significance of the difference in reaction rates is that carbonate absorbents--whether immobilized as liquid membranes or not--exhibit an apparent selectivity for absorption of H_2S in preference to CO_2, and membrane CO_2 permeability is much lower than that of H_2S.

The high degree of control which the membrane designer has over the gas-liquid interface permits him to further improve this inherent selectivity for absorption of H_2S over CO_2. Figure 5 shows how H_2S:CO_2 selectivity can be enhanced by splitting a given total membrane liquid film thickness into two or more liquid layers, each separated by a thin gas-filled space. This so-called "gas gap" is conveniently provided by a layer of a suitable non-wetting microporous polymer membrane. The rate of H_2S transport, being diffusion-limited, depends only on the total thickness of the membrane liquid films acting as diffusion barriers. Since the mass transfer resistance to H_2S of the intervening gas gap is entirely negligible, the H_2S permeability is not effected by this arrangement of the membrane sandwich. In contrast, the transport rate of CO_2 is diminished by dividing the membrane liquid film into multiple layers, since the CO_2 flux is sensitive to the rate of the relatively slow chemical reaction between CO_2 and membrane liquid and since these slow reactions are forced to occur an additional time for each new gas-liquid interface which is created. According to this much oversimplified description, the CO_2 transport rate is approximately halved by a single gas gap, decreased 3-fold with two gas gap interlayers, etc., with a corresponding increase in H_2S:CO_2 separation factor α at no cost in reduced H_2S permeability. It should be observed that the selectivity enhancement requires only that the CO_2 reaction be slow relative to that of H_2S, since competition between these two reactants for membrane carrier determines selectivity. The CO_2 absorption reaction might be fast compared to the diffusion process.

Figure 6 shows that this simple analysis describes experimental data quite adequately. The ratio of H_2S and CO_2 fluxes has been determined for three membrane sandwich configurations and plotted as a function of CO_2 partial pressure in the feed stream; inlet H_2S concentration was fixed. Multilayering is seen to improve H_2S:CO_2 selectivity as predicted by theory, as the spacing and slopes of the lines drawn through the three data sets indicate. With a double gas gap arrangement (three membrane liquid layers) and a synthetic coal gas feed containing 2.7 psi H_2S and 20 psi CO_2, the H_2S:CO_2 flux ratio is increased from about 0.5 (no gas gap) to 1.5, corresponding to a permeate composition enrichment from 33% to 60% H_2S in CO_2. Selectivity for H_2S absorption is particularly important for integrated combined cycle power generation from low Btu coal gas for reasons discussed below.

Permeation data such as the above are used in predicting the membrane area requirement for any given application. Since the permeability of facilitated transport membranes depends on reaction kinetics and equilibria, it is not possible to characterize membrane performance by a simple permeability "constant" as for polymeric membranes, and in fact the permeation constant varies significantly from permeator inlet to outlet in the following integration:

$$A = \int_{0}^{N_{H_2S}} \frac{dN_{H_2S}}{Pr_{H_2S}\,(P_{H_2S,\,F} - P_{H_2S,S})} = \frac{\delta \cdot F_t}{P_t} \int_{P_{H_2S,i}}^{P_{H_2S,o}} \frac{dP_{H_2S,\,F}}{Pr_{H_2S} \cdot \Delta P_{H_2S}}$$

where F_t and P_t are the volumetric flowrate and total pressure of the coal gas feed. The H_2S partial pressure difference across the membrane is calculated by material balance. For typical applications involving desulfurization of low-Btu coal gas produced from high sulfur coal, a range of 1-2 ft^2 of membrane area per kilowatt of generating capacity is predicted.

MEMBRANE H_2S SCRUBBING OF LOW BTU GAS

The conceptual layout of a liquid swept membrane H_2S scrubbing system is shown in Figure 7; it is very similar to the hot carbonate flowsheet with the exception of the replacement of the conventional absorber with the novel membrane permeator.

Many of the benefits of membrane H_2S scrubbing in the combined cycle power plant are due to the controllable, high membrane selectivity for H_2S absorption. Minimizing CO_2 removal increases the fuel gas mass flow to the gas turbine, decreases the turbine compressor air requirement, and thus increases the net shaft work delivered to the gas turbine generator. On the other hand, passage of large amounts of CO_2 through the H_2S removal and sulfur conversion trains is to be avoided for a number of reasons.

The total amount of acid gas flowing through the sulfur removal and conversion trains is less, of course, for the more selective process; specifically, three times less acid gas must be processed on a molar basis if the product stream from the H_2S stripper consists of 60% H_2S in CO_2 rather than 20% H_2S. A decrease in the total amount of absorbed acid gases to be stripped from solution should reduce the stripping steam requirement. Since insufficient waste heat is available in the plant to raise all the low pressure stripping steam required, a portion must be extracted from the steam turbine at a penalty in reduced power output; this penalty is minimized by high membrane selectivity. In short, less gasification, heat recovery, and gas and steam turbine equipment need be purchased per megawatt of exported power when selective membrane scrubbing is employed, and power plant first costs are thus reduced by more effective use of the energy available in the coal gas. The net plant heat rate is also improved by routing CO_2 to the turbines, reflecting lower operating as well as first costs.

A final consideration as regards the power plant is that a number of H_2S removal processes, including the membrane scrubber, employ concentrated solutions of alkali metal salts as absorbents. With conventional absorption columns, a possibility exists for alkali metal carryover due to entrainment or foaming. This is unacceptable in view of the extremely low gas turbine tolerance

for alkali metals in the fuel gas due to hot corrosion problems. The carbonate membrane solution, on the other hand, is quite effectively immobilized.

The high absorption selectivity afforded by membrane H_2S scrubbing also results in equipment and utility savings in the H_2S scrubbing process itself. Specifically, the effective absorbent carrying capacity for H_2S increases with selectivity, and a reduced solution recirculation rate is possible at a savings in pumping power. Since gas and liquor flowrates are down, the size of the stripping column is decreased, and a smaller acid gas condenser duty follows from the reduced stripping steam consumption.

The relatively high absorption temperature of 90-110°C is an advantage relative to processes which operate nearer ambient. The higher the absorption temperature, the less heat exchange area and heat rejection capacity that is required in the fuels plant. Energy losses due to incomplete heat recovery are minimized and less polluted condensate is generated. By operating at somewhat higher absorption temperatures and living with increased K_2CO_3 makeup requirements, the alkaline membrane liquid should be capable of absorbing carbonyl sulfide, if required, and hydrolyzing it to H_2S and CO_2 to facilitate its conversion to elemental sulfur in the Claus plant.

Finally, Claus plant capital cost is sensitive to H_2S concentration in the acid gas feed. Above 50% H_2S, the less expensive partial combustion process may be employed; at lower H_2S concentrations, the split-stream configuration is required in order to achieve stable combustion. Furthermore, since H_2S conversion to elemental sulfur is limited by equilibrium considerations, sulfur conversion efficiency increases with H_2S concentration for a given number of catalytic stages. Since the cost of the sulfur conversion plant will be as large as that of the H_2S removal plant, substantial cost savings can be realized here.

MEMBRANE LIFE

Because of the very severe operating environment of coal gas, an extensive life testing effort has been undertaken, focussing on the liquid swept membrane. The membrane has been operated at 90°C and a pressure of 300 psig with synthetic coal gas mixtures. Tests have also been performed on actual coal gas produced by the GEGAS-F atmospheric fixed bed gasifier. Both chemical and physical effects have been sought and solutions developed for membrane life-limiting problems as they have been identified. Promising life test results have been obtained which will soon be reported.

CONCLUSIONS

The superior performance of facilitated transport immobilized liquid membranes makes possible the use of membranes to do industrially significant gas separations. The extremely high permeability and H_2S:CO_2 selectivity of carbonate liquid membranes

makes them particularly suitable in low Btu coal gas-combined cycle power plant applications. In addition to high performance, reasonable membrane life is being demonstrated.

ACKNOWLEDGEMENTS

The membrane scrubber development is based in large part on the invention and experimental ingenuity of W.J. Ward and C.S. Herrick of this laboratory.

REFERENCES

(1) Ward, W.J., Browall, W.R., Salemme, R.M., "Ultrathin Silicone/Polycarbonate Membranes for Gas Separation Processes", Journal of Membrane Science, 1, March, 1976.

(2) Browall, W.R., Kimura, S.G., "Ultrathin Membranes for Oxygen Enrichment", Presented at VI Interamerican Congress of Chemical Engineers, July, 1975.

(3) Kimura, S.G., Browall, W.R., "Permselective Membranes for Oxygen Enrichment", General Electric Publication, 1976.

(4) Ward, W.J., "Immobilized Liquid Membranes" from Recent Developments in Separation Science, N. Li ed., Chemical Rubber Company, 1974.

(5) Stein, W.D., The Movement of Molecules Across Cell Membranes, Academic Press, 1967.

(6) Ward, W.J., Robb, W.L., "Carbon Dioxide-Oxygen Separation: Facilitated Transport of Carbon Dioxide Across a Liquid Film" Science, 156, 3781, June 16, 1967.

(7) Ward, W.J. "Analytical and Experimental Studies of Facilitated Transport" AIChE Journal, 16, 3, May, 1970.

(8) Schultz, J.S., Goddard, J.D., Suchdeo, S.R., "Facilitated Transport Via Carrier Mediated Diffusion in Membranes" AIChE Journal, 20, 3, May, 1974 and 20, 4, June, 1974.

(9) Tosh, J.S., Field, J.H., Benson, H.E., and Haynes, W.P., "Equilibrium Study of the System K_2CO_3, $KHCO_3$, CO_2, and H_2O, U.S. Bureau of Mines, Report of Investigations 5484, 1959.

FIGURE 1.
FACILITATED TRANSPORT OF HYDROGEN SULFIDE

$$H_2S + CO_3^= \rightleftharpoons HS^- + HCO_3^-$$

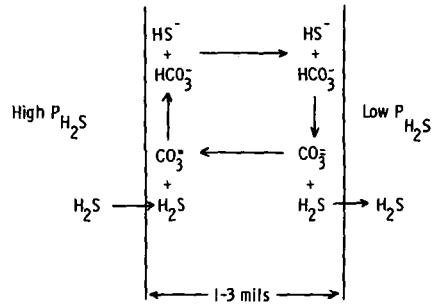

Immobilized K_2CO_3 Solution

SIMILAR REACTION FOR FACILITATED TRANSPORT OF CO_2

$$CO_2 + CO_3^= + H_2O \rightleftharpoons 2HCO_3^-$$

FIGURE 2.

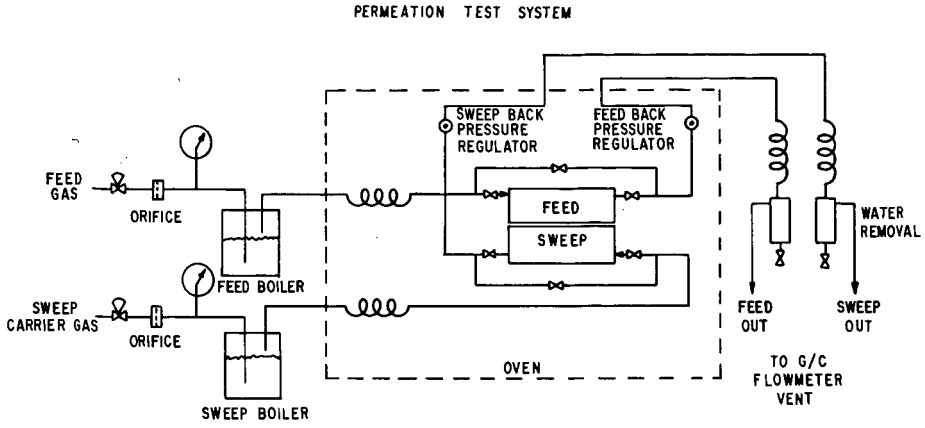

FIGURE 3.

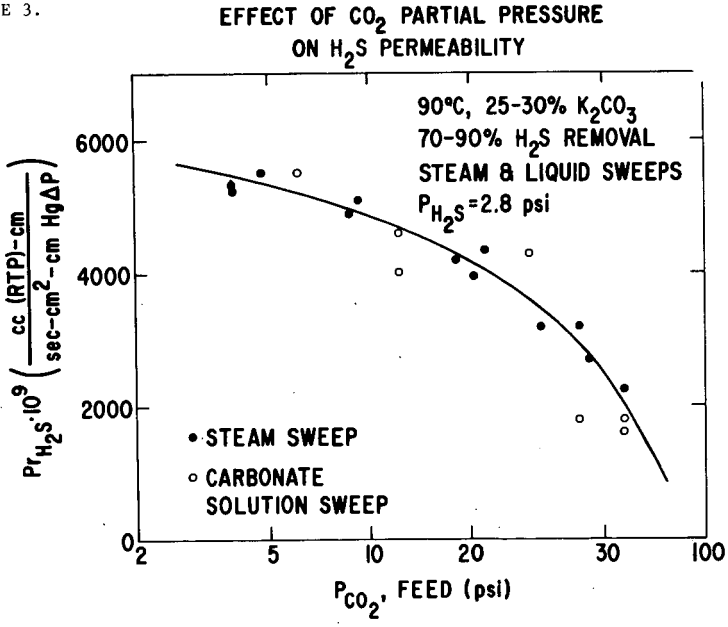

FIGURE 4.

H_2S PERMEABILITY MAP AT 90°C, 30 PSI CO_2 IN FEED

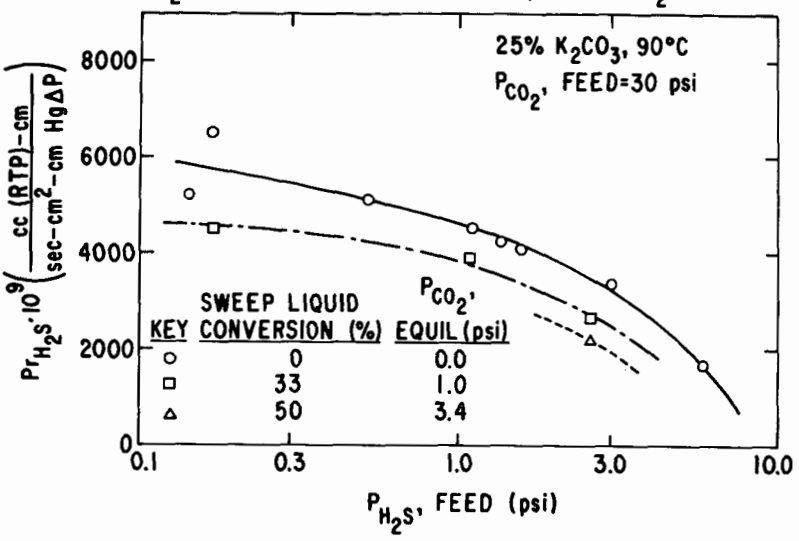

FIGURE 5.

IMPROVEMENT OF H_2S/CO_2 SELECTIVITY BY GAS GAP

DIFFUSION LIMITED H_2S TRANSPORT:

$$N_{H_2S} \propto \frac{1}{(\text{TOTAL LIQUID FILM THICKNESS})}$$

REACTION RATE LIMITED CO_2 TRANSPORT:

$$N_{CO_2} \propto \frac{1}{(\text{NUMBER OF GAS-LIQUID INTERFACES})}$$

I. TWO ILM'S IN CONTACT

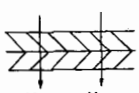

II. TWO ILM'S SEPARATED BY GAS GAP

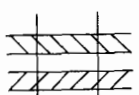

$$\therefore \alpha_{II} \approx 2\alpha_I$$

FIGURE 6.

ENHANCEMENT OF MEMBRANE H_2S/CO_2 SELECTIVITY BY GAS GAP

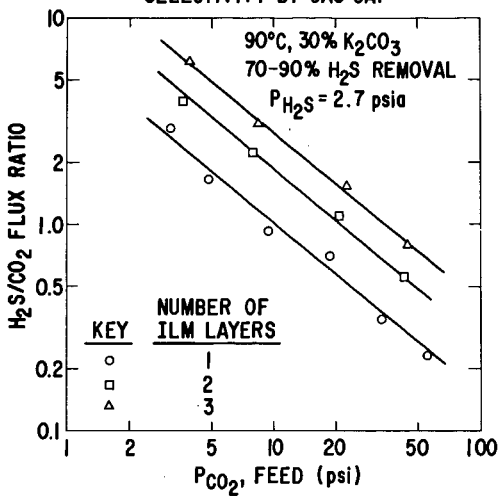

FIGURE 7.

MEMBRANE H_2S SCRUBBING SYSTEM (LIQUID SWEEPING)

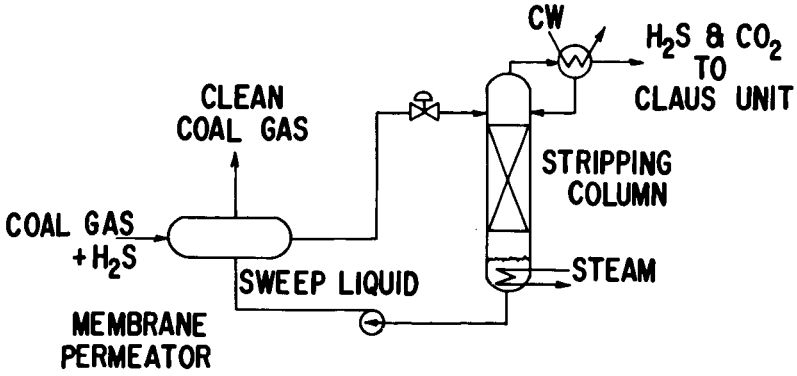

Hot Low-Btu Gas Purification with Coal Ash, O. J. Hahn and M. R. Heilig, Institute for Mining and Minerals Research, University of Kentucky, Lexington, KY 40506.

An experimental study was carried out to evaluate the removal of H_2S and other sulfur compounds from hot low Btu producer gas using gasifier ash. The present work emphasized thermogravimetric studies of the basic absorption and regeneration of ash as a function of temperature, particle gas size composition and residence time. The gas composition studied include (H_2S, N_2), (H_2S, H_2, N_2), (H_2S, H_2, CO, N_2), (H_2S, CH_4, H_2, CO, N_2), (H_2S, CH_4, H_2, CO, CO_2, N_2) and (H_2S, COS, H_2, CO, N_2). The temperature range varied from 800 to 1600°F. The absorption of H_2S in the iron oxide matrix is preceded by the reduction of the iron to the elemental form.

In the case of (H_2S, N_2) gas the absorption was restricted by the formation rate of H_2.

HOT GAS CLEANUP PROCESS FOR REMOVING H_2S FROM LOW-BTU GASES USING IRON OXIDE ABSORBENTS

E. C. Oldaker and D. W. Gillmore

Energy Research and Development Administration
Morgantown Energy Research Center
Morgantown, West Virginia

INTRODUCTION

Research is continuing at the Morgantown (West Virginia) Energy Research Center, Energy Research and Development Administration, to develop a hot gas cleanup process using solid regenerable sorbents to remove hydrogen sulfide from hot (1000°-1500°F) low-Btu fuel gas made from coal. A suitable process is needed whereby sulfur can be removed from low-Btu gases so that high sulfur coals can be utilized to provide clean energy and meet the environmental standards regulating the amount of sulfur released to the atmosphere. Removal of hydrogen sulfide without cooling the gas would conserve the heat lost in conventional gas purification methods, thus increasing the thermal efficiency by 15 percent.

The use of iron oxide to remove H_2S from industrial gases has been practiced for many years. Indeed, research by the Appleby-Frodingham Steel Company during the late fifties led to the construction and operation of a plant desulfurizing about 2½ million cubic feet of coke oven gas per day followed by construction of a 32 million cubic feet per day plant before operational problems and economic costs shut down the operations. The crude coke oven gas was passed through a fluidized-bed of sintered iron oxide powder (-16 mesh + 100 mesh) where reaction with H_2S and Fe_2O_3 took place at temperatures approaching 400°C. This process, as reported by Reeves et al (1), removed 95-98 percent of the H_2S from the coke oven gas. The principal problems encountered, as far as the use of iron oxide was concerned, were massive attrition and replacement of the fines, plugging and erosion of pipes transporting the iron oxide. These difficulties encountered by the Appleby-Frodingham process have been overcome by placing the iron oxide particles on a supporting matrix composed of fly ash, or silica, by thoroughly mixing the two components, extruding the paste-like mixture into 1/4-inch diameter by 3/4-inch long cylinders and sintering at 1800°F.

The chemistry involved in absorption and regeneration using iron oxide shows that iron sulfides are produced when H_2S reacts with Fe_2O_3 with the empirical composition approaching $FeS_{1.5}$

$$Fe_2O_3 + 3H_2S \rightarrow 2FeS_{1.5} + 3H_2O$$

However, according to Imperial Chemical Industries Catalyst Handbook (2), fresh iron oxide is converted to Fe_3O_4 in the presence of hydrogen and at temperatures above 650°F. Therefore, the reaction would be written as

$$Fe_3O_4 + 4H_2S \rightarrow 2FeS + FeS_2 + 4H_2O$$

During regeneration, air oxidizes the FeS and FeS_2 to Fe_3O_4 and SO_2:

$$6FeS_{1.5} + 13O_2 \rightarrow 2Fe_3O_4 + 9SO_2$$

However, in the presence of excess oxygen, the Fe_3O_4 is converted to Fe_2O_3. If this condition exists, then upon the start of another absorption cycle, some hydrogen is consumed from the raw producer gas while conversion to Fe_3O_4 is taking place

$$3Fe_2O_3 + H_2 \rightarrow 2Fe_3O_4 + H_2O$$

A review of the literature reveals that coke oven gases have been desulfurized in both fixed and fluid beds of iron oxide at temperatures up to 752°F (1). Abel et al (3) and Shultz (4) reported the results of laboratory-scale investigations of solid sorbents to remove hydrogen sulfide from hot (1000°-1500°F), clean, simulated low-Btu fuel gas. Clay and Lynn (5) reported the use of iron oxide supported on alumina to remove NO_x and SO_x from powerplant stack gases at temperatures approaching 1000°F, using an injected stream of synthesis gas (CO + H_2) to reduce the SO_2 to H_2S and NO to N_2 before passing the flue gases over the catalyst. Oldaker et al (6,7,8,9) reported the results of tests involving fly ash-iron oxide and silica-iron oxide sorbents to remove H_2S from hot (1000°-1500°F) low-Btu gases.

EXPERIMENTAL WORK

The Research conducted thus far has been two-pronged; lab scale investigations for the development of an efficient sorbent for removing H_2S from hot low-Btu gases made from coal, and process development to identify the major parameters required for scale-up design criteria utilizing data from bench scale operations up to 9000 scfh gas flows.

The absorbent research has been directed toward the development of sorbents with the following criteria:

a. Efficient removal of H_2S at temperatures above 1000°F;
b. Physical strength required to withstand handling;
c. Economic feasibility; and
d. Process feasibility--regenerability, form and composition and acceptable life.

Attrition of the iron oxide sorbent resulting in unacceptable carry over and absorbent replacement, plugging or fouling of system components, led to development of a more suitable matrix support for the iron oxide. Fly ash and silica satisfied this requirement and permitted adequate gas contact for removal of H_2S, while withstanding process temperatures.

The next step toward the development of the sorbent hinged on the necessary preparation techniques required to strengthen these sorbents in the categories of H_2S absorption capacity and efficiency, physical strength, and economic costs.

Several tests were carried out to determine the effects of additives on the physical strength and absorption capacities. It was found that one percent bentonite added to the fly ash-iron oxide mixture produced a superior sorbent having good physical strength and absorption capacity. This was not true when using silica-iron oxide mixtures as both the physical strength and absorption capacity were reduced. On the other hand, using sodium silicate as the additive produced an excellent sorbent when using either fly ash or silica as the support material. Data are shown in table 1.

Another major difference between the support materials is the amount of iron oxide that can be admixed. It was found that 25 percent iron oxide added to the fly ash was the maximum amount that could be tolerated without reducing both the physical strength and the absorption capacity, whereas 45 percent iron oxide could be added to the silica without any detrimental effects on the physical strength or absorption capacity of the sintered sorbent. This increased amount of iron oxide accounts for the much higher H_2S absorption capacities shown in table 1 for the silica sorbents.

The temperature limitations imposed on each type of sorbent is significant because of the highly exothermic reaction taking place during the regeneration of the sorbents. Using fly ash as the support material imposes a temperature limitation

of 1500°F for the sorbent to have a good level of absorption capacity and life expectancy. This is because fly ash acts as a glass-fusing at around 1500°F. The fusing characteristic would cause loss of pores thus cutting down on surface area available for good gas contact and eventually rendering the sorbent useless for removing H_2S from hot producer gas.

Silica, on the other hand, has a much higher fusion temperature permitting higher temperature operation without affecting the ability of the sorbent to perform. The recommended operating temperature indicated by limited data is believed to be in the range of 1700°-1800°F. This range is well above most if not all coal gasification processes being developed at this time. Provided that the present work being carried out on other than low-Btu gases does not contain constituents detrimental to the sorbent material or reactions, the two sorbents could be used on most coal gasification processes efficiently and economically. Particulate matter carried over from the gasification process may cause detrimental effects especially if the fixed bed concept is utilized, although the lab scale investigations indicate the carbonaceous material is burned off during the regeneration cycle. There is much research work going on at the present time on hot particulate removal from coal-derived gases, which is essential to projected combined cycle and turbine applications.

Figure 1 is a flow diagram of the laboratory apparatus used to test and evaluate the various sorbents. Generally, the gases were metered into the system to simulate the actual composition of producer gas. Coal was fed into the system at rates up to 500 grams/hr through the carbonizer to provide the actual tars and particulates found in producer gas. After being preheated, the producer gas flows into the absorber containing approximately 700 grams of prepared sorbents. The H_2S is monitored at the input and output of the absorber by means of the Tutwiler technique (10) to determine the absorption capacity and efficiency of the particular sorbent being tested. The temperature of the absorbent bed is maintained at operating temperature by means of electric heaters, usually at 1100°F. The gas output is also monitored by analyzers for CO and H_2.

Life expectancy is another major parameter used to evaluate the worth of a high temperature solid absorbent for H_2S removal. Therefore, an iron oxide-fly ash absorbent was tested on the lab scale unit using simulated producer gas containing tars and particulates to determine some degree of life expectancy. Thirty complete absorption-regeneration cycles were completed on the same absorbent. It was found that the recycling of the sorbent did not affect the ability of the sorbent to remove H_2S from the hot producer gas maintaining an average absorption capacity of 10 wt.-pct. during the tests. Upon completion of these tests, the sorbents were in excellent condition without any signs of physical deterioration or caking between the individual sorbents. Figure 2 indicates the sorption capacities achieved during the thirty runs. These tests were conducted at 1100°F. Regeneration was accomplished by using 12 scfh air flow rate through the absorber for approximately two hours. During regeneration, the bed temperature increased to 1700°F momentarily in the actual wave front or zone of reaction. Although this temperature reached 1700°F momentarily, without apparent harm, it is believed that 1500°F would be the highest temperature fly ash-iron oxide sorbents should be exposed for optimum life expectancy. Further life tests are now being conducted where an optimum sorbent is recycled until the H_2S absorption capacity decreases significantly so that better defined limits can be predicted. Table 2 shows the typical data from six of the thirty sorption capacity tests using the fly ash-iron oxide sorbent. Note that the H_2S absorption efficiency is given using 400 grains/100 scf as the break through limit. These percentages would be much higher using 150 grains/100 scf as the stopping point for absorption.

Further testing, using much higher gas flows and increased amounts of sorbent material was believed necessary to generate data that are required for scale-up criteria. A 9000 scfh atmospheric producer and hot gas cleanup facility has been designed, built and installed at MERC for this purpose.

The general overall range of operating conditions include:

Space velocities	500-3500 vol/vol/hr
Coal feed rates	60-200 lb/hr
Pressures	3-15 psig
Temperatures	600°-1500°F
Make gas flows	5000-9000 scfh
Gas analyses	CO-H_2-CO_2-H_2S-N_2-CH_4-COS-CS_2-C_2H_6-O_2-SO_2

The overall flowsheet is shown in figure 3. The detailed instrumentation has been removed to permit better understanding of the process. Also, it is well to remember that particular designs or instrumentation shown here are only tools needed to procure design criteria and not necessarily the approach that would be used for commercial application.

Air and steam are fed into the 16-inch diameter producer through the revolving, eccentric grate into the combustion zone to gasify the coal. The depth of the coal bed can be varied depending on operating conditions required. Normally, the bed depth averages about 32-36 inches. An agitator-stirrer mechanism providing continuous vertical and circular movement permits stirring in various levels of the coal to minimize agglomeration or break up voids while running on bituminous coal. The coal is choke-fed downward through the coal feed tube, the length of which establishes the bed height. From shakedown operations, it has been necessary to revise the coal feed system. The extremely slow movement of the coal through the coal feed tube permitted the coal particles to become somewhat plastic or sticky and adher to tube walls eventually blocking coal feed to the producer. This system is now being revised by feeding the coal through a pocket feeder and metering screw. The bed level will be established by the speed of the screw and monitored by nuclear gauges similar to those on the MERC 42-inch diameter pilot scale producer (11).

The make gas exits from the producer into a standard-design refractory cyclone to remove the larger dust particles--above 10 micron--and is then piped into either of the two absorbers, which are loaded with fly ash or silica supported iron oxide absorbents. For testing at 2500 space velocity using 7500 scfh gas flow, around 225 pounds of sorbent would be used. The absorbent bed temperature is held above 900°F by maintaining the sensible heat of the exit gas through insulation, refractory, and the circulation of hot gases from a gas-fired POC heater. During regeneration, which is accomplished with air, the heat from the highly exothermic reaction is controlled by dilution gases and/or the natural heat-sink effect of the refractory lined vessel.

The off gases from the absorber are then piped through a back pressure regulator and a metering orifice to the flare stack.

Three sampling ports are located in the flow system for gas analyses. One gas sampling point is located immediately downstream from the cyclone, where the raw producer gas is continuously monitored by a gas chromatograph. Another sampling point is located downstream from the absorbers in the piping system handling the make gas. This point continuously monitors the H_2S concentration remaining in the make gas after passing through the iron oxide sorbents. The last gas sampling port is located in the exit gas piping carrying the SO_2 enriched stream to the vent stack. This port continuously monitors the SO_2 concentration in the off gas during regeneration cycle.

Figure 4 is a cross sectional view showing the interior arrangement of the producer. The most important parts are the eccentric, cone crusher-type grate, the 16-inch water cooled combustion zone, the agitator-stirrer mechanism, and the coal feed tube.

Figure 5 is a cross sectional view of the refractory lined absorber which is 12-inches inside diameter. The absorber gas flow is down flow during absorption and up flow for regeneration. This flow pattern is presently being reversed in an attempt to prevent build-up of particulates on top of the sorbent bed.

Preheated gas from a gas fired POC heater enters through the bottom of the absorber and passes through the sorbent bed to provide the heat-up necessary before the start of an absorption cycle. As shown, thermocouple ports are located 18 inches apart in order to measure temperatures and thus identify the wave front or zone reaction as it passes through the sorbent bed.

Preliminary data generated thus far on the bench scale unit fairly well parallels data taken on the lab scale apparatus. For instance, the data generated while using the lower temperature extreme of 616^{o}F while using anthracite coal provides almost the same absorption capacity--6.43 wt.-pct., although the space velocity was increased from approximately 500 on the lab unit to 2500 vol/vol/hr on the bench scale facility. Also, a slightly higher bed temperature of 672^{o}F increased the absorption capacity by 18 percent to 7.62 wt.-pct. This shows that increased temperatures give better absorption results. Previous tests on laboratory apparatus showed the highest absorption results were obtained around 1500^{o}F, the limit of the fly ash-iron oxide sorbents. Table 3 shows typical data generated at these lower temperatures on the bench scale facility. The data indicate also that efficiency decreases as temperature during absorption is lowered. More data generated on the bench scale facility will be made available in the immediate future after shakedown operations and equipment design modifications are completed.

CONCLUSION

The research results thus far indicate that the hot gas cleanup process is an acceptable alternative for removing H_2S from low-Btu fuel gases derived from coal. The solid absorbents performed well at temperatures between 1000^{o}-1500^{o}F.

Further engineering development is needed on hot particulate removal and it is being intensely investigated at this time by several firms. Several independent studies are also being made on various regenerative techniques, using recycled SO_2, for instance, to increase the SO_2 concentration in the effluent gas stream to permit more efficient processing to elemental sulfur. Engineering studies concerning the geometry of the absorber-reactor are being made with particular emphasis on heat transfer mechanisms to handle the high temperatures during regeneration. Fluid bed and moving bed concepts along with the fixed bed are being evaluated and some testing programs are already underway.

REFERENCES

1. Reeve, L. Desulfurization of Coke Oven Gas at Appleby-Frodingham. J. Inst. Fuel, Vol 31, No. 210, July 1958, pp 319-324.

2. Catalyst Handbook, Imperial Chemical Industries, Ltd., Distributed by Springer-Verlag, Inc., New York (1970), p 53.

3. Abel, W. T., F. G. Shultz, and P. F. Langdon. Removal of Hydrogen Sulfide from Hot Producer Gas by Solid Absorbents, BuMines RI 7947, 1974.

4. Shultz, F. G. Removal of Hydrogen Sulfide from Simulated Producer Gas at Elevated Temperatures and Pressures. Proc. 2d Internat. Conf. on Fluidized-Bed Combustion, National Air Pollution Control Assoc., Hueston Woods State Park, College Corner, Ohio, October 4-7, 1970, 1972, pp III-5-1-III-5-5.

5. Clay, P. T. and Scott Lynn. Iron-Catalyzed Reduction of NO by CO and H_2 in Simulated Flue Gas. General Motors Symposium on NO Reduction, October 7-8, 1974.

6. Oldaker, E. C., A. M. Poston, and W. L. Farrior. Removal of Hydrogen Sulfide from Hot Low-Btu Gas with Iron Oxide-Fly Ash Sorbents. MERC/TPR-75/1, February 1975.

7. Oldaker, E. C., A. M. Poston, and W. L. Farrior. Hydrogen Rulfide Removal from Hot Producer Gas with A Solid Fly Ash-Iron Oxide Sorbent. MERC/TPR-75/2, June 1975.

8. Farrior, W. L., A. M. Poston, and E. C. Oldaker. Regenerable Iron Oxide-Silica Sorbents for Removal of H_2S from Hot Producer Gas. 4th Energy Resource Conf., University of Kentucky, January 6-7, 1976.

9. Oldaker, E. C., A. M. Poston, and W. L. Farrior. Laboratory Evaluation of Properties of Fly Ash-Iron Oxide Sorbents for H_2S Removal from Hot Low-Btu Gas 170th National Meeting ACS, Vol 20, No. 4, pp 227-237, August 24-29, 1975, Chicago, IL.

10. Altieri, V. J. Gas Analyses and Testing of Gaseous Materials, American Gas Association, New York, 1st Edition, pp 339-340, 1945.

11. Friggens, G. R. and A. W. Hall. Nuclear Gages for Monitoring Coal Bed of Commercial Scale Pressurized Gas Producers. BuMines RI 7794, 1973.

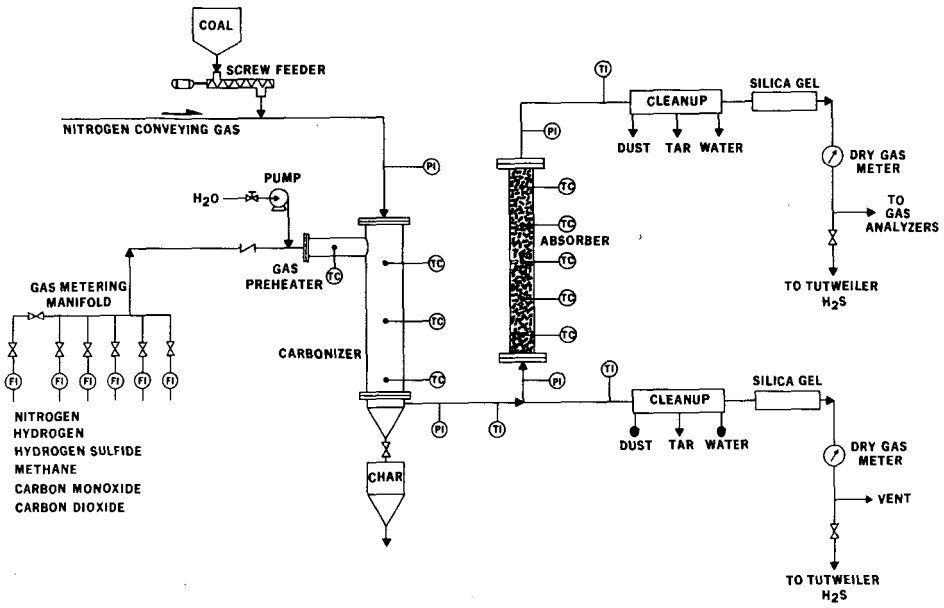

FIGURE 1. — Flow Diagram of Apparatus for Measuring Sorption Capacity

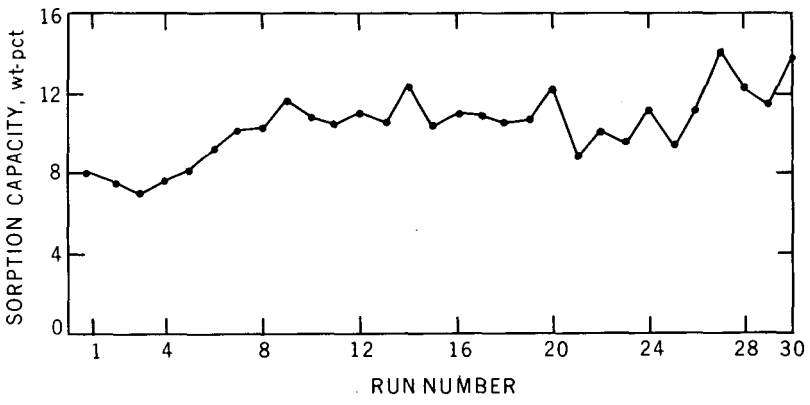

FIGURE 2. — Sorption Capacities Achieved During Thirty Absorption Regeneration Tests

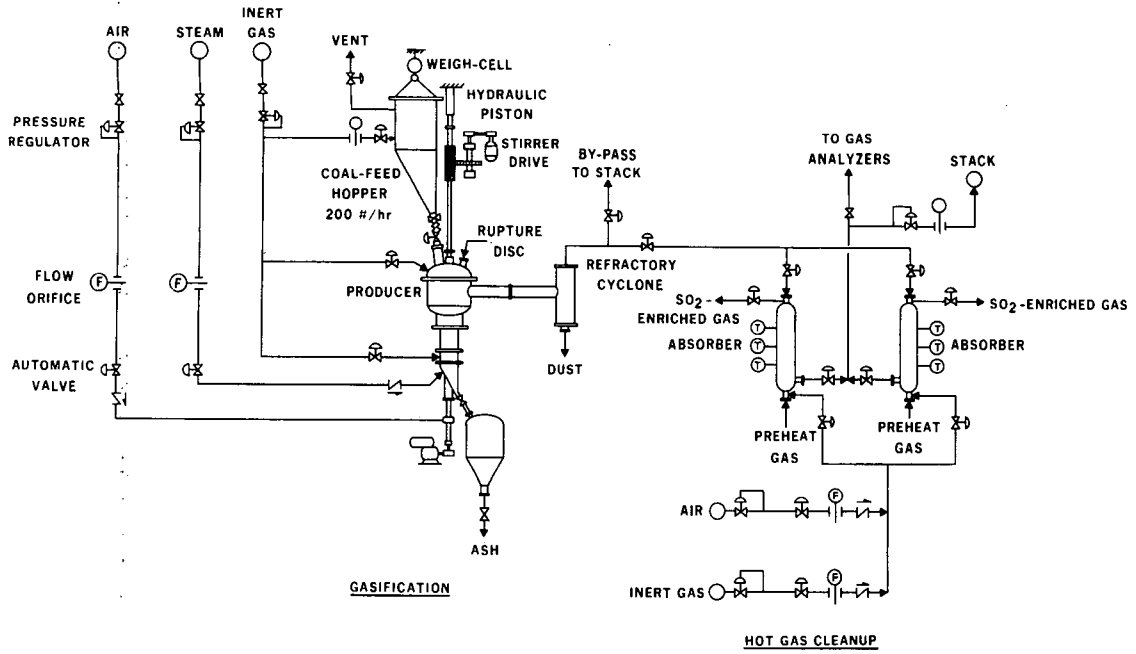

FIGURE 3. — Bench Scale Producer and Hot Gas Cleanup Facility.

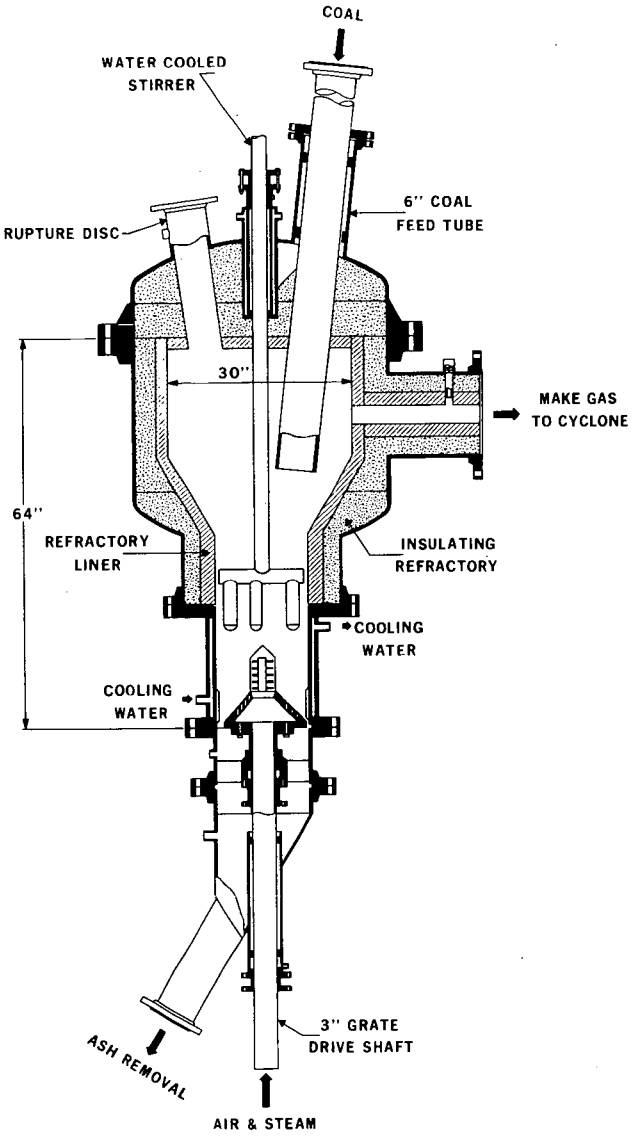

FIGURE 4. — 16-inch Gas Producer for Bench Scale Hot Gas Cleanup Facility. 88

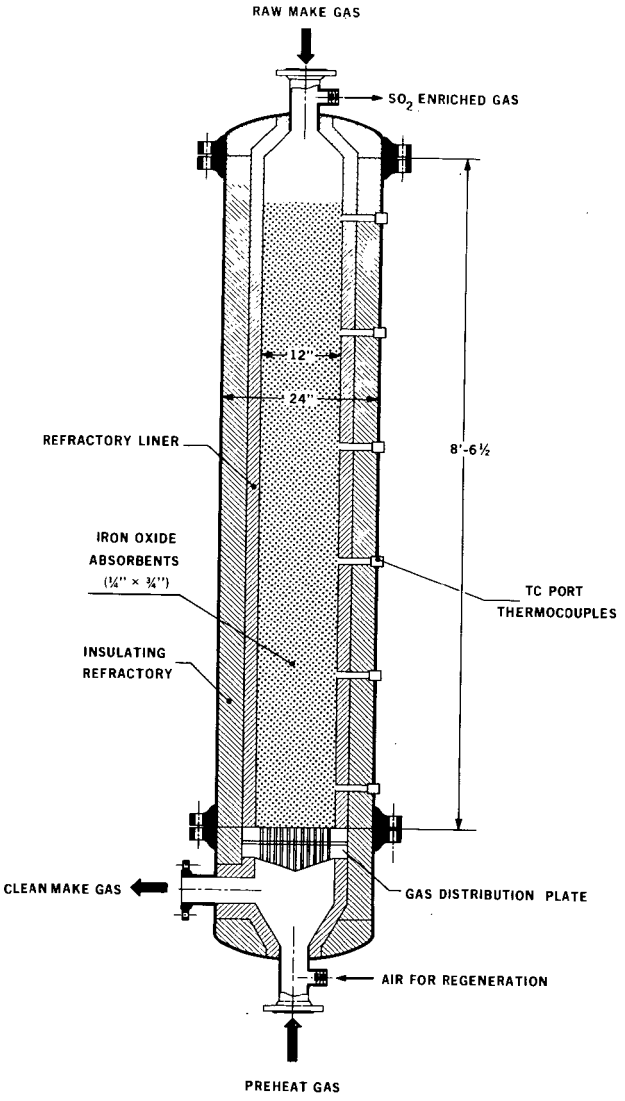

FIGURE 5. — 12—inch Absorber Vessel for Bench Scale Hot Gas Cleanup Facility.

Sorbent Composition	Physical Strength lb/cm	Surface Area m^2/gm	H_2S Sorption Capacity wt.-pct.
55% silica + 45% Fe_2O_3	75	2.5	16.1
55% silica + 45% Fe_2O_3 + 1% bentonite	31	4.3	14.5
55% silica + 45% Fe_2O_3 + 6 ml sodium silicate/lb	68	2.1	22.8
75% fly ash + 25% Fe_2O_3	16	0.9	11.5
75% fly ash + 25% Fe_2O_3 + 1% bentonite	59	1.5	10.5
75% fly ash + 25% Fe_2O_3 + 10 ml sodium silicate/lb	69	---	10.4

TABLE 1 — Data Indicating Effect of Additives On Sorption Capacity and Physical Strength

Total gas flow, std. cu. ft.	Gas flow rate, std. cu.ft./hr.	Run duration, hr.	Space velocity, vol/vol/hr	H_2S absorption			Total quantities through bed	
				Total grains	wt.-pct.	Efficiency pct.	Tar, gms	Dust, gms
89.62	14.27	6.28	501	1118	10.35	92.5	31.5	.2
91.83	15.97	5.75	563	1193	11.04	95.0	30.8	.6
94.14	16.37	5.75	570	1180	10.92	93.5	28.2	.4
90.07	16.38	5.50	587	1135	10.51	93.1	33.5	.5
91.40	15.23	6.00	529	1159	10.73	94.2	32.3	.5
109.38	15.09	7.25	549	1332	12.33	92.2	33.4	.5

TABLE 2 — Typical Data From Six of Thirty Sorption Capacity Tests

Average Bed Temp.	616°F	672°F
Time to breakthrough, hrs	4.66	5.60
Producer gas flow rate, scfh	7500.00	7322.94
Space velocity, vol/vol/hr	2500	2450
Gas to breakthrough, scf	34,975	40,992
Total H_2S absorbed, grams	6544.8	7711.2
Weight percent	6.43	7.60
Percent of total (using 100 grains/100 scf as breakthrough)	82.61	82.07

TABLE 3 — Sorption Data Obtained During Regeneration Study on Bench Scale Hot Gas Cleanup Facility

HIGH TEMPERATURE SULFUR REMOVAL SYSTEM DEVELOPMENT FOR THE WESTINGHOUSE FLUIDIZED BED COAL GASIFICATION PROCESS

D. L. Keairns, R. A. Newby, E. P. O'Neill, D. H. Archer
Westinghouse Research Laboratories
Pittsburgh, Pennsylvania 15235

ABSTRACT

High temperature sulfur removal can be achieved with calcium based sorbents (e.g. dolomite) in fluidized bed coal gasification systems now being developed for power generation. The use of dolomite offers the opportunity to meet environmental emission standards, to minimize energy losses, and to reduce electrical energy costs.

In addition to achieving the removal of sulfur from the low Btu gas, the complete sulfur removal system must be integrated with the total power plant and environment to assure compatibility. Critical requirements to achieve a commercial system include establishing criteria for "acceptable" sorbents, establishing integrated sulfur removal/gasification process design parameters, predicting trace element release, predicting sorbent attrition, developing an economic regeneration and/or once-through process option, developing a spent sorbent processing system, and establishing safe and reliable disposition options for spent sorbent. Design and operating parameters are being developed and potential process limitations identified.

This work is being performed as part of the Westinghouse Coal Gasification Program. The project is being carried out by a six-member industry/government partnership comprising ERDA, Public Service of Indiana, Bechtel, AMAX Coal Co., Peabody Coal Co. and Westinghouse. This work has been funded with federal funds from the Energy Research and Development Administration under contract E(49-18)-1514. The content of this publication does not necessarily reflect the views or policies of the funding agency.

INTRODUCTION

The production of a low Btu fuel gas from coal for combined cycle electric power generation provides the potential for improved thermal efficiency and reduced power costs compared with conventional power plants with flue gas desulfurization and can provide acceptable environmental impact. The ability to produce the low Btu gas at elevated pressure (e.g. 1500 kPa) with removal of sulfur and particulates from the high temperature gas (e.g. 800-900°C) will enable the maximum thermal efficiency to be achieved. Calcium-based sorbents, such as limestone and dolomite, have been proposed for the high temperature sulfur removal.

Westinghouse has been working on the development of a multi-stage fluidized bed gasification process for combined cycle power generation since 1970.[1,2] The goal of the program is the integration and operation of a gasifier/power-generating plant on a scale which will demonstrate the commercial operation of the process. An integrated program is underway to proceed from bench-scale laboratory research through pilot scale development and system design and evaluation to the operation of a demonstration plant. The pilot development is now being carried out in a 15 ton/day process development unit.

Westinghouse is investigating gas cleaning systems for high temperature operation (800-900°C), intermediate temperature operation (e.g. 650°C), and low temperature operation. Work has been carried out on both sulfur removal and particulate control systems. This document is limited to an overview of the high temperature sulfur removal system development work on calcium-based sorbents. This system was selected for the base concept based on the potential for high system efficiency and the high kinetic efficiency of removing hydrogen sulfide under the proposed operating conditions with an economically available sorbent. Alternate systems, such as the use of iron oxide or low temperature processes, have not been excluded as candidates for the demonstration plant and are also being studied. An intermediate temperature process is attractive in that it reduces the materials problems while maintaining a relatively high plant efficiency.

The approach to the development of the calcium-based sulfur removal system includes laboratory experimental programs utilizing pressurized thermogravimetric analysis, pressurized fluidized bed reactors, and physical and chemical characterization to develop basic data and to develop screening techniques; data analysis to develop design criteria; systems analyses to assess the technical, economic, and environmental impact of alternate sulfur removal system concepts and to assess the impact of these alternatives on the total power plant.

SULFUR REMOVAL SYSTEM

The basic gasification process utilizing the high temperature calcium-based sorbent system is illustrated in Figure 1. The gasification process has been described.[1,2] The sulfur removal process options are indicated in Figure 1: in-bed desulfurization and external desulfurization. In situ desulfurization of the fuel gas within the recirculating bed devolatilizer combines the sulfur removal and coal devolatilization in a single vessel. This approach requires compatible coal and sorbent behavior and the ability to separate sorbent and char. The external desulfurizer requires a separate vessel and associated components but provides greater flexibility. Both systems are being assessed through process simulations, PDU operation, and engineering analyses.

Two basic sulfur removal systems have been identified and investigated: once-through sorbent operation and regenerative operation. The reference once-through system and regenerative system concepts are illustrated in Figure 1. An alternate once-through system concept is also indicated which has been considered. A number of spent sorbent processing and regeneration processes have been investigated. Similarly, a number of disposal and utilization options are available. These process alternatives will be discussed in the following sections. Other options such as pretreatment of the sorbent to improve its attrition behavior or sulfur capacity and the addition of "getters" to remove alkali metals to prevent gas turbine corrosion are also being considered.

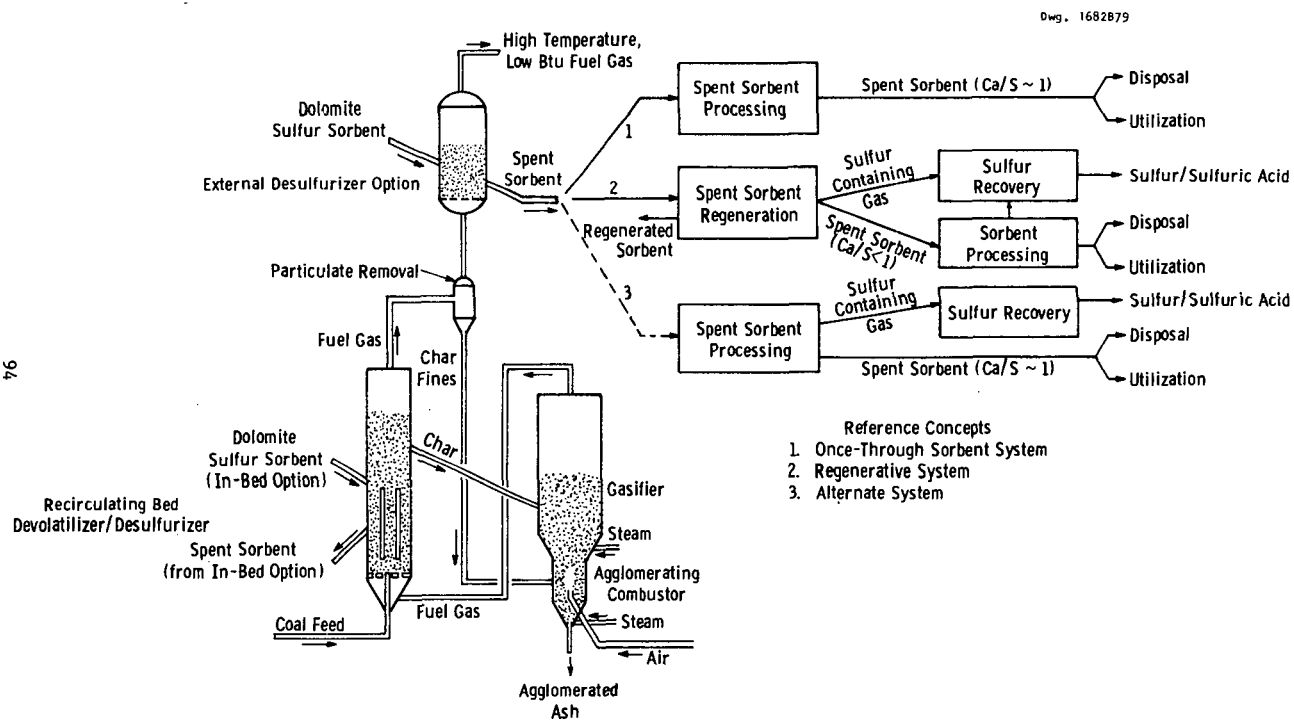

Fig. 1—Westinghouse multistage fluidized bed gasification/desulfurization process utilizing calcium-based sulfur removal system

SULFUR REMOVAL

Laboratory and engineering studies are being carried out to evaluate two areas critical to sulfur removal: sulfur removal process options and sorbent selection. These efforts parallel development work planned for the process development unit related to these areas.

Process Options

The technical and environmental performance and economic aspects of sulfur removal process options are being evaluated in order to provide a basis for selection and to define process development requirements. Two major options have been identified: once-through sorbent operation versus regenerative sorbent operation and in situ (devolatilizer) desulfurization versus external dessulfurization.

Both once-through sorbent and regenerative sorbent desulfurization behavior are being developed. The PDU is currently designed for once-through sorbent operation. Trade-offs between once-through and regenerative sulfur removal exist with factors such as sorbent consumption, sorbent attrition, trace element release, and system complexity and operability being important considerations.

Sorbent Selection

Both limestone ($CaCO_3$) and dolomite ($MgCa(CO_3)_2$) can be used as sulfur sorbents under full gasification conditions at high fuel temperatures, but laboratory studies show that there are several factors which restrict their use under specific design conditions, and which impact on both the desulfurization process, and the overall power generation plant.

Limestone reacts with hydrogen sulfide only when it has calcined, a kinetic rather than a thermodynamic restriction.[3] For atmospheric pressure applications, calcined limestone should achieve 90% desulfurization of fuel gases at calcium to sulfur molar feed ratios of $\sim$1.8/1.[4] Recent fixed-bed tests by the Bureau of Mines confirm this projection.[5] However for desulfurizing low Btu gas at pressure, calcium carbonate is the stable form of the reacting sorbent, and limestone is inactive.[6]

For dolomite, at Ca/S feed ratios of < 1.2/1.0, projections from laboratory data show that almost complete reaction of the calcium content may be attained while fixing 90% of the fuel sulfur in solid form, for particle sizes up to 2000 microns.[7] For larger particle sizes reaction is apparently limited by diffusion of reactant into the solid. No significant variation was noted in testing dolomites ranging from the relatively pure massive-grained Canaan dolomite (Connecticut), through the sucrose-type dolomites (Glasshouse, Ohio), to the impure Tymochtee dolomite (Ohio).[2c] Fluidized-bed tests by Conoco Coal Development Co.* have demonstrated the excellent sulfur capture abilities of dolomite with simulated fuel gases.[8] The Bureau of Mines tests showed that half-calcined dolomite demonstrated improved sulfur removal at 1500°F over that noted at 1400°F.[5] However when they increased the desulfurizing temperature to 1600°F, they noted a drastic loss of desulfurizing action as the dolomite decomposed to the fully-calcined state. While this test has not been simulated in laboratory tests, precalcined dolomites have shown similar sulfidation reaction rates to those noted with half-calcined dolomite. Further tests are evidently required to explore this discrepancy.

The major limitations on using dolomites arise from trace-element emissions, attrition rates, and suitability for processing by direct air oxidation for disposal.

One of the major concerns in operating a gas turbine with the low Btu gas is the extent to which corrosion and erosion will limit the lifetime of the metal alloys used in the blades and stators.[2c] The alkali metals, particularly sodium, induce hot corrosion (accelerated oxidation or sulfidation attack of the metal) by depositing oxygen-excluding liquid films of sulfates on the metals. Dolomites contain sodium and potassium as impurities, and they are found both as clay mineral components, and as more volatile compounds - probably chlorides, in the carbonate rock. The range of these impurities in dolomites is enormous, e.g. Na (5-330 ppm), and K(5-6,500 ppm).[2c] Recent studies

* Conoco Coal Development Co. and Consolidation Coal Co. are used in this paper. Consolidation Coal Co. is used when work was performed under that organizational name.

of the release of alkalis from dolomites into fuel gas have demonstrated that significant fractions of the alkali can enter the gas stream, and that this release is essentially complete within a short fraction of the expected sorbent residence times.[2c] The resulting alkali level in the turbine feed gas is substantially in excess of that permitted by current empirical specifications for oil-fired turbines (~10 ppb Na). There are several approaches which may be taken to avoid this problem. First of all, a low-alkali dolomite may be chosen as sulfur sorbent. This is likely to be the result of an unusually fortuitous selection of power plant site. Although the available analysis of dolomites show significant variations in alkali content within a particular geological stratum from quarry to quarry and from stratum to stratum within a quarry, the majority of the analyses are of sufficient vintage to be suspect. However we have noted a consistant increase in alkali content with increasing quarry depth, so that material quarried at a depth of 100 ft may contain one order of magnitude more alkali than that quarried near the surface.[9]

An alternative to selecting a "clean" dolomite, is to pre-heat the material to release the alkalis before using the stone as a sulfur sorbent. The bulk of the alkali release occurs within 20 minutes of heating the stone to ~870°C, and after this initial release the rate of alkali loss is extremely low. The third possibility is to add materials such as aluminosilicates to the sorbent bed, or at a particulate filtration stage to getter the alkalis. It should be emphasized that several critical questions cannot be satisfactorily answered without further research. The extent to which chlorine from the coal may strip alkalis from dolomite and coal char must be investigated. In addition the turbine tolerance to the combined presence of sodium and potassium requires further experimental and theoretical investigation.[2c] The chemical fate of minor elements such as the alkalis in coal gasification is not well known. Recent studies at the Bureau of Mines show considerable

release of chlorine to the gas phase - presumably as HCl.[2c] However the mass balance for alkalis in the input and output solids was not sufficiently precise to estimate the levels of alkali in the gas phase.

It should also be noted that the turbine tolerance to alkalis is theoretically a function of total chlorine (as HCl) levels in the gas phase. The combination of high chlorine and high alkali levels may avoid corrosive sulfate deposits. This apparent advantage will be limited by direct gaseous attack of the protective oxide scales on the turbine alloys.

SORBENT REGENERATION

The consumption of sorbent by the power plant sulfur removal system may be minimized by utilizing a processing step to regenerate the utilized sorbent to an active form. Ideally the sorbent would be entirely reconstituted by the regeneration process, but in reality fresh sorbent will be required due to deactivation of the regenerated sorbent and attrition losses. Regeneration of the sulfided sorbent requires that the captured sulfur be converted to some other form, preferably elemental sulfur of commercial quality. The purge stream of spent sorbent must be processed to some environmentally acceptable or useful form. This combination of functions, sorbent regeneration-sulfur recovery-spent sorbent processing, must result in an integrated process which is compatible with the coal gasification process and is economically and environmentally acceptable.

Regeneration Process Options

A variety of potential regeneration process concepts have been evaluated for technical feasibility. Two concepts have been selected for further engineering assessment: (1) Sorbent regeneration by reaction of sulfided sorbent with steam and carbon dioxide to generate carbonated sorbent and a hydrogen sulfide gas stream; (2) sorbent regeneration by reaction of sulfided sorbent with oxygen to generate the oxide form of the sorbent and a sulfur dioxide gas stream. The chemical reactions are written, respectively.

$$CaS + H_2O + CO_2 \rightleftharpoons CaCO_3 + H_2S \qquad (1)$$

and

$$CaS + 3/2\ O_2 \rightleftharpoons CaO = SO_2 \qquad (2)$$

Steam and CO_2 Regeneration Scheme

A schematic flow diagram for the sorbent regeneration system based on the steam and CO_2 regeneration reaction is shown in Figure 2. This process is also being evaluated by Consolidation Coal.[8]

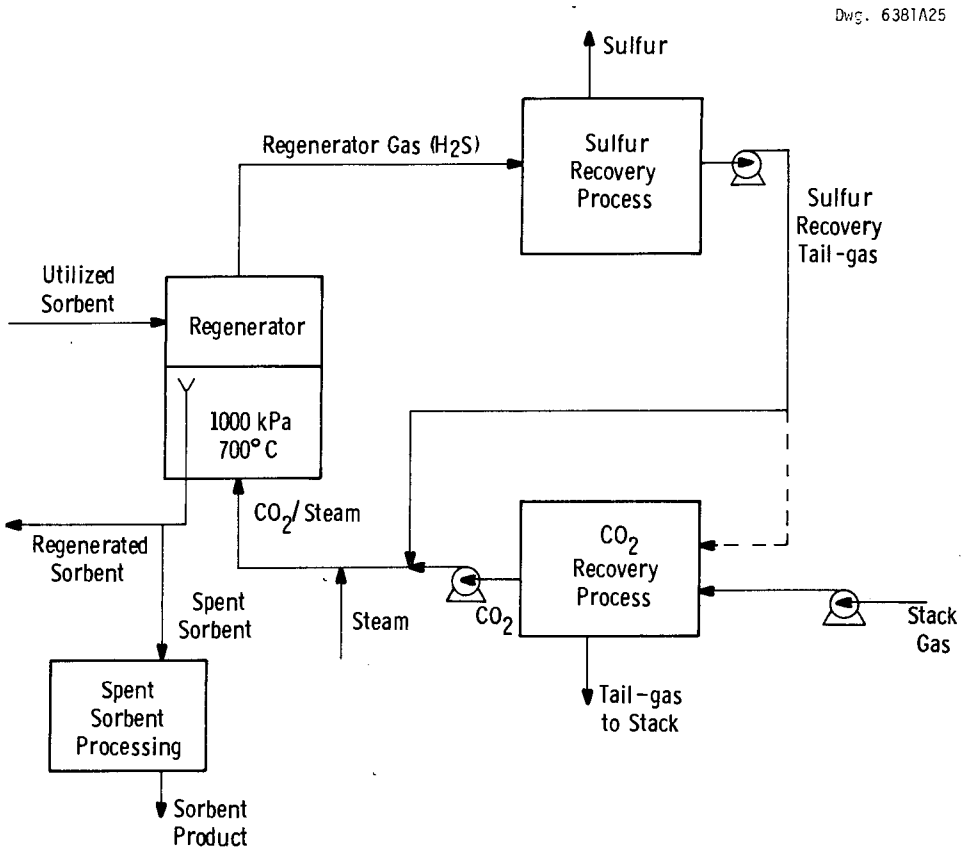

Fig. 2 — Sorbent regeneration by steam and CO_2 reaction

Three major components are involved in the sorbent regeneration system: the regenerator reaction vessel, the sulfur recovery process and the CO_2 recovery process. A number of commercial processes are available for sulfur recovery from H_2S gas streams. The specific process selection will depend largely on two factors - the level of H_2S in the regenerator gas and the optimum scheme for steam and CO_2 utilization. An H_2S volume percent of about 15% will permit the application of conventional Claus process technology. Lower H_2S concentrations will require either preliminary concentrating of the H_2S-gas, followed by Claus sulfur recovery, concentrating and recycle of the Claus plant tail-gas, or application of alternate sulfur recovery processes suitable for low H_2S concentrations such as the Stretford process (Ralph M. Parsons Co. and Union Oil Co. of California).

Make-up CO_2 for the regeneration reaction can be supplied by power plant stack gas purification. A portion of the sulfur recovery tail-gas may also require purification in order to maintain low levels of impurities (N_2, O_2, etc.) in the CO_2/steam reactant stream. Numerous commercial processes are available for CO_2 recovery - Selexol, Benfield, Catacarb, Sulfinol, and many others. The economics and environmental performance of each of these processes will differ for this application and require evaluation.

The single most important factor influencing the economics and performance of this regenerative scheme is the regenerator gas H_2S concentration. The size of the regenerator reaction vessel, the size and complexity of the sulfur recovery process, and the rate of steam consumption and auxiliary power usage all increase as the H_2S concentration is reduced. Estimates of the H_2S concentration based on reaction kinetics and thermodynamics are about 3-5 volume %.

Other factors such as regenerated sorbent activity, the required rate of sorbent circulation, the effect of the regeneration process on the power plant availability, etc., are also important to the process feasibility.

Oxygen Regeneration Scheme

A schematic flow diagram of the sorbent regeneration system based on the oxygen regeneration reaction is shown in Figure 3. An atmospheric pressure version of this process has been applied by Esso (U.K.) for their CAFB gasification process.[10]

This regeneration process is conceptually simpler than the steam/CO_2 regeneration process since only two major process components are involved: the regenerator reaction vessel and the sulfur recovery process. On the other hand, the oxygen regeneration process is necessarily a higher temperature regeneration scheme with the potential for greater sorbent deactivation. The regenerator could be operated at pressures of 200 to 1000 kPa (2 to 10 atmospheres) and temperatures of 1000 to 1100°C with SO_2 volume percents of 2 to 4 expected for the high pressure system and up to 10% for the low pressure system.

Sulfur recovery from dilute SO_2 streams is generally more expensive and complex than from dilute H_2S streams. The most highly commercialized sulfur recovery process for this application is the Allied Chemical direct reduction process (using methane or clean liquid fuels as reductant) which will work effectively on SO_2 streams down to about 4 volume % SO_2 depending upon the oxygen content of the gas.[11] For lower SO_2 concentrations a commercial concentrating step such as the Wellman-Lord process must be used. Other sulfur recovery processes applicable to SO_2 streams which are in early stages of commercialization are the Foster Wheeler RESOX process (which uses coal as the SO_2 reductant), the ASARCO-Phelps Dodge process, the Bureau of Mines Citrate process, the Westvaco activated carbon process, and the Stauffer Aquaclaus process.

While the low pressure oxygen regeneration results in a much greater SO_2 concentration in the regenerator gas, the technological and reliability problems involved in circulating the hot sorbent between vessels with greatly different operating pressures may not be easily overcome. Again, as in the steam/CO_2 regeneration process,

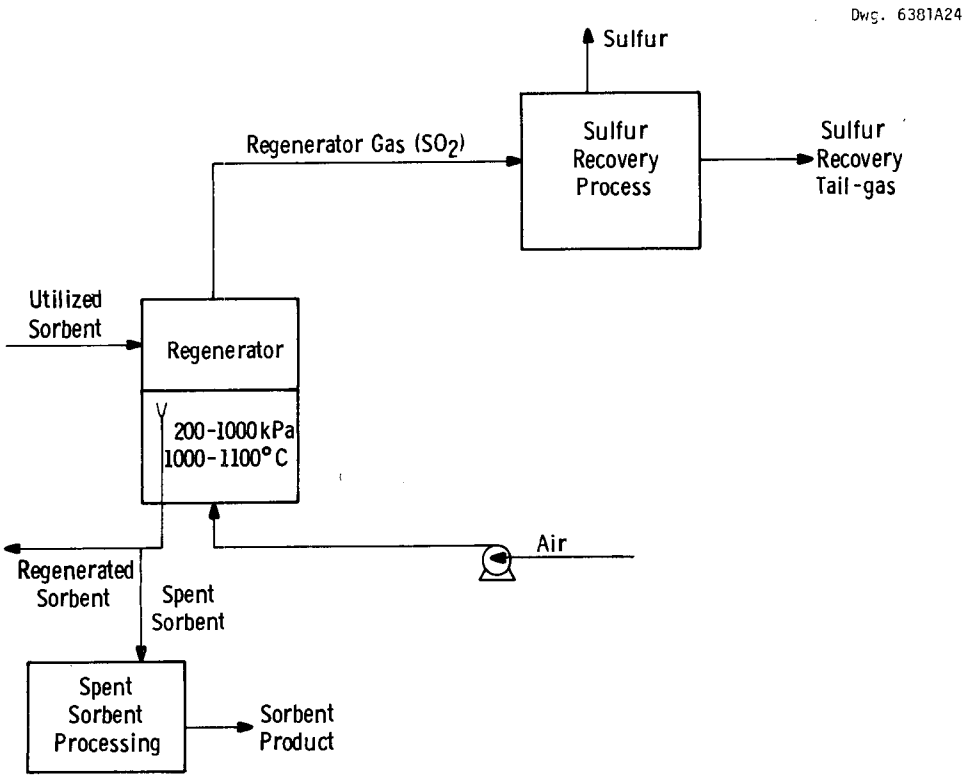

Fig. 3 – Sorbent regeneration by oxygen reaction

the concentration of the sulfur-bearing species in the regenerator gas has a dominant influence on the economics and performance of the regeneration system. Increased operating temperatures will provide greater SO_2 concentrations (thermodynamically) but may increase sorbent deactivation.

The overall economics, technical performance and environmental impact of these two sorbent regeneration concepts must be evaluated in order to determine the feasibility of sorbent regeneration, in order to select the most promising regeneration scheme and in order to identify the optimum components to be utilized in the regeneration scheme. The critical interfaces between the coal gasification system, the power generation system, the spent sorbent processing system and the sorbent regeneration system are being considered in the evaluation.

Regeneration Chemistry

It was noted by Mellor[12] that the equilibrium $CaS + H_2O + CO_2 \rightleftharpoons CaCO_3 + H_2S$ cannot be used to reform calcium carbonate, because of the low concentration of hydrogen sulfide produced. This problem may be overcome by carrying out the reaction at pressure.[13] However the early work by Pell[14] showed that calcium sulfide is rapidly deactivated, and TG studies show that only 20% of the calcium sulfide is readily converted to calcium carbonate after 10 cycles of sulfidation/regeneration, at 704°C.[b]

An encouraging feature is that the rate of sulfidation decreases very slowly as the stone is recycled and the regenerated sorbent is almost as reactive as fresh stone.[6]

The initial rate of regeneration is very fast and is apparently limited by production of the equilibrium level of hydrogen sulfide, since the initial rate increases on dropping the temperature from 700°C to 650°C. However, when the regeneration has proceeded to a certain stage (50% after 2 cycles, or 20% after 10 cycles), the rate

falls off by more than one order of magnitude. At this stage the rate can be increased by increasing the reaction temperature, so that at 870°C, all the sulfide is readily regenerated. However, the equilibrium concentration of H_2S becomes so unfavorable that this is not a technically feasible solution.

The deactivation of calcium sulfide thus becomes a chemically limiting step in regeneration. An additional clue to the mechanism of deactivation is given by the fact that when calcium sulfide is prepared by reduction of calcium sulfate, at 820 or 850°C, for 2 hours, only 26% of the calcium sulfide is regenerable.[15] This increased deactivation may be partly due to the longer residence time at higher temperatures than is customary in sulfidation reactions, since sulfidation takes about 15 minutes. Recent studies by Sun[16] have shown that longer exposure at high temperatures (871°C) during sulfidation, reduces the extent of regeneration, as does increasing the temperature of sulfidation to 950°C, while lowering the sulfidation temperature to 750°C increases the extent of regeneration. The deactivation of the calcium sulfide is always accompanied by some growth of calcium sulfide particle size, and by extensive growth of magnesium oxide crystallites in proximity to the calcium sulfide as determined by X-ray diffraction line-widths.

It can be concluded that a continuous regeneration system must operate with a low sulfur differential between the calcium sulfide content of the desulfurizer and regenerator exit streams.

Squires[17] has demonstrated that the extent of regeneration improves dramatically with partial pressures of steam of 15 atmospheres, and that 50% of the calcium sulfide is regenerable. While his sulfidation reaction conditions (700°C) may not have been severe enough to cause growth of the magnesium oxide around the calcium containing crystallites, the improved diffusivity of the reactant gases through the solid caused by raising the H_2O/CO_2 ratio may significantly improve the extent of regeneration before the reaction rate dwindles. Pell's

experiments carried out at a 1/1 ratio at 15 atm indicate little if any improvement over the TG value for extent of regeneration. The average extent of regeneration for 20 cycles is ∿13%, so that each mole of calcium will remove 2.7 moles of sulfur via the regenerator, and one mole of sulfur via the spent sorbent stream.

The calcium to sulfur molar make-up feed rate required is therefore 0.25/1 unless attrition losses are greater than 5% of the total calcium per cycle, in which case reducing the attrition loss becomes more important than improving the regenerability of the stone. Consolidation Coal Co.[8] have reported attrition loss rates of less than 1% per cycle; however it is not known if such performance can be projected to large scale units.

SPENT SORBENT DISPOSITION

The once-through and regenerative process options will produce a dry, partially utilized dolomite or limestone with particles up to 6 mm in size. In addition, fine particles of sorbent (with some ash and char) will be collected in the gas particulate collection systems. The composition of the sorbent for disposition will depend on the characteristics of the original stone, the coal feed, the selection of the sorbent processing system, and the process operating conditions. The major compounds in the waste stone from the desulfurizer or regenerator utilizing dolomite are calcium carbonate ($CaCO_3$), magnesium oxide (MgO), and calcium sulfide (CaS). Trace elements from the sorbent and coal will also be present.

Direct disposal or utilization of this material is not considered to be an option which will be generally available. Thus, processing of the spent sorbent has been incorporated in the sulfur removal system. The ultimate selection and development of a spent sorbent processing scheme will depend on many factors related to the development of the desulfurization system and the regeneration system. These factors will determine the nature of the spent sorbent and the processing required for the spent sorbent processing system. Among the factors that will affect the disposition of the sorbent are the quantity of spent sorbent, its chemical characteristics, regulations, geographical location, and the market size in the case of utilization.

Processing

A variety of spent sorbent processing schemes have been identified which could potentially convert the spent sorbent produced in a once-through or regenerative operation into a material suitable

for direct disposal or utilization.[4,19] Processing alternatives have been developed to convert calcium-based sorbents containing calcium sulfide to environmentally acceptable forms for disposal or utilization. Work by Westinghouse on the CAFB fluidized bed gasification/desulfurization process, under contract to EPA, has identified spent sorbent processing options.[4] Experimental programs are now being carried out as an extension of this work to permit technical and economic assessments of these processes. These tests will provide information directly applicable to the subject coal gasification/desulfurization process. Spent sorbent processing systems being considered include dry oxidation, oxidation plus carbonation, deadburning, slurry carbonation, dry sulfation, high temperature processing with coal ash, and low temperature processing with coal ash.

A dry oxidation process which converts the spent sorbent (calcium sulfide) from a once-through or regenerative operation into a calcium sulfate material has been selected as the base spent sorbent processing scheme. Experimental studies and process studies for the dry oxidation process are being performed as part of the current program.

Thermogravimetric studies of the direct oxidation of calcium sulfide to calcium sulfate have revealed some important features of the reaction which must be considered in process evaluation.

First, in most dolomitic stones, complete oxidation of the sulfided stone occurs rapidly in air at 800°C, while sulfided limestones containing more than 30 molar % CaS and the sulfides of large-grained dolomites are oxidized incompletely.

Secondly, the reaction is extremely exothermic, $\Delta H_{298} = -912$ kJ mole^{-1}, and if the temperature of the reacting solid is permitted to rise to higher temperatures, sulfur dioxide will be

emitted by one of two mechanisms. In the first mechanism direct oxidation to the oxide may occur: $CaS + 3/2\ O_2 \rightarrow CaO + SO_2$. However if low partial pressures of oxygen are developed in the system as a result of the primary reaction, then calcium sulfide and calcium sulfate interact to reject sulfur dioxide according to the reaction

$$3\ CaSO_4 + CaS \rightarrow 4\ CaO + 4\ SO_2.$$

By carrying out the oxidation reaction in a fluidized bed reactor at 800°C in excess air, both of these competing reactions may be avoided. In thermogravimetric tests at 800°C, sulfur dioxide transients in the exit gas stream were accompanied by temperature excesses. Typically 32 moles of cold air per mole of calcium are required for heat balance in a system operating at a 2/1 calcium to sulfur mole ratio in the desulfurizer. Because of the large excess of air entering the system, >3X stoichiometric, the particles should oxidize at much the same rate as they do in the TG apparatus; stone residence times greater than 30 minutes are projected to ensure that oxidation is almost complete (>90%).

The third feature of this reaction is that regenerated stone which has experienced multiple sulfidation/regeneration cycles is not completely oxidizable. A function of the calcium sulfide which is inert in the regeneration reaction is also inert in the oxidation reaction.

Based on the information available, the dry oxidation process is considered attractive for once-through operation with most dolomites. This process does not appear as attractive for once-through operation with limestones or for regenerative operation. The primary concern is the environmental impact from sorbent disposal. Further work is required to permit a comprehensive assessment of dry oxidation. Work is proceeding to investigate other processing options.

Disposal

The environmental impact of any disposed material is a function of its physical and chemical properties and the quantity involved. Two disposal alternatives will be investigated: land and ocean dumping. Environmental impact tests are planned to study the direct disposal of material from the spent sorbent processing system. These tests will be carried out using material produced in laboratory units to investigate the affect of operating conditions and in the process development unit to determine the environmental impact from material produced in the integrated process.

Westinghouse has carried out environmental impact tests on related materials as part of the CAFB fluidized bed gasification and the fluidized bed combustion programs being carried out under contract to EPA.[4,18,19,20] Leaching and activity tests have been developed at Westinghouse to assess the potential water contamination and heat release from disposing a spent bed limestone directly from a gasification process and from the spent limestone after further processing. These studies indicate the leachability and activity can be significantly reduced by further processing. Spent dolomite from fluidized bed combustion processes has also been tested[18] which indicates that if the calcium sulfide in the dolomite can be converted to calcium sulfate through the dry oxidation process, the material will be environmentally acceptable.

Utilization

The direct disposal of sorbent may not be possible or permitted in all cases. Utilization of spent sorbent is an alternative which has the potential to provide technically and economically attractive by-product. Potential applications of processed or unprocessed spent sorbent include soil stabilization, land fill, concrete, refractory brick, gypsum, municipal waste treatment. Preliminary work has been carried out in this area.[4,20,21]

ASSESSMENT

High temperature sulfur removal with a fluidized bed coal gasification system appears attractive based on available information. A number of processing options are being developed which consider integration of the sulfur removal system with a low Btu gasification - combined cycle power plant and consider the total sulfur removal system from sorbent selection to sorbent disposition. Assessment of the sulfur removal system includes:

Sulfur Removal: Dolomites are the preferred sorbent for the Westinghouse coal gasification process. Sulfur removal efficiencies of 90% are projected with mean particle sizes between 1000 and 2000 μ and a calcium to sulfur molar ratio of 1.2/1.0 for a once-through system. Combined devolatilization/desulfurization is considered attractive but compatibility must be demonstrated. The external desulfurizer option offers an alternative with greater flexibility. There appear to be ample supplies of dolomite available.

Sorbent Regeneration: Two regeneration concepts have been selected for further study. Regeneration by carbon dioxide and steam is technically feasible and is the preferred option. Calcium to sulfur molar feed make-up is projected to be 0.25/1 based on attrition losses < 5% of the sorbent per cycle. Commercial technology is available for sulfur recovery from dilute H_2S or SO_2 gas streams and for CO_2 recovery. Advanced systems, which may reduce costs, are not being incorporated into the current development effort.

Spent Sorbent Disposition: In general, spent sorbent processing will be required for once-through or regenerative operation due to the calcium sulfide present in the sorbent. Alternate processing schemes are under investigation to permit disposal or utilization of the material.

A dry oxidation process is attractive for once-through operation with most dolomites. Preliminary oxidation tests and environmental impact tests indicate this processing option will be economic and environmentally acceptable. Preliminary tests on related materials indicates utilization of the spent sorbent may be practical.

Sorbent Selection: General factors to be considered in the selection of a sorbent are the desulfurization performance, the sorbent regenerability, the spent sorbent properties, sorbent attrition behavior and trace metals release behavior. Sodium, potassium, and chlorine release is of particular importance to control gas turbine corrosion. Trace metals release to the fuel gas may be controlled by selecting a "pure" sorbent, pretreating the sorbent or utilizing a getter in the fuel gas cleaning system. Available data indicate the trace elements can be controlled to meet turbine protection requirements. Further work is required to specify the preferred method of operation.

A once-through sulfur removal system utilizing dolomite with a dry oxidation spent sorbent processing system has been selected for the reference design. Further development evaluation of the technical performance, economics, and environmental impact of the alternative sulfur removal systems under consideration must be carried out to select the most promising system. The integration of the alternative processing schemes into an optimum high temperature sulfur removal system which is compatible with the coal gasification power plant is the object of the development effort.

REFERENCES

1. Archer, D. H., E. J. Vidt, D. L. Keairns, J. P. Morris, J. L. P Chan, "Coal Gasification for Clean Power Generation," Proceedings Third International Conference on Fluidized Bed Combustion, November 1972 (NTIS Number PB-231 977).
2. "Advanced Coal Gasification System for Electric Power Generation," Westinghouse Electric Corp., Contract reports to ERDA/FE:
   a) Interim Report No. 1, NTIS No. PB-236 971;
   b) Interim Report No. 2, NTIS No. FE-1514-T-4;
   c) Interim Report No. 3
3. O'Neill, E. P., D. L. Keairns, and W. F. Kittle, "Kinetic Studies Related to the Use of Limestone and Dolomite as Sulfur Removal Agents on Fuel Processing," Proceedings Third International Conference on Fluidized Bed Combustion, November 1972, NTIS No. PB-231 977
4. Keairns, D. L., R. A. Newby, E. J. Vidt, E. P. O'Neill, C. H. Peterson, C. C. Sun, C. D. Buscaglia, and D. H. Archer, "Fluidized Bed Combustion Process Evaluation - Residual Oil Gasification/Desulfurization Demonstration at Atmospheric Pressure," two volume contract report to EPA, March 1975, EPA report number EPA-650/2-75-027 a and b, NTIS No. PB-241 834 and PB-241 835.
5. Abel, W. T., and E. P. Fisher, "Limestone to Reduce Hydrogen Sulfide from Hot Produced Gas." U.S.E.R.D.A., MERC/RI-75/3, January 1976.
6. Keairns, D. L., E. P. O'Neill and D. H. Archer, "Sulfur Emission Control with Limestone and Dolomite in Advanced Fossil Fuel Processing," Symposium Proceedings - Environmental Aspects of Fuel Conversion Technology, EPA-650/2-74-118, October 1974.
7. O'Neill, E. P. and D. L. Keairns, "Selection of Calcium-Based Sorbents for High-Temperature Fossil Fuel Desulfurization," Paper presented at the 80th National A.I. Ch. E. Meeting, Boston, September 1975, to be published in AIChE Symposium Series Volume.

REFERENCES (continued)

8. Carran, G. P., J. T. Clancey, B. Pasck, M. Pell, G. D. Rutledge and E. Gorin, "Production of Clean Fuel Gas from Bituminous Coal," Consolidation Coal Co. report to EPA, EPA-650/2-73-049, December 1973.
9. Data Supplied by the Indiana Geological Survey.
10. Esso Research Centre, England, "Chemically Active Fluid-Bed Process for Sulfur Removal During Gasification of Heavy Fuel Oil," EPA-650/2-74-109, November 1974.
11. Hunter, W. D., Fedoruk, J. C., Michener, A. W., Harris, J. E., "The Allied Chemical Sulfur Dioxide Reduction Process for Metallurgical Emissions," in Sulfur Removal and Recovery from Industrial Processes, J. B. Pfeiffer, ed., American Chemical Society, Washington, D. C., 1975.
12. Mellor, J. W., "A Comprehensive Treatise on Inorganic and Theoretical Chemistry," Vol. III, Longmans, London, 1923.
13. Squires, A. M., "Cyclic Use of Calcined Dolomite to Desulfurize Fuels Undergoing Gasification," in "Fuel Gasification" Advances in Chemistry Series NO69, American Chemical Society, Washington, D. C., 1967.
14. Pell, M., Ph. D. Thesis, Chemical Engineering Department, The City University of New York, 1971.
15. Kearns, D. L., D. H. Archer, R. A. Newby, E. P. O'Neill, E. J. Vidt, Evaluation of the Fluidized Bed Combustion Process, Vol. I. Environmental Protection Agency, Westinghouse Research Laboratories., Pittsburgh, Pa., EPA-650/2-73-048 a. NTIS PB-231 162/9. December 1973.
16. Sun, C. C., Unpublished work, Westinghouse, 1976.
17. Squires, A. M., "Programs for Gasification of Coal in High Velocity Fluidized Beds and Hot Gas Cleaning," paper presented at Symposium "Clean Fuels from Coal", Institute of Gas Technology, Chicago, Illinois, June 1975.

REFERENCES (continued)

18. Sun, C. C. and D. L. Keairns, "Environmental Impact of Solid Waste Disposal from the Fluidized Bed Coal Combustion Process," paper presented at the San Francisco ACS Meeting, August 29 - September 3, 1976.

19. Keairns, D. L., C. H. Peterson, and C. C. Sun, "Disposition of Spent Calcium-Based Sorbents Used for Sulfur Removal in Fossil Fuel Gasification," paper for presentation at the Annual AiChE Meeting, Chicago, Illinois, November 1976.

20. Keairns, D. L., D. H. Archer, J. R. Hamm, S. A. Jansson, B. W. Lancaster, E. P. O'Neill, C. H. Peterson, C. C. Sun, E. F. Sverdrup, E. J. Vidt, and W. C. Yang, "Fluidized Bed Combustion Process Evaluation - Pressurized Fluidized Bed Combustion Development," contract report to EPA, September 1975; EPA report No. EPA-650/2-75-027c, NTIS No. PB-246 116.

21. Peterson, C. H., M. Gunnasekaran, and S. M. Ho, "Utilization of Spent Limestone from a Fluidized Bed Oil Gasification/ Desulfurization Process on Concrete," Proceedings Fifth Mineral Waste Utilization Symposium, Chicago, Illinois, April 1976.

REACTION OF H_2S WITH HALF-CALCINED DOLOMITE IN A REGENERABLE PROCESS

G. P. Curran, B. Pasek, M. Pell, and E. Gorin

Research Division
Conoco Coal Development Company
Library, Pennsylvania 15129

Introduction

The Conoco hot desulfurization process makes use of the reaction of half-calcined dolomite with H_2S,

$$CaCO_3 \cdot MgO + H_2S = CaS \cdot MgO + CO_2 + H_2O \qquad (1)$$

to remove H_2S from a fuel gas and also to regenerate sorbent dolomite. The Conoco gasification process yields a gas fairly high in H_2O, about 13%. This necessitates a high desulfurization temperature if a goal of 95% desulfurization is to be met. The conditions called for in the current design are as follows:

Desulfurization:	914°C; 13% H_2O, 8% CO_2 inlet; 0.02% H_2S exit
Regeneration:	704°C; 35% H_2O, 64% CO_2 inlet; 3.6% H_2S exit

The entire process runs at 15 atmospheres. Desulfurization operates at the equilibrium H_2S concentration, and regeneration is assumed to operate at about 90% approach to equilibrium. The above conditions provided the base case point about which experimental work was conducted. However, equipment limitations required the desulfurization temperature to be reduced to 871°C for most of our work.

Continuous Cycling Runs

Experiments were carried out in a three-inch diameter gas desulfurizer and a two-inch diameter regenerator. Both vessels contained fluidized beds and were continuously fed with both gas and solids. Details of the experimental technique have been given elsewhere.[1,2] Dolomite was cycled through the vessels for numerous cycles so that the nature of the decline in activity could be studied. Detailed data on the conditions of these cyclic runs are presented in Tables 1 and 2.

It was found that the desulfurization reaction proceeded rapidly, and that a low concentration of H_2S was maintained until the supply of $CaCO_3$ was essentially exhausted. However, the regeneration reaction was incomplete, typically yielding but a fraction of the original $CaCO_3$ in an hour's residence time.

The regeneration activity, defined as mols $CaCO_3$ produced/100 mols CaS fed, declined as the stone was cycled. The activity decline is pictured in Figure 1. It can be seen that the decline is logarithmic in character. Thus, although a severe decline occurs in cycles 1 to 10, the stone contains modest residual activity even out to 100 cycles. This means that a regenerable process is feasible. The data presented in Figure 1 are for Canaan dolomite, our base case stone. Similar data were obtained for other dolomites.

Figure 2 presents deactivation data for three regeneration temperatures. The data lines are roughly parallel, but this is believed to be fortuitous and unlikely to hold for all conditions. The data indicate that at 593°C, the fractional regeneration is quite low, amounting to less than 10% within only 7 cycles. Only at low regeneration temperatures is the equilibrium H_2S concentration high enough for processing by a conventional Claus process. The Conoco process, however, uses a liquid-phase Claus reaction which is uniquely suited to handling low H_2S concentrations. Out interest therefore centered around the 704°C temperature where stone utilization is higher.

TABLE 1

Conditions and Results for Gas Desulfurizer with Canaan Dolomite Feed

System Pressure: 15 atm (206 psig)
System Temperature: 871°C (1600°F)

Run Number	A7	A15	A16	A20A	A21	A22A	A36A
Canaan Dolomite Batch Number	← 1 →			← 2 →			
Acceptor Size Consist, Tyler Mesh	← 28 x 35 →			← 35 x 48 →			20 x 28
Feed Rate, gm/hr (half-calcined basis)	2950	3040	1500	1810	1840	1892	2120
Nominal Solids Residence Time, min	33	32	65	52	51	50	42
Input, SCFH(1)							
Recycle to Bed	175	178	178	148	148	148	310
H_2O	33	33	33	21	21	21	60
H_2	40	40	40	25	25	25	55
CO	33	33	33	23	23	23	62
CO_2	21	21	21	8.8	8.8	8.8	21
N_2	96	96	96	66	66	66	152
H_2S	3.5	3.5	1.8	1.6	1.6	1.6	1.8
Purges (CO_2) to Bed	← 5 →						
Purges (N_2) above Bed	← 15 →						
Recycle Acceptor Lift Gas, above Bed	← 71 →						110
Output in Cycle No.	2	6	1	23	18	8	4
Exit Gas Rate, SCFH (dry basis	215	213	215	143	144	144	338
Composition, Mol %							
H_2	17	17.5	18.2	16.5	16.6	16.6	17.5
CO	18	17.9	18.0	17.0	16.8	16.1	17.0
CO_2	12	9.9	9.7	9.8	9.9	10.3	9.4
N_2	53	54.4	54.0	56.6	56.3	57.0	56.0
H_2S	0.05	0.207(2)	0.048	0.03	0.03	0.03	0.04
Outlet Gas, Top of Bed							
Composition, Mol %							
H_2O	9.7	10.0	9.5	8.1	8.0	8.5	8.3
H_2	15.4	16.4	17.1	16.0	16.1	16.0	16.5
CO	15.9	16.8	16.9	16.5	16.3	15.5	16.0
CO_2	11.2	9.3	9.2	9.5	9.6	10.0	8.9
N_2	47.7	47.3	47.3	49.9	49.6	50.0	50.3
H_2S	0.046	0.194	0.045	0.029	0.029	0.029	0.038
Flow Rate, SCFH, Top of Bed	416	418	418	300	301	303	690
Fluidizing Velocity, ft/sec	0.60	0.60	0.60	0.43	0.43	0.43	0.99
Attrition, % of Feed Rate	0.7	0.77	0.89	0.68	0.84	0.48	1.4(3)
Duration of Circulation with H_2S Feed, hr	25.2	35.1	42.7	117	145	89	71
Removal of Feed Plus Recycle Sulfur, %	95.3	79	90	94.6	94.6	94.5	86.7
% H_2S in Outlet/Equilibrium % H_2S	1.4	6.8	1.7	1.3	1.3	1.1	1.7
Conversion of Acceptor/Pass, Mol % of Total Ca	19	16	18	13.8	13.6	13.2	12.6

(1) Input is given after shift reaction and hydrolysis of CS_2 have taken place.
(2) Gas sample taken after breakthrough had occurred.
(3) Includes 20-30% +100 mesh particles.

TABLE 2

Conditions and Results for Regenerator with Canaan Dolomite Feed
System Pressure: 15 atm (206 psig)

Run Number	A7	A15	A16	A20A	A21	A22A	A36A
Temperature, °C (°F)	704 (1300)	593 (1100)	593 (1100)	704 (1300)	704 (1300)	760 (1400)	704 (1300)
Nominal Solids Residence Time, min.	37	36	74	60	59	57	52
Input, SCFH							
Recycle to Bed	←		0.0		→ 102	0.0	0.0
H_2O	110	100	109	53	47	48	108
H_2	0.0	12	12	8.0	3.0	8.0	11
CO_2	110	118	118	91	50	86	205
Purges (N_2) to Bed	8	8	8	7	10	10	10
Purges (N_2) above Bed	10	10	10	10	0.0	10	0.0
Purges (CO_2) above Bed	5	5	5	4	15	4.5	15
Output in Cycle No.	1	6	1	23	18	8	4
Exit Gas Rate, SCFH (dry basis)	133	154	152	120	33	116	236
Composition, Mol %							
H_2	ND	8.0	8.3	5.0	3.9	3.9	2.1
CO	ND	0.76	1.01	3.95	5.2	3.7	2.6
CO_2	85.7	78.4	77.4	71.8	83.1	71.4	94.1
N_2	13.5	11.4	12.8	18.3	5.2	19.4	0.6
H_2S	0.7	1.41	0.46	0.82	2.54	0.94	0.62
COS	ND	0.02	Trace	0.04	0.11	0.04	0.03
Outlet Gas, Top of Bed							
Composition, Mol %							
H_2O	48.3	41.6	44.1	32.9	29.0	32.9	33.5
H_2	--	5.15	5.14	3.8	3.1	3.0	1.5
CO	--	0.49	0.63	3.0	4.1	2.8	1.8
CO_2	47.8	48.5	46.0	52.0	57.5	51.8	62.4
N_2	3.5	3.2	3.9	7.6	4.1	8.5	0.4
H_2S	0.4	0.91	0.28	0.62	2.03	0.72	0.44
COS	--	0.01	Trace	0.03	0.09	0.031	0.02
Flow Rate, SCFH, Top of Bed	228	238	245	158	169	151	333
Fluidizing Velocity, ft/sec	0.63	0.60	0.61	0.44	0.47	0.44	0.92
% H_2S in Outlet/Equilibrium % H_2S	0.09	0.04	0.01	0.18	0.61	0.43	0.11
Regeneration of Acceptor/Pass, Mol % of Total Ca	5.1	11.5	7.5	8.8	7.4	9.3	11.0

ND - Not determined.

FIGURE 1

DEACTIVATION OF CaS IN CANAAN DOLOMITE
AT 704°C (1300°F)

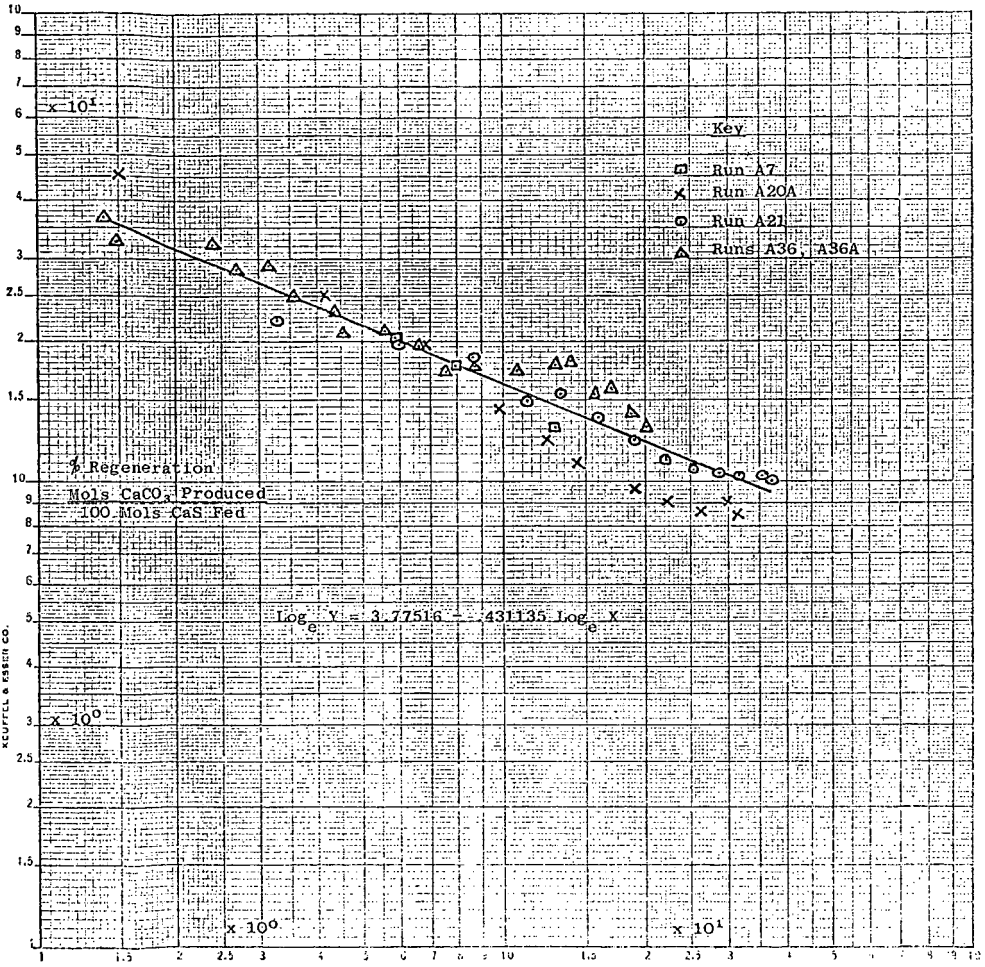

FIGURE 2

DEACTIVATION OF CaS WITH
TEMPERATURE AS A PARAMETER

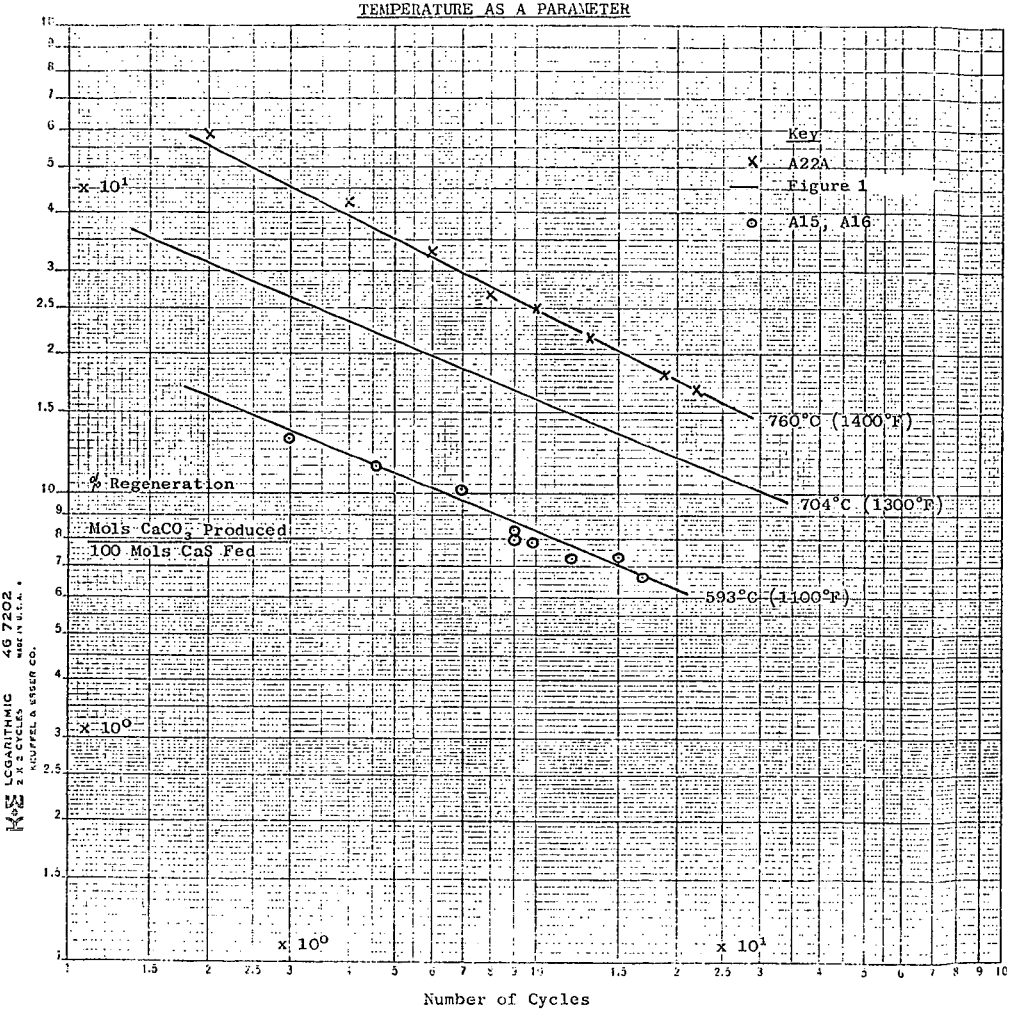

Batch Regeneration

As a limiting step appeared to be regeneration, a batch regeneration program was set up to further explore the variables affecting the system. Results of these runs are given in Table 3. A statistical analysis of the data showed percent regeneration to increase with increasing temperature and decreasing age of stone. The effect of increasing temperature causing an increase in conversion was more pronounced for cycled stone than for fresh stone.

The effect of bed depth was unusual. It was expected that since the deeper bed ran at an H_2S outlet concentration closer to equilibrium, there would be less driving force for reaction and the regeneration conversion would be lower. In all six test pairs exactly the opposite was found. The runs with the deeper beds, i.e., higher H_2S outlet concentration, gave higher conversions. This is consistent with earlier conclusions that increasing the H_2S concentration does not adversely affect conversion in the regenerator.

In the course of running cyclic operations, the H_2S concentration in the outlet gas of the regenerator ranged from about 10% to 100% of the equilibrium value, and there was no detectable change in the rate of regeneration as the H_2S content approached equilibrium. It had been concluded that there would be no difficulty in running the regenerator close to the equilibrium H_2S concentration in the outlet gas.

Regeneration Kinetics

Regeneration kinetics were examined by recording the H_2S concentration in the exit gas as a function of time as the batch runs progressed. The total mols of H_2S produced were normalized to match the total mols of CaS reacted, and conversion as a function of time was then plotted. These results are presented in Figures 3 to 5 in the form of $(1 - X)$ versus time, where X is the fractional conversion of the CaS feed.

In all cases, the rate continuously decreased. It appeared that the reaction would eventually cease while there was still considerable CaS left. This is consistent with the notion that much of the CaS is simply unreactive. The initial reaction rate was faster for fresh stone than for cycled stone at all temperature levels. Additionally, the rate seemed to slow sooner for the cycled stone. The curves also show that the effect of bed depth is present even at the early stages of all reactions; the deeper beds had a higher reaction rate at all times.

While the reaction kinetics are complicated, they may be approximated by a simple first order rate constant for the short times (about an hour) of interest to the process. The reaction model would then be:

$$Kt = -\ln (1 - X)$$

where K = rate constant, hr^{-1}, whose function of gas concentration is yet to be determined.
t = time, hours
and X = fractional conversion of the CaS fed.

The value of K was taken from the slope of the data from 5 to 50 minutes in Figures 3 to 5, and is tabulated in Table 4. The data of Table 4 are plotted in Figure 6. The activation energies for cycled and fresh stone are shown to be the same, about 19 kilocalories.

The kinetic mechanism proposed here allows one to calculate the effect of changing conditions of temperature or residence time upon fractional conversion of CaS (percent regeneration).

TABLE 3

Results of Regenerator Runs
All Runs 15 atm, 60% CO_2, 35% H_2O Inlet

Run No.	Dolomite	Bed Height, inches	% Regeneration	Maximum Approach to Equilibrium, %	Run Time, hours	Maximum % H_2S, Dry Basis	Temperature, °F (°C)	Gas Residence Time, sec	10^3 x Mols CaS Available / Mols (CO_2 + H_2O)/hr
A68	Sulfided Fresh	35.3	61.6	13.0	7.2	1.77	1200 (649)	4.9	20.6
A69		36.1	47.4	47.4	8.0	2.78	1300 (704)	4.7	24.8
A70		36.8	80.8	93.7-102.8(1)	5.7	2.68-2.94(1)	1400 (760)	4.6	26.5
A71		16.1	57.5	3.0	8.4	.41	1200 (649)	2.2	8.6
A72		16.9	71.2	13.5	8.0	.79	1300 (704)	2.2	11.0
A73		16.2	78.3	50.0	4.7	1.43	1400 (760)	2.0	11.4
A74	Sulfided Cycled	37.9	14.5	2.8	9.1	.38	1200 (649)	5.3	5.39
A75		36.5	31.5	14.2	8.1	.83	1300 (704)	4.8	10.8
A76		38.9	55.4	31.5	10.0	.90	1400 (760)	4.8	19.9
A77		15.9	10.9	0.7	3.7	.09	1200 (649)	2.0	1.71
A78		15.3	23.0	3.4	7.8	.20	1300 (704)	2.0	3.38
A79		17.1	42.6	13.6	8.0	.39	1400 (760)	2.1	6.8

(1) The high value is extrapolated where a portion of the chart was unreadable.

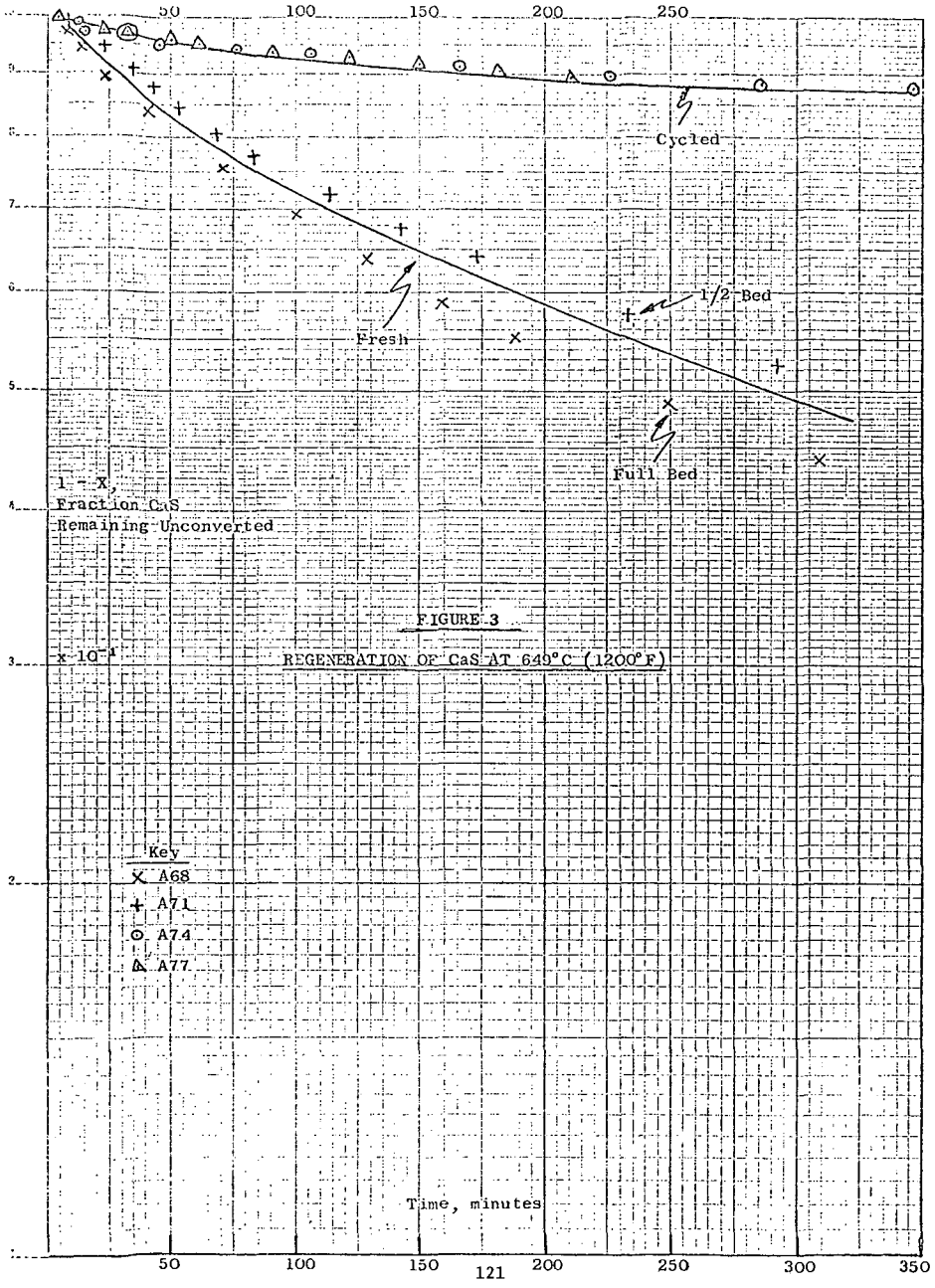

FIGURE 3

REGENERATION OF CaS AT 649°C (1200°F)

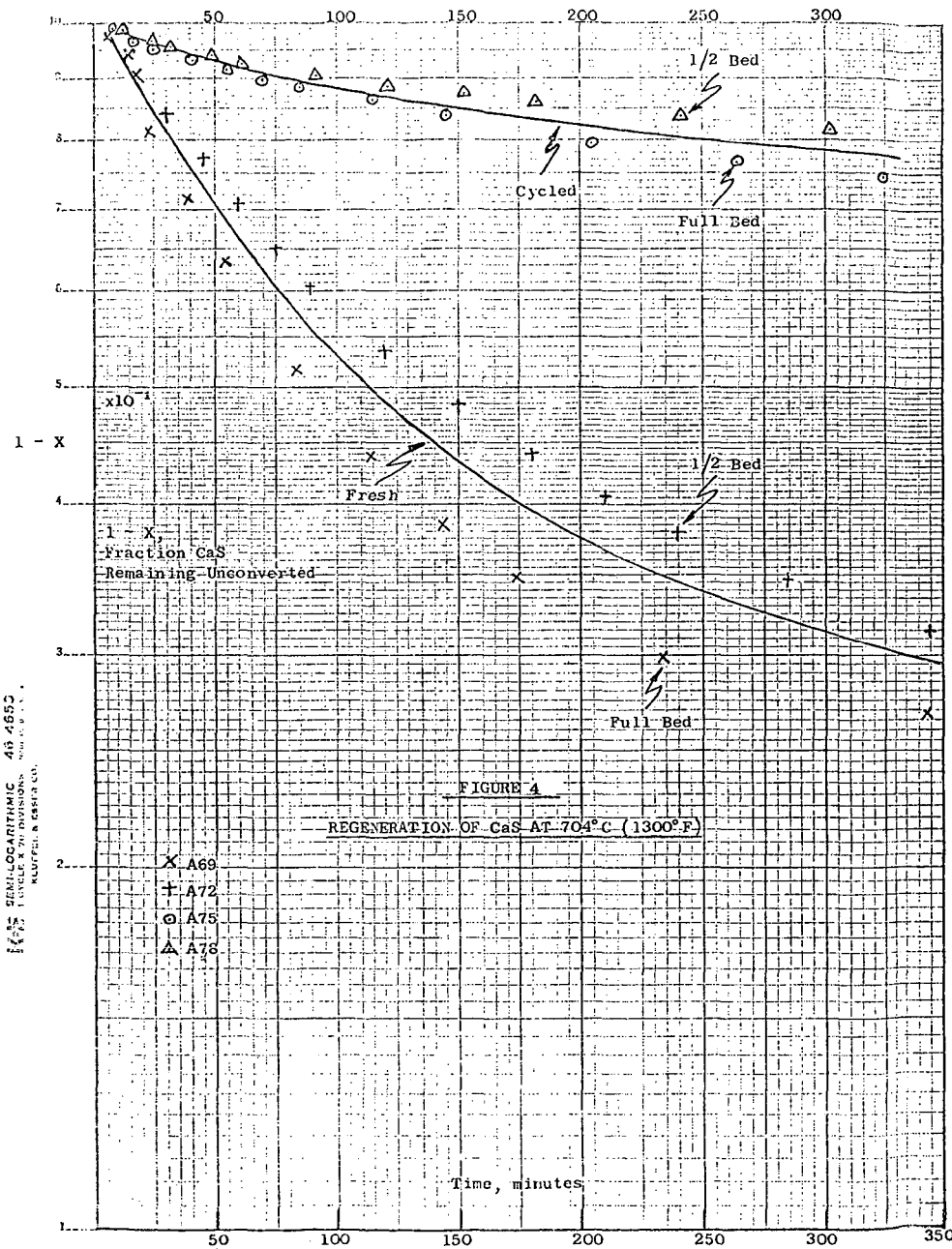

FIGURE 4

REGENERATION OF CaS AT 704°C (1300°F)

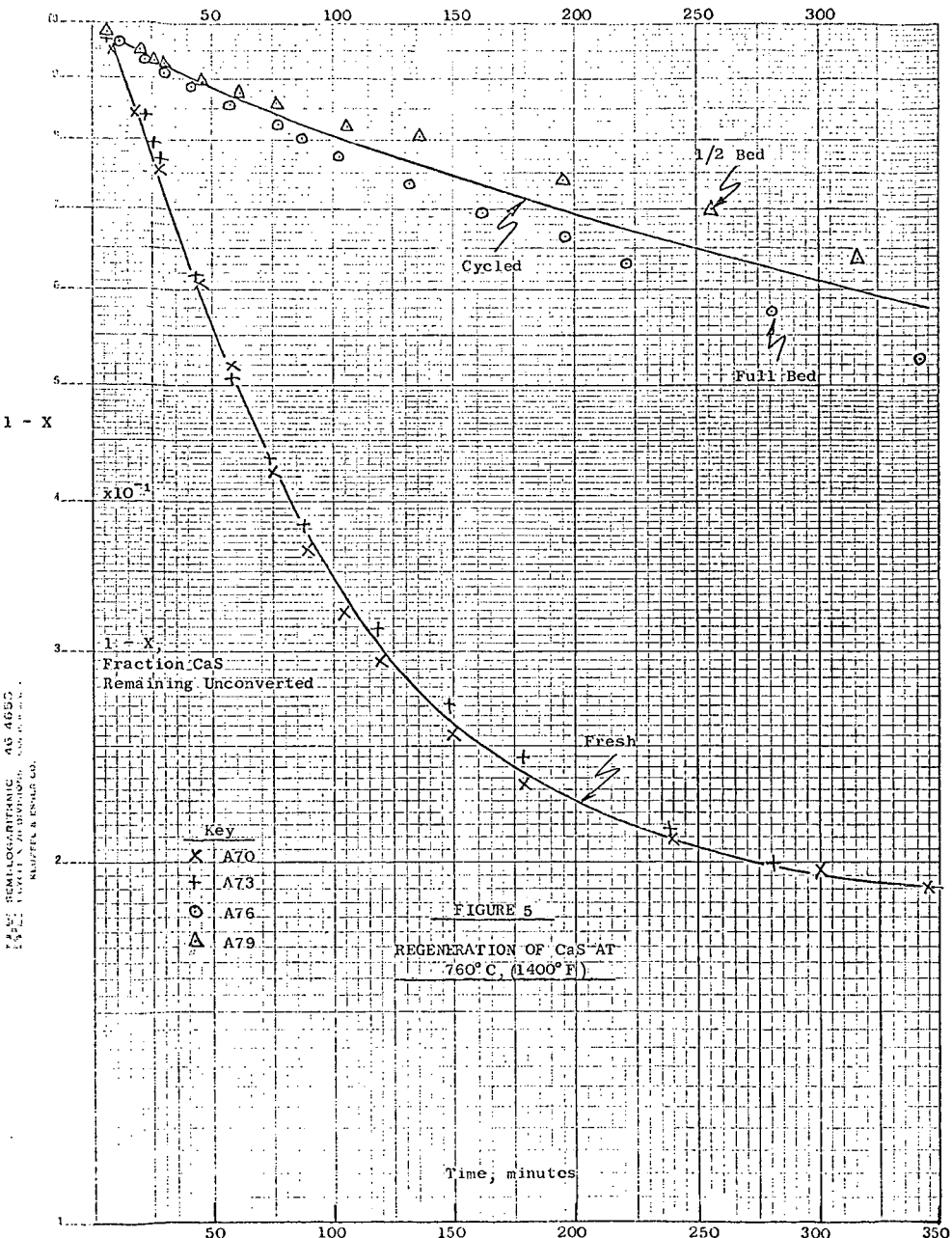

FIGURE 5

REGENERATION OF CaS AT 760°C. (1400°F)

TABLE 4

Initial Rate Constants for Regeneration Kinetics

System Pressure: 15 atm
Feed: 35% H_2O, 60% CO_2, 5% H_2

Temperature, °C (°F)	k, hr^{-1}	
	Cycled	Fresh
649 (1200)	.063	.247
704 (1300)	.098	.468
760 (1400)	.170	.747

FIGURE 6

EFFECT OF TEMPERATURE ON REGENERATION KINETICS

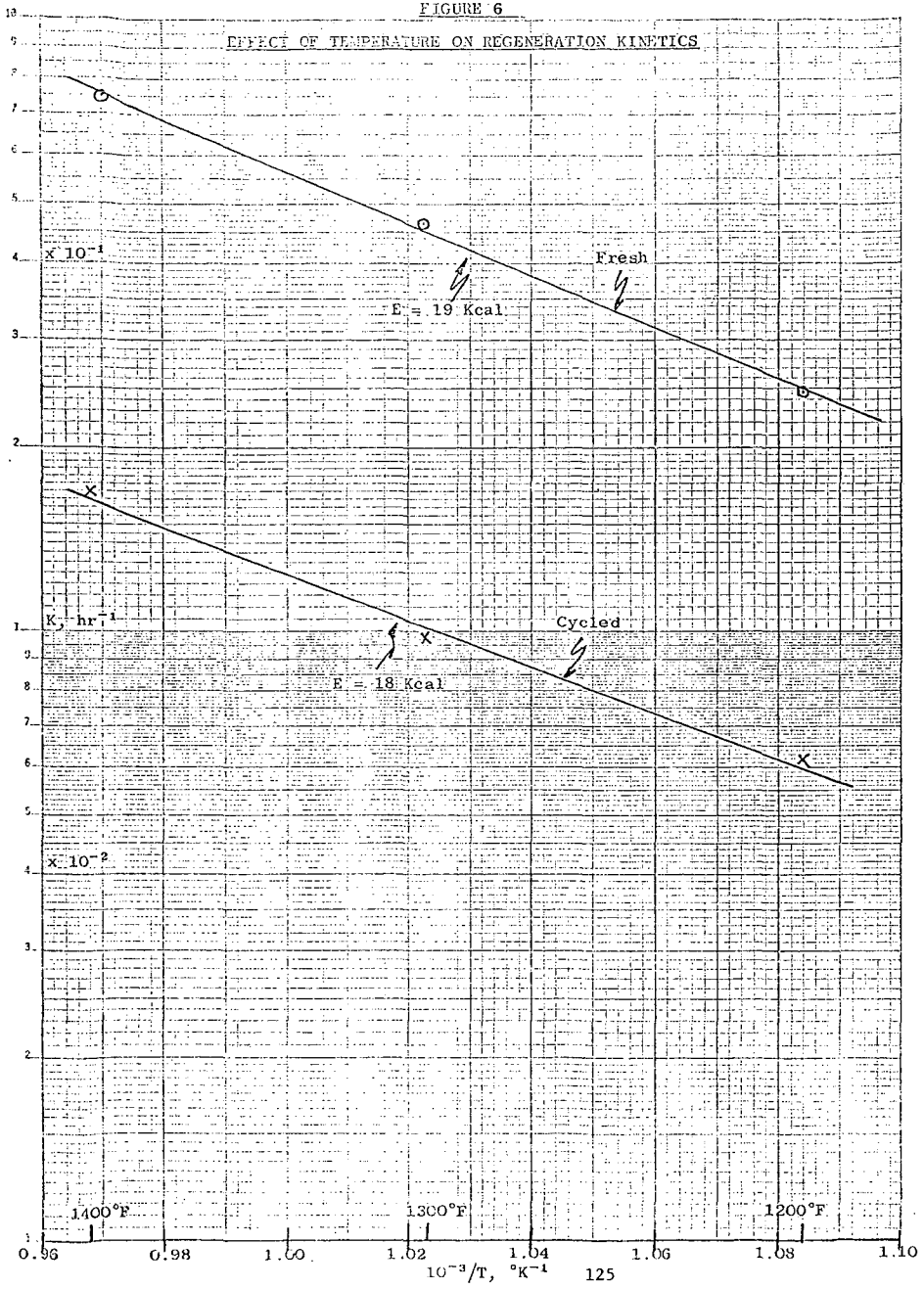

Cycling with Varying Residence Times

Four batch cycling runs were made employing the possible combinations of 20 or 60 minutes residence time for sulfur absorption and regeneration. Results are presented in Figure 7. Tymochtee 11 dolomite was the feedstock, and each run lasted for 11 cycles.

The effect of reducing residence time in the gas desulfurizer was striking. At 10 cycles, going from 60 to 20 minutes in the gas desulfurizer increased regeneration activity from 15 to 40% at 60 minutes regenerator time and from 15 to 23% at 20 minutes regenerator time. Conversely, going from 60 to 20 minutes regenerator time had no effect at the 60 minute desulfurizer level. Another effect observed was that attrition rates were highest at the short gas desulfurizer residence time, 2.3% average for 20 minutes versus 0.8% for 60 minutes.

It is believed that deactivation of stone takes place primarily in the gas desulfurizer due to crystal growth and particle sintering. This would explain the dramatic effect of time on activity. The results of the above runs are highly significant since they indicate the potential for greatly increasing the stone's capacity for sulfur absorption.

Scanning Electron Microscope Data

Selected samples of cycled stone were examined under an electron microscope equipped for energy dispersive X-ray analysis. It was found that cycled stone contained very large grains of CaS. The $CaCO_3$ which was present tended to be concentrated in smaller sizes. Both of the calcium species were larger than the MgO crystals or grains. It is believed that the larger CaS grains are unreactive in the regeneration step of the process.

Model for the Deactivation Process

The regeneration reaction suffers from deactivation of the CaS even from cycle 1. The model postulated below fits the behavior of the system so far. The part dealing with regenerator variables was developed jointly with A. M. Squires of The City College Clean Fuels Institute.

Deactivation of the dolomite occurs mainly in the gas desulfurizer due to the elevated temperature. Two mechanisms are operating. Crystal growth of $CaCO_3$ and CaS segregates the calcium crystals from the MgO and produces a material tending toward a limestone rather than a dolomite. Simple sintering and densification take place as well, and this both hardens the stone and tends to reduce porosity.

In the regenerator, densification does not occur. However, the reaction starts rapidly and then tails off to an insignificant rate. Using the same feed, it can be shown that the conversion at which reaction essentially ceases is a strong function of temperature, the lower temperature producing the lower conversion. It has further been observed that introducing product H_2S does not retard the rate of reaction, but conversely increases the ultimate level of conversion attainable.

The phenomenon of the products of reaction increasing the conversion of calcium in the sulfur-calcium system is not new. Pell[3] found that H_2O increased the conversion of CaO to CaS in the reaction of H_2S with calcined dolomite, and Ruth[4] showed that either CO_2 or H_2O could increase the conversion of $CaCO_3$ to CaS in the reaction of H_2S with half-calcined dolomite. Furthermore, both studies demonstrated the effect of the reaction flagging at lower and lower conversion levels as the reaction temperature decreased. Ruth[5] proposed the following mechanism after examination of electron microscope results on various samples. "High levels of CO_2 . . . . may promote the formation of large numbers of fine

FIGURE 7

Runs A129 to A132 - Deactivation of CaS at 704°C (1300°F)

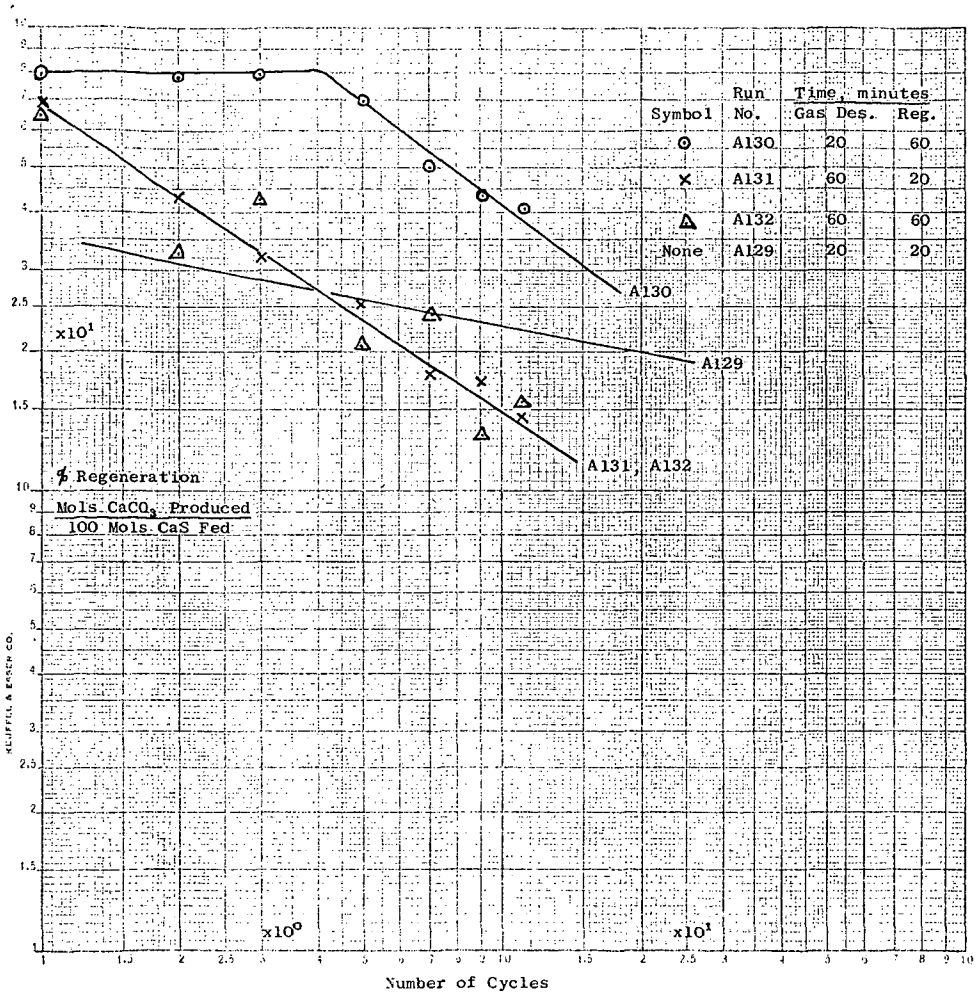

crystallites of CaS that do not protect the underlying $CaCO_3$ . . . . On the other hand, at low levels of CO_2 a smaller number of large CaS crystals formed and grow together to close off the surface, thereby protecting the remaining $CaCO_3$ from further reaction."

Ruth's careful analysis of his data showed that in the presence of reaction products, the reaction was indeed slower initially. However, within a short time the conversion associated with the product-rich environment soon surpassed that in the product-poor environment.

It is postulated that a similar model fits the regeneration reaction. At low levels of H_2S, the $CaCO_3$ formed grows in large crystals shutting off the interior of the grain from further reaction. At high levels of H_2S, the reaction nucleates at many sites to produce many small crystals which leave the interior of the grain open to further reaction. Via such a mechanism, the presence of H_2S would enhance conversion in the regenerator. This is in full concordance with our experimental results.

Acknowledgment

Appreciation is expressed to the Environmental Protection Agency for financial support of the work presented in this paper and for permission to publish the results given.

References

1. Curran, G.P., Clancey, J.T., Pasek, B., Pell, M., Rutledge, G.D., and Gorin, E., "Production of Clean Fuel Gas from Bituminous Coals," (1973), EPA No. EPA-650/2-73-049, NTIS No. PB 232-695/AS.

2. Curran, G.P., Koch, B.J., Pasek, B., Pell, M., and Gorin, E., "High Temperature Desulfurization of Fuel Gas," Report to EPA under Contract No. 68-02-1333, in preparation.

3. Pell, M., "Reaction of Hydrogen Sulfide with Fully Calcined Dolomite," Ph.D. Thesis, The City University of New York (1971).

4. Ruth, L.A., Squires, A.M., and Graff, R.A., "Desulfurization of Fuels with Half-Calcined Dolomite: First Kinetic Data," Env. Science & Tech., 6, 1009-1014, 1972.

5. Ruth, L.A., "Reaction of Hydrogen Sulfide with Half-Calcined Dolomite," Ph.D. Thesis, The City University of New York (1972).

High Pressure TGA Studies on the Cyclic Use of Half-Calcined Dolomite to Remove Hydrogen Sulfide

George L. Kan, Arthur M. Squires, Robert A. Graff

The Clean Fuels Institute
Department of Chemical Engineering
The City College of New York
New York, N.Y. 10031

Candidate solids for absorption of hydrogen sulfide from a fuel gas at elevated pressure are the composite of iron oxide and fly ash developed by the U.S. Bureau of Mines (1), fully-calcined dolomite (2-4), and half-calcined dolomite (2,5).

Half-calcined dolomite absorbs hydrogen sulfide by the reaction:

$$[CaCO_3+MgO] + H_2S = [CaS+MgO] + H_2O + CO_2$$

For a given fuel gas at a given pressure, desulfurization by this reaction is best accomplished at a temperature just a bit below the temperature at which calcium carbonate would decompose at the partial pressure of carbon dioxide prevailing in the fuel gas.

Regeneration of the solid absorbent is by the reverse reaction, preferably conducted at the lowest possible temperature in order to obtain the highest possible concentration of hydrogen sulfide in the offgas, facilitating conversion of this species to elemental sulfur in a subsequent operation.

Absorption and regeneration cycles at atmospheric pressure and 750°C give the results seen in Figure 1. Although the absorption reaction is rapid, the regeneration reaction is slow, requiring more than 1 hour. There is a decline in capacity of the solid to about 23% of the total calcium after 6 cycles.

Cycling trials at elevated pressure have been carried out with a duPont thermogravimetric analyzer modified for operation at total pressures up to 30 atmospheres, with high partial pressures of steam, and with corrosive gases such as hydrogen sulfide. This equipment is described in reference 6.

In contrast to the results at one atmosphere, cycling at elevated pressure gives little change in capacity or reactivity beyond the first several cycles. Figure 2 gives results from 15 cycles carried out at 300 psig and 731°C. Absorption for 15 minutes was alternated with regeneration for 10 minutes. The capacity settles out at 40%. Figure 3 shows the course of the reactions in the first, 7th, and 15th cycles, and illustrates our finding that the reaction rates do not change much with cycling; only capacity changes. The regeneration reaction at 300 psig is extremely fast, running most of its course in the order of one minute.

Figure 4 shows 30 cycles with absorption for 19 minutes and regeneration for 5 minutes at 550°C. The 19 minutes absorption time

includes 13 minutes at 700°C and 6 minutes cooling time.

Figure 5 shows sulfur capacity versus cycle number for three runs, and illustrates the decline in capacity with decline in regeneration temperature.

Figure 6 illustrates the course of reactions in the last cycle of each of the three cycles plotted in Figure 5. It is fascinating that the observed reaction rates do not seem much to depend upon temperature. This suggests that the true rates are extremely fast, and that the observed rates are controlled by diffusion.

In the series of runs depicted in Figure 7, we varied the ratio of steam to carbon dioxide in the regeneration step to see if this is an important factor in the final capacity of the solid. It appears from Figure 7 that the capacity suffers at a low ratio of steam to carbon dioxide, such as 25/75. Above about 50/50, the ratio does not seem to have much effect. It may be noted that we have succeeded in a run of 15 cycles with a steam partial pressure in the vicinity of 19 atmospheres.

The effect of temperature in absorption and regeneration is shown in Figures 8 and 9. In both figures the duration of the absorption and regeneration steps are 21 and 4 minutes respectively, the time required for heating and cooling being included in the absorption time. Increasing absorption temperatures reduces capacity. The data in Figure 8 show a "deactivation energy" of 22 kcal/gmole. Capacity increases with regeneration temperature, but the temperature effect is not as strong as in absorption. From the data of Figure 9, the "activation" energy is 9 kcal/gmole.

Figure 10 shows the last cycle reaction rates for the four runs plotted in Figure 8. Figure 11 shows the capacity versus cycle number for the same runs.

The effect of steam and CO_2 level on regeneration rate was explored in the presence of partial pressures of H_2S. Figures 12 and 13 show five regeneration steps for the same stone in which only the regeneration atmosphere was changed from one cycle to the next. The sample reactivity was first stabilized by conducting 6 cycles in the same regeneration atmosphere (50% H_2O, 40% CO_2, 10% H_2). In all cases the a sorption conditions were unchanged. Lower initial rates result from the presence of H_2S as well as decreased H_2O and CO_2 partial pressures. With high CO_2 pressures (Figure 12), increasing the steam partial pressure increases the initial rate and the capacity. The effect is much more dramatic at low CO_2 pressures (Figure 13).

The complexities of the kinetic situation illustrated in Figures 12 and 13 are reminiscent of the "kinetic curiosities" reported eariler for the absorption reaction (5), and like them, the new complexities appear to reflect differences in the way in which crystallites of $CaCO_3$ or CaS grow within the solid microstructure. Examinations of microstructural properties of solids arising in this research will be reported elsewhere (7).

Acknowledgments

This research was supported by the Empire State Electric Energy Research Corporation, Project EP4-3. We thank Richard D. Harvey and his colleagues at the Illinois State Geological Survey for their cooperation.

REFERENCES

1. W.T. Abel, F.G. Schultz, P.F. Langdon, U.S. Bureau Mines Rep. Invest. 7947, 1974.
2. A.M. Squires, Adv. Chem. Ser., vol. 69 (1967), p. 205.
3. A.M. Squires, R.A. Graff, M. Pell, A.I.Ch.E. Symp. Series, vol. 67, no. 115 (1971), p. 23.
4. M. Pell, R.A. Graff, A.M. Squires, "Reaction of CaO with H_2S", in Sulfur & SO_2 Developments, A CEP Technical Manual, 1971, p. 151.
5. L.A. Ruth, R.A. Graff, A.M. Squires, Environmental Sci. & Tech., vol. 6 (1972), p. 1009.
6. S. Dobner, G. Kan, R.A. Graff, A.M. Squires, Thermochemica Acta. in press.
7. R.D. Harvey, G. Kan, R.A. Graff, A.M. Squires, "Behavior of Dolomite in Absorption of H_2S from Fuel Gas", Proceedings of the AIME Fall Meeting, Sept. 1-3, 1976. Denver Colorado.

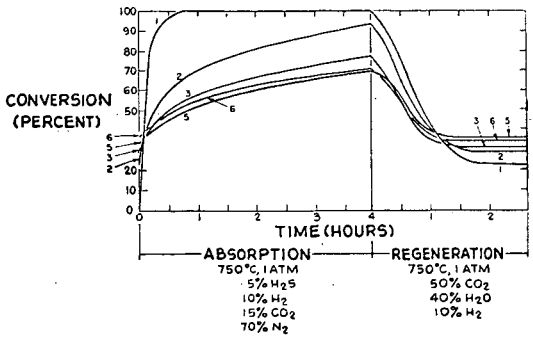

Figure 1. Sulfur absorption and regeneration cycles for half-calcined dolomite at 1 atm and 750°C.

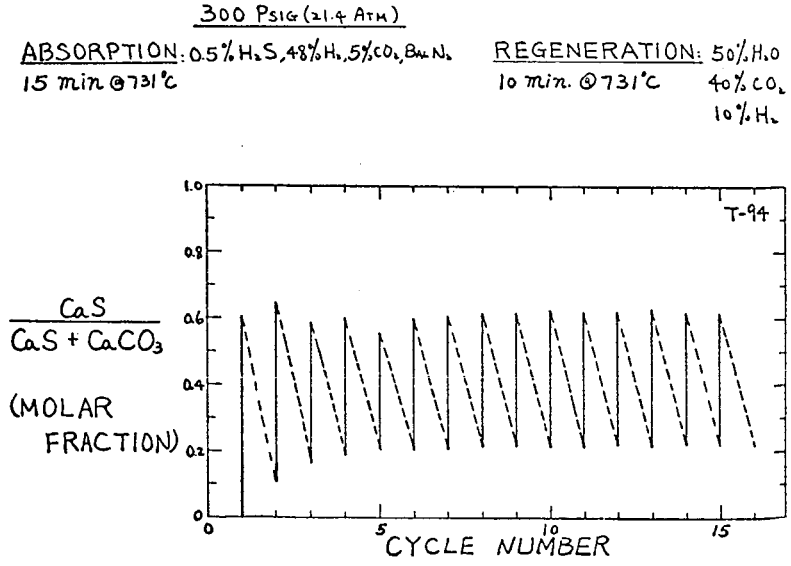

Figure 2. Molar fraction of calcium sulfide in half-calcined dolomite used in 15 cycles for absorption of hydrogen sulfide from simulated fuel gas.

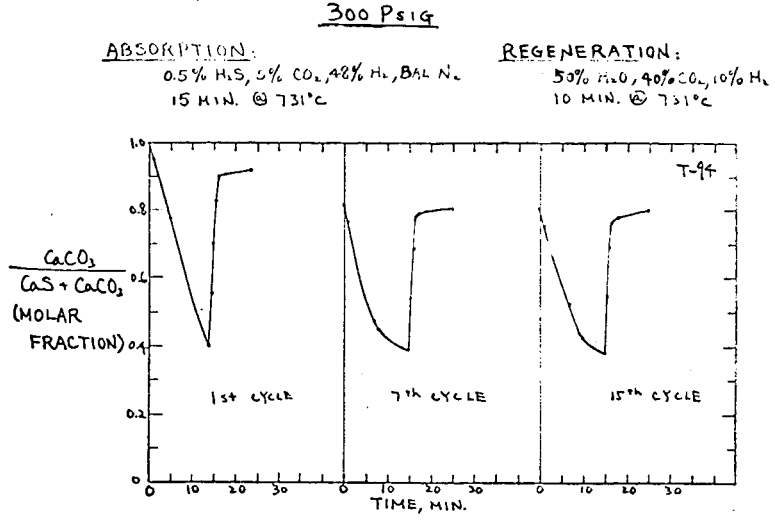

Figure 3. Course of reactions in first, 7th, and 15th cycles of Figure 2.

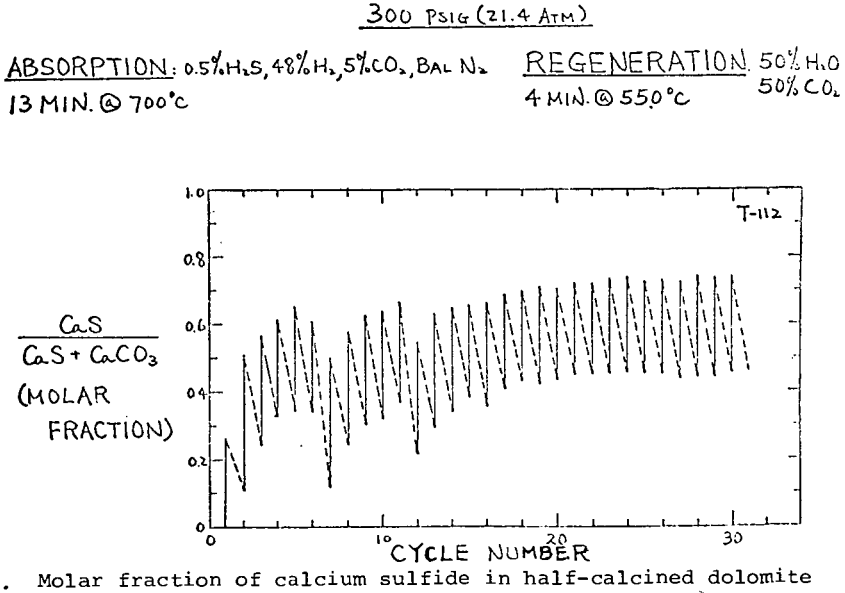

Figure 4. Molar fraction of calcium sulfide in half-calcined dolomite used in 30 cycles for absorption of hydrogen sulfide from simulated gas. Heating took about two minutes without H_2S present, cooling took about 6 minutes with H_2S mixture present.

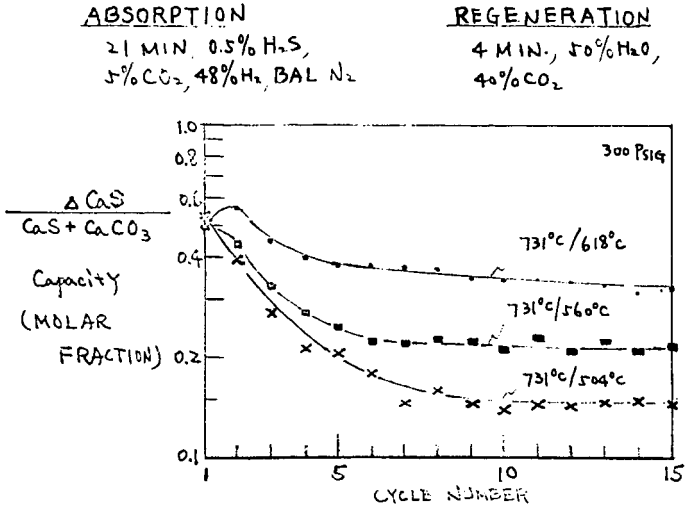

Figure 5. Capacity versus cycle number for three runs with absorptions at 731°C (the first temperature designated alongside each curve) and regenerations at 618°C, 560°C, and 504°C (the second temperature).

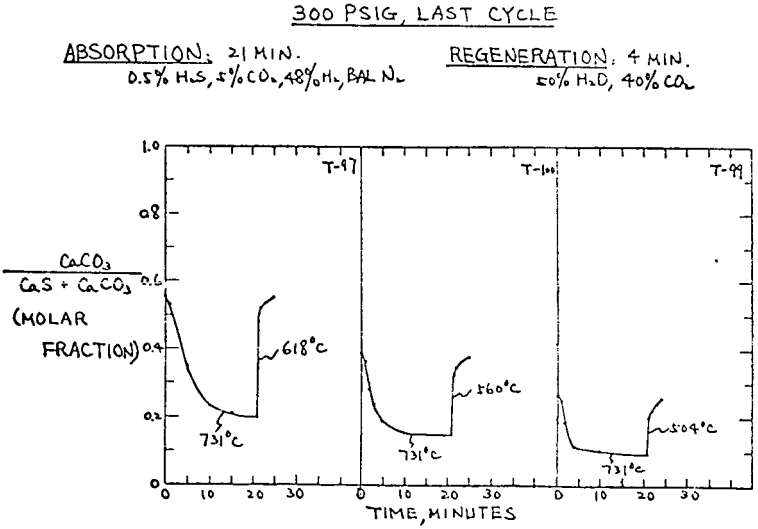

Figure 6. Cycle of absorption and regeneration for each of the three runs of Figure 5.

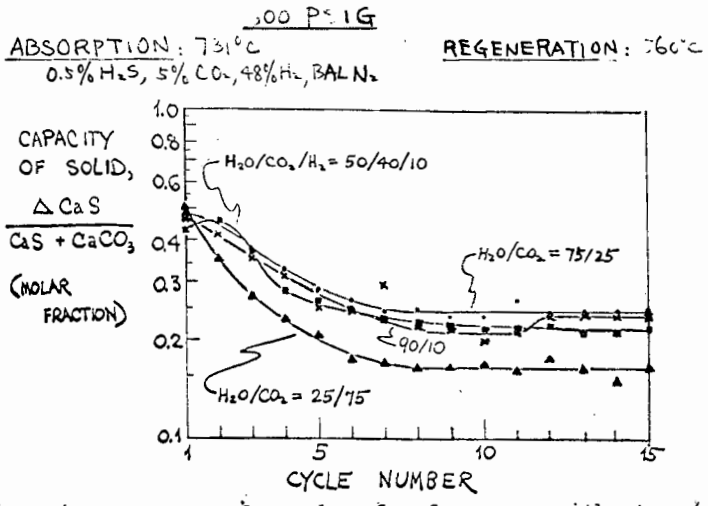

Figure 7. Capacity versus cycle number for four runs with steam/carbon dioxide/hydrogen ratios in regeneration gas as shown alongside the curves.

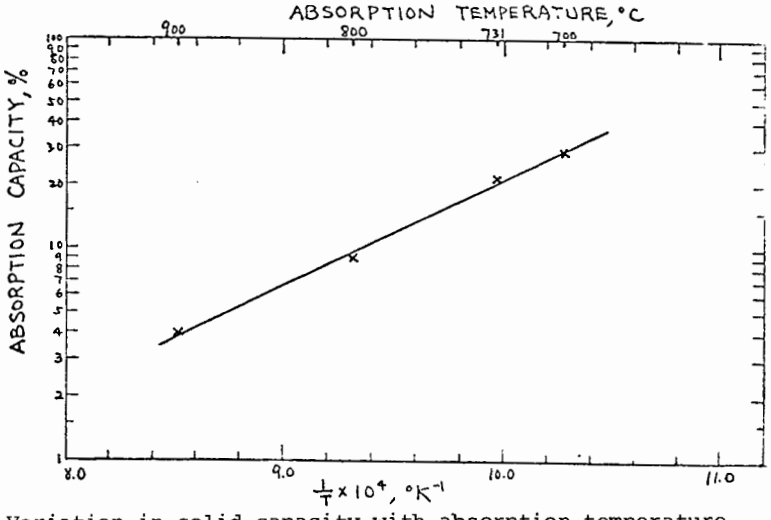

Figure 8. Variation in solid capacity with absorption temperature, for regeneration at 560°C. Absorption = 21 minutes (including heating and cooling); regeneration = 4 minutes.

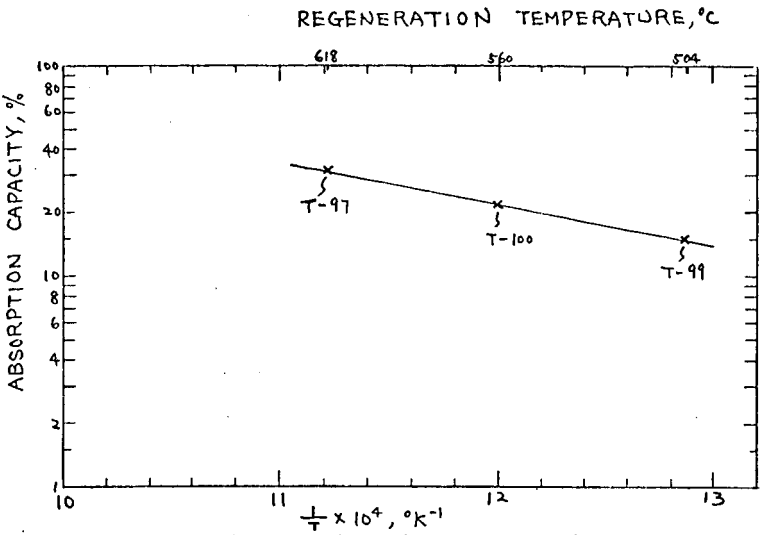

Figure 9. Variation in solid capacity with regeneration temperature, for absorption at 731°C. Times are same as in Figure 8.

300 PSIG, LAST CYCLE

RUN	ABSORPTION	REGENERATION
T-110	*26MIN*, 0.5%H_2S, 30%CO_2, 48%H_2, Bal N_2	4MIN., 50%H_2O, 50% CO_2
T-111	*21MIN*, 0.5%H_2S, 10%CO_2, 48%H_2, Bal N_2	4MIN., 50%H_2O, 50% CO_2
T-112	*19MIN*, 0.5%H_2S, 5%CO_2, 48%H_2, Bal N_2	4MIN., 50%H_2O, 50% CO_2
T-114	*19MIN*, 0.5%H_2S, 5%CO_2, 48%H_2, Bal N_2	4MIN., 50%H_2O, 40%CO_2, 10% H_2

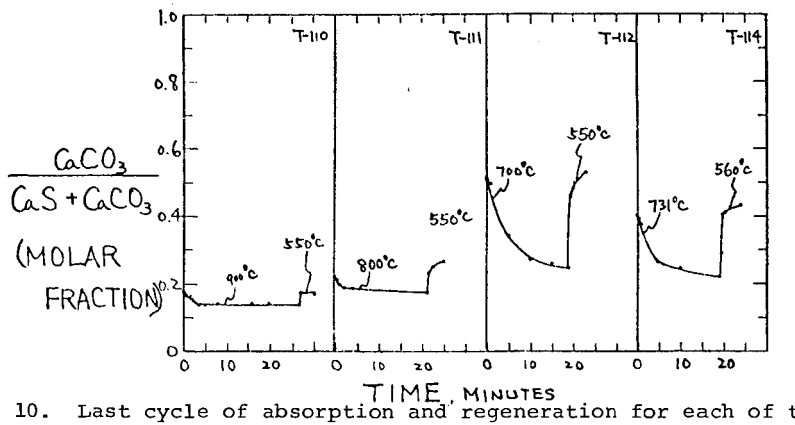

Figure 10. Last cycle of absorption and regeneration for each of the four runs of Figure 8.

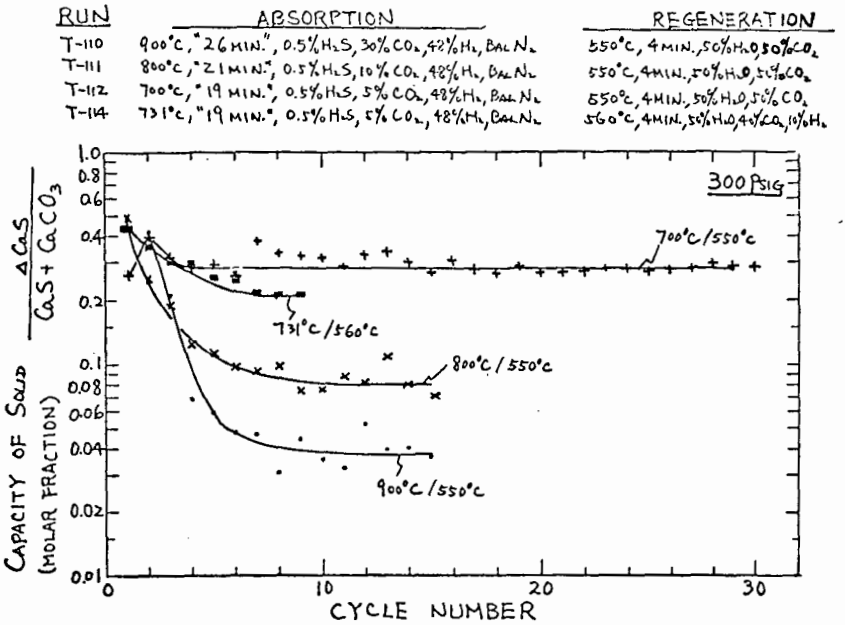

Figure 11. Capacity versus cycle number for the four runs of Figure 8.

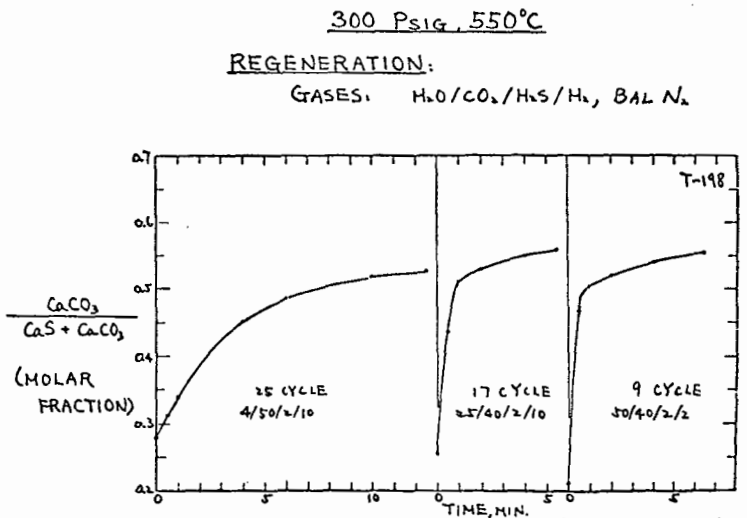

Figure 12. Effect of steam on regeneration rate at high CO_2 partial pressure in presence of H_2S. Three cycles of the same sample. Absorption at 700°C, 0.5% H_2S, 5% CO_2, 48% H_2, balance N_2.

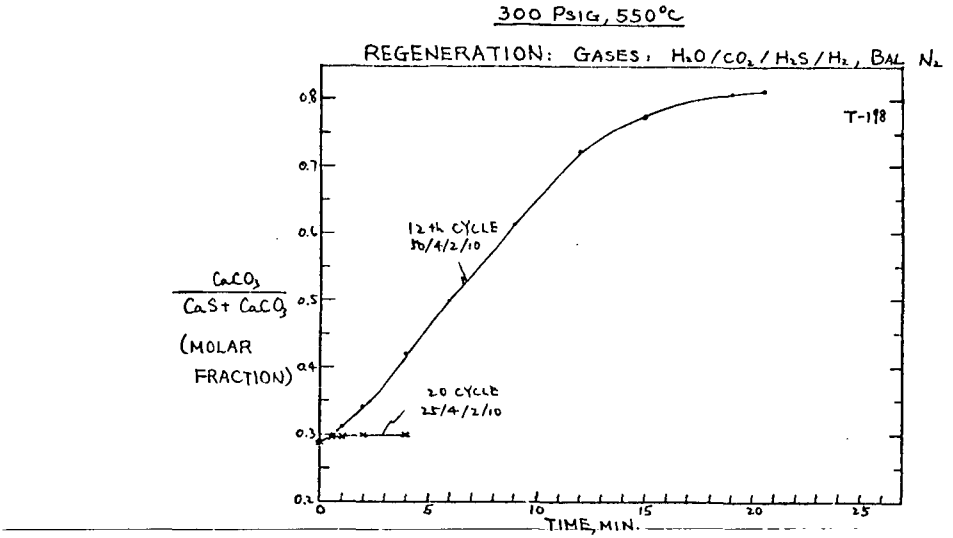

Figure 13. Effect of steam on regeneration rate at low CO_2 partial pressure in presence of H_2S. Same sample and absorption conditions as in Figure 12.